UNESCO Chair on
Coastal Geo-Hazard Analysis
Research Institute for Earth Sciences
Geological Survey of Iran

Abstract:

Lake Urmia is one of the most important and valuable water ecosystems in Iran and is known as the largest and saltiest permanent lake in Iran and one of the largest supersaturated lakes in the world, and because of its unique ecological values as an international park and wetland and because of the nature suitable for the permanent and temporary living of all kinds of rare birds of the world and the natural beauty of its coasts and islands have been introduced as a biosphere reserve by "UNESCO" in 1976.

The catchment area of Lake Urmia with an area of about 5,801 square kilometers. This basin is located in the northwest of Iran and is surrounded by the northern part of Zagros mountains, the southern slope of Sabalan Mountain and the northern, western and southern slopes of Sahand mountain.

ISBN: 978-622-5858-86-2

2024

UNESCO Chair on
Coastal Geo-Hazard Analysis
Research Institute for Earth Sciences
Geological Survey of Iran

UNESCO Chair on
Coastal Geo-Hazard Analysis
Research Institute for Earth Sciences
Geological Survey of Iran

Standard Instruction for Salt Extraction from Urmia Lake with Enviromental Considerations (part I)

UCCGHA 021-I

2024

Standard Instruction for Salt Extraction from Urmia Lake with Environmental Considerations (part I)

سرشناسه : لک، راضیه، ۱۳۴۵ – پورشعبان، اردشیر، ۱۳۵۳

Lak, Razyeh, 1966 – Pourshaban, Ardeshir, 1974

عنوان و نام پدیدآور : Standard instruction for salt extraction from Urmia Lake with environmental considerations (part I)[Book]/ author Razyeh Lak...[et al.]; employer Geological survey of Iran, Academic Jihad of Shahid Beheshti Unit; supervisors Razyeh Lak, Ardeshir Pourshaban; head of the Executive Council Razyeh Lak; summarized and translated into English Manouchehr Ghorashi; with cooperation UNESCO Chair on Coastal Geo-Hazard Analysis.

مشخصات نشر : تهران: نشر خزه، ۱۴۰۳ = ۲۰۲۴ م.

مشخصات ظاهری : ۲۴۰ ص.: مصور(رنگی)، جدول(رنگی)، نمودار(رنگی)؛ ۱۴/۵ × ۲۱/۵ سم.

شابک : 978-622-5858-86-2

وضعیت فهرست نویسی : فیپا

یادداشت : author Razyeh Lak, Ardeshir Pourshaban, Mahsa Adl, Mohammad Hasan Tavakol, Sepideh Yasemi Khiabani, Mahdi Dashti, Maryam Moejezi, Golbarg Dastfarshan

یادداشت : عنوان به فارسی: تهیه دستورالعمل استاندارد برداشت اصولی نمک از دریاچه ارومیه با رعایت ملاحظات زیست محیطی (بخش ۱)

یادداشت : کتابنامه: ص. ۲۱۷، ۲۴۰

موضوع : دریاچه ارومیه -- اوضاع زیست‌محیطی – برداشت اصولی نمک

موضوع : Urmia Lake (Iran) -- Environmental conditions – Standard Instruction for Salt

شناسه افزوده : لک، راضیه، ۱۳۴۵ -

شناسه افزوده : Lak,Razyeh- 1966-

شناسه افزوده : پورشعبان، اردشیر، ۱۳۵۳-

شناسه افزوده : Pourshaban, Ardeshir, 1974-

شناسه افزوده : یونسکو. کرسی مخاطرات زمین شناختی ساحلی- سازمان زمین‌شناسی و اکتشافات معدنی کشور

شناسه افزوده : UNESCO Chair on Coastal Geo-Hazard Analysis- Geological Survey and Mineral Exploration of Iran

رده بندی کنگره : DSR۲۱۶۱

رده بندی دیویی : ۳۳۳/۹۵۵

شماره کتابشناسی ملی : ۹۵۲۶۸۵۷

Standard Instruction for Salt Extraction from Urmia Lake with Environmental Considerations (part I)

Author:

Razyeh Lak, Ardeshir Pourshaban, Mahsa Adl, Mohammad Hasan Tavakol, Sepideh Yasemi Khiabani, Mahdi Dashti, Maryam Moejezi, Golbarg Dastfarshan

نشرخزه

اطلاعات گزارش

عنوان: تهیه دستورالعمل استاندارد برداشت اصولی نمک از دریاچه ارومیه با رعایت ملاحظات زیست‌محیطی (بخش ۱)

مجری: سازمان زمین‌شناسی و اکتشافات معدنی کشور، جهاد دانشگاهی واحد شهید بهشتی

زبان مرجع: فارسی

خروجی: گزارش، نقشه، مقاله، داده های الکترونیکی

ناظران علمی: راضیه لک، اردشیر پورشعبان

نویسندگان: مهسا عدل، محمد حسن توکل، سپیده یاسمی خیابانی، مهدی دشتی، مریم معجری، گلبرگ دستفرشان

رئیس کرسی یونسکو در مخاطرات زمین شناختی ساحلی: حمید نظری

مسئول شورای اجرایی: راضیه لک

خلاصه‌نویسی و ترجمه به انگلیسی: منوچهر قرشی

ناشر: نشر خزه

با همکاری کرسی یونسکو در مخاطرات زمین شناختی ساحلی

چاپ اول: ۱۴۰۳

شمارگان: ۵۰ نسخه

صفحات: ۲۴۰

شابک: ۹۷۸-۶۲۲-۵۸۵۸-۸۶-۲

khazepub@gmail.com

Report Information

Title: Standard Instruction for Salt Extraction from Urmia Lake with Environmental Considerations (part I)

Employer: Geological survey of Iran, Academic Jihad of Shahid Beheshti Unit

Original language: Persian

Output: Report, Map, Paper, Digital Meta Data

Supervisors: Razyeh Lak, Ardeshir Pourshaban

Authors: Mahsa Adl, Mohammad Hasan Tavakol, Sepideh Yasemi Khiabani, Mahdi Dashti, Maryam Moejezi, Golbarg Dastfarshan

Chairholder in the UNESCO Chair on Coastal Geo-Hazard Analysis: Hamid Nazari

Head of the Executive Council: Razyeh Lak

Summarized and translated into English: Manouchehr Ghorashi

Publisher: Khazeh Publication

with cooperation UNESCO Chair on Coastal Geo-Hazard Analysis

First Edition: 2024

Edition number: 50

Page: 240

Shabak: 978-622-5858-86-2

khazepub@gmail.com

Scientific Council

Name	Affiliation
Ara Avagyan	IGS: Institute Geological Sciences
Rick J Bailey	IOC-UNESCO Indian Ocean Tsunami Warning and Mitigation System/ UNESCO
Aram Fathian Baneh	University of Calgary
Wenjiao Xiao	Chinese Academy of Sciences
Magdi Guirguis	Institut français d'archéologie orientale du Caire
Richard Walker	University of Oxford
Philippe Agard	University of Sorbonne
Justin Ahanhanzo	Intergovernmental Oceanographic Commission of UNESCO (IOC-UNESCO)
Alice Aurelie	UNESCO Water Sciences Division
Eric Barrier	University of Sorbonne
Jean-François Ritz	University of Montpellier
Martin Hanz	German under water archaeology association
Klaus Reicherter	Aachen University
Judith Thomalsky	German Archaeological Institute Tehran Branch
Hamid Alizadeh Lahijani	Iranian National Institute for Oceanography and Atmospheric Science
Abbas Banj Shafiei	Urmia University
Yahya Djamour	Shahid Beheshti University (SBU)
Hassan Fazeli Nashli	University of Tehran
Razyeh Lak	Research Institute for Earth Sciences
Mohammad Mokhtari	International Institute of Earthquake

	Engineering and Seismology
Hamid Nazari	Research Institute for Earth Sciences
Jafar Omrani	Geological Survey of Iran
Morteza Talebian	Research Institute for Earth Sciences
Mohammad Tatar	International Institute of Earthquake Engineering and Seismology
Mahdi Zare	International Institute of Earthquake Engineering and Seismology
Stefano Salvi	National Institute of Geophysics and Volcanology (INGV)
Ryo Anma	Tokushima University
Yeong Bae Seong	Korea University
John Lambert	Deltares, UNESCO
Issa El-Hussain	Sultan Qaboos University
Ekkehard Holzbecher	German University of Technology in Oman
Egor Krasinskiy	Underwater research center Russian Geographical Society
Audemard Franck A.	Department of Geology, Central University of Venezuela
Executive Committee	
Name	**Affiliation**
Nasir Ahmadi	Environmental Protection Organization of Mazandaran Province
Arash Amini	Golestan University
Alireza Amrikazemi	Scientific Coordinator, Qeshm Island UNESCO Global Geopark
Parviz Armani	Imam Khomeini International University
Ataollah Dadashpour	Geological Survey of Iran, Sari branch

Asghar Dolati	Kharazmi University
Hasan Fazelinashli	University of Tehran
Fahimeh Foroghi	Iranian National Institute for Oceanography and Atmospheric Science
Abdolazaim Ghanghormeh	Golestan University
Habibolah Ghasemi	Shahrood University of Technology
Mohammad reza Ghasemi	Research Institute for Earth Sciences
Manouchehr Ghorashi	Research Institute for Earth Sciences
Jafar Hassanpour	University of Tehran
Ataollah Kavian	Environmental Protection Organization of Mazandaran Province
Mohammadreza Kazemzadeh	Superme Audit Gourt
Razyeh Lak	Head of RIES and Executive Manager
Mahmoudreza Majidifard	Research Institute for Earth Sciences
Ali Akbar Momeni	Shahrood University of Technology
Babak Moradi	Iranian National Institute for Oceanography and Atmospheric Science
Seyed Mohsen Mortazavi	Hormozgan University
Hasan Nasrollah Zadeh Saravi	Caspian Sea Ecological Research Center
Ehsan Pegah	Kharazmi University
Abdolwahed Pehpouri	Qeshm Island UNESCO Global Geopark
Ahmadreza Rabani	University of Science and Technology of Mazandaran
Mahdi Rahmanian	Shargh Daily newspaper
Ahmad Rashidi	International Institute of Earthquake Engineering and Seismology
Masoud Sadri Nasab	University of Tehran
Mohammad Salamati	Respina Company

Mohammad Tatar	International Institute of Earthquake Engineering and Seismology
Alireza Vaezi	Research Institute for Earth Sciences
Mojtaba Yamani	University of Tehran
Ahmed Hadidi	German University of Technology in Oman (GUTECH)
Secretariat	
Name	**Affiliation**
Elnaz Aghaali	Research Institute for Earth Sciences
Keivan Ajdari	Research Institute for Earth Sciences
Hourieh AliBeygi	Research Institute for Earth Sciences
Sedigheh Ghanipour	Research Institute for Earth Sciences
Hamoon Memarian	Research Institute for Earth Sciences
Shirin Safavi	Research Institute for Earth Sciences
Aazam Takhtchin	Research Institute for Earth Sciences
Mehrnoosh Pour Saeid	Graphic Designer
Hanieh Bakhshaei	Geological Survey of Iran
Reza Behbahani	Geological Survey of Iran
Javad Darvishi khatooni	Geological Survey of Iran
Mohammadreza Ensani	Geological Survey of Iran
Marziyeh Estrabi Ashtiyani	Geological Survey of Iran
Gholamreza Hoseinyar	Geological Survey of Iran
Mojtaba Kavianpour Sangno	Geological Survey of Iran

Contents

Table of Figures

Table of Table

Management summary

Lake Urmia, as the largest and saltiest permanent lake in Iran and one of the largest supersaturated lakes in the world, due to the problems that have occurred in recent years, lost a large volume of its water and natural reserves, and is a critical zone in environmental topics of the country. In this regard, the drying up of the lake and the emergence of more salt domes and salt sheets, caused traditional and sometimes industrial salt extraction, therefore resultant salt dust, to become important incident in this region. In this eonnexion, the present report deals with the compilation of guide lines as a framework for environmental considerations in salt extraction sites.

This report consists of two main parts. In the first part, extraction processes and the results of modelling, instruction for minimal effects of salt withdrawal is present.

The second part examines the issues and discussions related to the modelling of particle distribution resulting from extraction activities. In this connection, a hypothetical mine with a capacity of 1,250 tons per day, which is equivalent to the traffic of about 50 large trucks (18-wheel vehicle) and the emission coefficients resulting from the traffic of a three-axle truck and a dump-truck have been considered. In terms

of location, Qabadlo region (southeast of Urmia lake), and two other hypothetical extraction sites located on the coast of Urmia city (west of the lake), and near Salmas city (northern coast of Qarabagh village) are also considered. By using the CFD and ADMS models, the release of fine dusts in above mention sites was modelled. It is worth to mention that, the main activities that lead to the production of pollution include the traffic of trailers, blowing from the surface of salt piles, as well as the accumulation and extraction of salt piles. The deflation from the surface of piles by using CFD modelling and considering the related standards determined. Finally, by determining the emission coefficients for other activities according to the existing standards, together with preparing meteorological files as well as preparing the topography file of the region, modelling of particles in the mentioned three sites was done. At the end of this part, there is a checklist that must be completed by environmental expert and then send it to the environmental protection department of the province.

1- Generalities

1-1- Introduction

Lake Urmia is one of the most important and valuable water ecosystems in Iran and is known as the largest and saltiest permanent lake in Iran and one of the largest supersaturated lakes in the world, and because of its unique ecological values as an international park and wetland and because of the nature suitable for the permanent and temporary living of all kinds of rare birds of the world and the natural beauty of its coasts and islands have been introduced as a biosphere reserve by "UNESCO" in 1976 (Kelts & Shahrabi, 1986).

The catchment area of Lake Urmia with an area of about 5,801 square kilometers is located between the geographical coordinates of 44° 14' - 47° 53' E and 35° 46' - 38° 30' N. This basin is located in the northwest of Iran and is surrounded by the northern part of Zagros mountains, the southern slope of Sabalan Mountain and the northern, western and southern slopes of Sahand mountain (Shah Hosseini et al., 2003) (Figure 1).

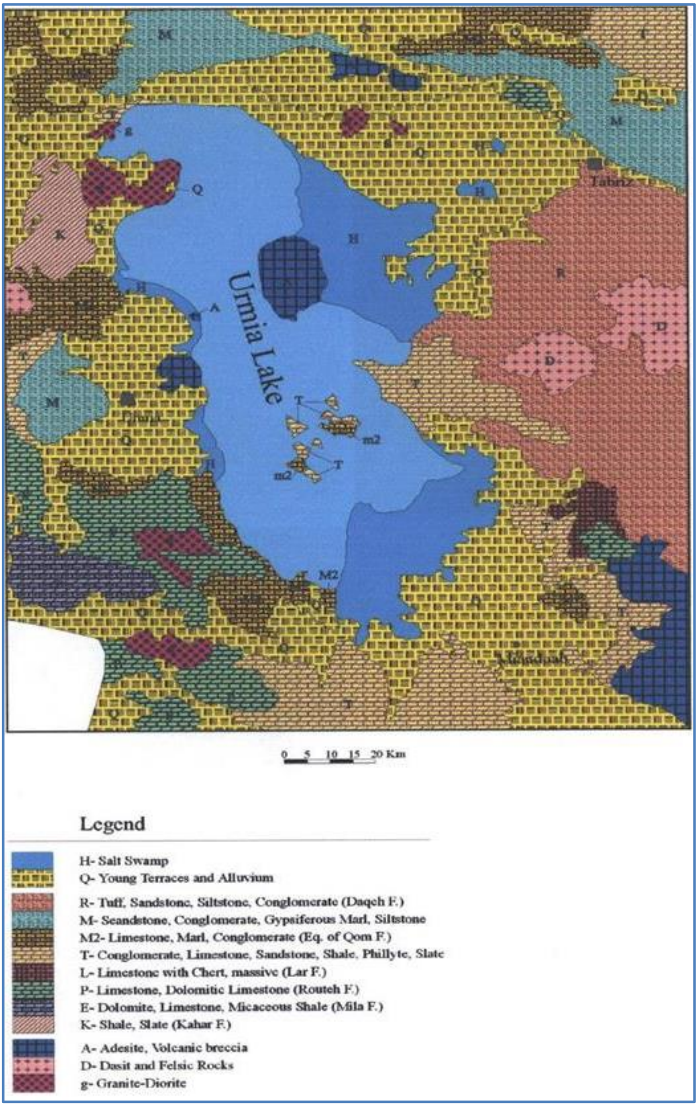

Figure 1: Geology around the lake (Shah Hosseini et al., 2003)

The most important rivers of the Urmia Basin are: Zarrineh Rud, Simineh Rud, Mahabad chai, Gadarchai, Baranduz chai, Shahr chai, Rouzeh chai, Nazlu chai, Zola chai (Permanent river) and Tasuj chai (Seasonal River) that pass through different geological formations around the lake (Darvishi Khatouni et al., 2010) (Figure 2 &Figure 3 &Figure 4).

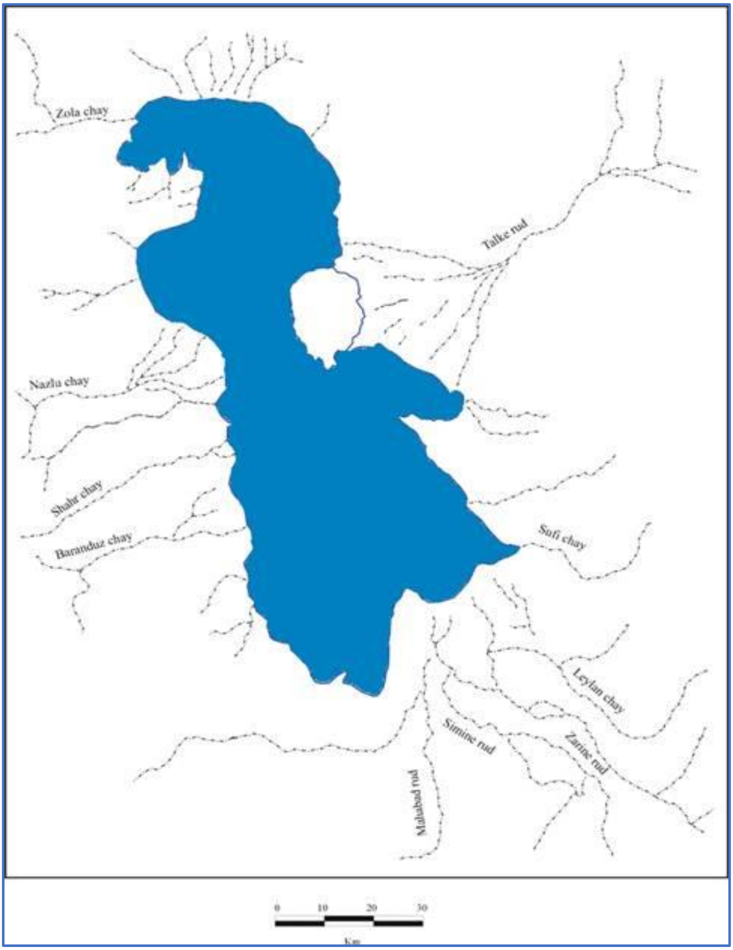

Figure 2: Important rivers of the Urmia Lake drainage basin (Darvishi Khatouni et al., 2010)

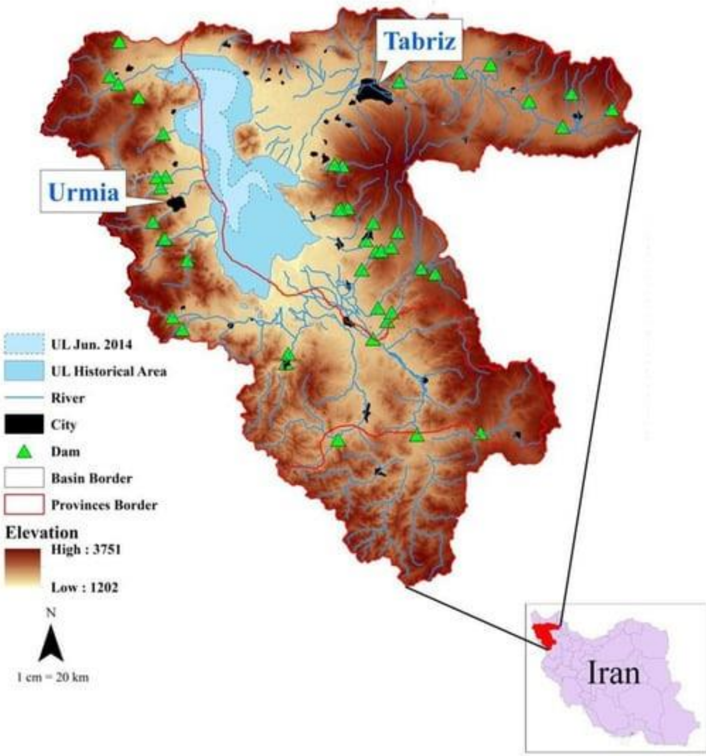

Figure 3: Urmia Lake drainage basin in northwest of Iran.

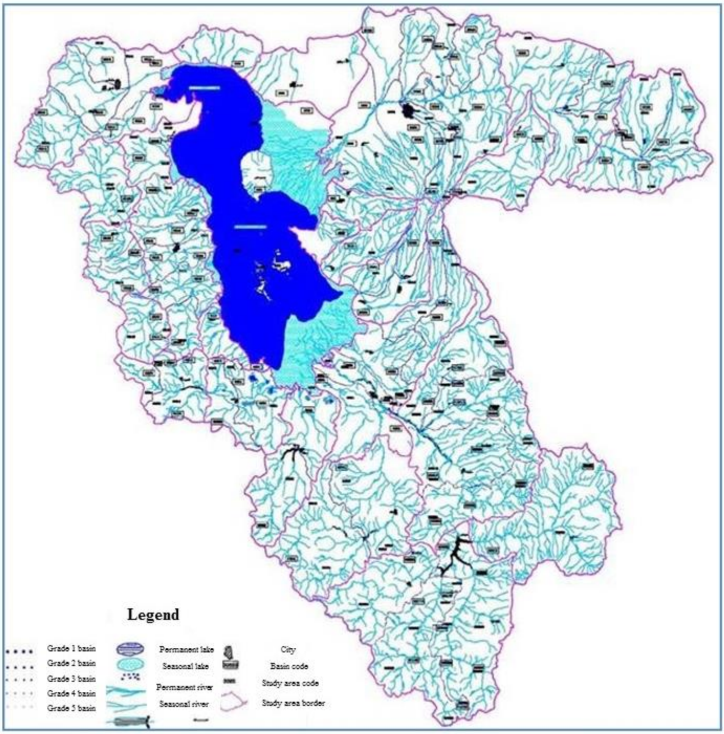

Figure 4: Urmia Lake drainage basin (Darvishi Khatouni et al., 2010).

The average amount of salt entering the lake is 2.2 million tons per year, of which 54% (1.18 million tons) is related to the Ajichai River, followed by the Zarrineh rud River, which carries 463,000 tons of salt to the lake annually. Due to the entry of the Ajichai river to the northeast of the lake and the lack of proper flow exchange by the Urmia lake causeway, the difference in the sediments between north and south of causeway is completely evident (Aghanbati, 2006).

It is worth noting that the salinity of Lake Urmia is the natural process of it becoming saltier, in other words, the annual entry of 4.6 billion cubic meters of surface flows into the lake, which contain 2.2 million tons of salts, and on the other hand, the evaporation of the same amount of fresh water from the lake causes more concentration of the remaining salts in the lake, and the process of water becoming more salty continues.

Despite high salinity, green algae such as Dundella, crustaceans like *Artemia salina* and bacteria are among the living organisms of the lake, and these organisms play an effective role in the durability of the lake and prevent its annihilation (Aghanbati, 2006) (Figure 5).

Figure 5: The difference in the type of sediments north and south of Shahid Kalantari highway (Aghanbati, 2006)

Due to the construction of several dams (such as Olavian, Sahand, Hasanlu, Shahcha, Zolu, Drik, Qala chai etc.) in recent years, as well as the increase in height of the Zarineh rud dam, the Lake Urmia, today faces a serious risk of totally dried up and annihilatation. It is worth to mention that Zarineh rud River supplies more than 50% of the lake's water, which has now reduced the water input to the lake to 7 billion cubic meters. The increase in the salinity of Urmia lake water and its reaching to supersaturation limit (more than 340 grams per liter), caused the death of birds as a result of salt deposition on their wings and feathers and their bodies, and finally the inability to move and feed, and disrupting traffic of vessels. In addition the ineffectiveness of the docks built on the shores of Sharafkhaneh, Rashkan, Golmankhaneh and Ashk and Kabodan islands, the emergence of salt marsh lands of at least 150 thousand hectares, especially in the low-lying areas around the lake and, the attachment of the nine islands of the National Park (location Breeding of important species of migratory birds as well as the protected area of wildlife) to the southern shores of the lake (appearance of the land connection of the above islands with the shores), decrease in population and non-breeding of important birds living in the lake (white pelicans and flamingos), reducing the migration of birds to the habitat of the National Urmia Lake, a sharp reduction in cyst production in conditions where the water salinity is higher than normal, are among of major problems during droughts. In the current state even Artemia of the Lake Urmia (*Artemia Urmiana*) produces cysts, but the amount of this production has also decreased drastically (Darvishi Khatouni, 2011)

As mentioned earlier construction of a 15-kilometer causeway in Urmia Lake on November 2008 resulted in the drying up of more than 80% of the distance between the two western-eastern sides of the lake. The construction of this causeway has caused the disconnection of the northern and southern half and has imposed serious changes on the hydrodynamics of the region and the ecological characteristics of the lake. This bridge has a direct effect on the lake's water circulation and has caused the unmonotonousness salinity of the lake. As a result, due to the lack of water exchange in the southern and northern parts, the water salinity has greatly increased in the northern part and has reached 300 grams per liter, and the life of *Artemia Arumiana* in this half has been severely threatened (Najafi & Najafi, 2013).

1-2- Objectives and necessity of investigation

The environmental crisis and the drying up of Lake Urmia is one of the biggest geological risks of the country especially in NW Iran. The reduction of the water level and the size of the lake, is a national and trans-regional phenomenon, and this necessitates the investigation and carrying out more research regarding the reduction of the percentage of salts the lake, preventing the wastage of water resources in the catchment area, and to protect the aquifers around the lake from further infiltration of salt water into them to prevent the generation of salt dusts in the future.

Three main goals of this research are as follows:

- Providing environmental requirements in order to minimize the negative effects of salt extraction (focusing on preventing the creation of salt dusts)

- Preparation of executive instructions for extraction salt in compliance with environmental considerations
- Obligatory instruction for contractors to comply with environmental principles in extraction

1-3- Exploitation and extraction of salt

Most of the salt in the world is soluble in ocean water between 1 and 5% and its average amount is around 3.5%. The variation in the amount of salt in the seas and oceans depend on the amount of evaporation, the percentage of ice and the amount of salt in the river waters. On the coasts of intracontinental lakes, where the rate of seawater evaporation is high, are suitable for salt extraction.

Salt is found naturally in two forms:

1) solid (rock salt)
2) Salt water (brine) which includes the second form of huge sources of salt.

As the proportion of salts in the lake water increases, different salts, which include carbonates, sulfates, chlorides, and finally potassium and magnesium salts, are deposited.

In general, there are 3 ways of exploitable brines in terms of evaporating solutes:

1) Brine Saltwater lakes or saturated lakes
2) Intercrystalline brine between crusts or salt layers
3) Salty underground water tables or salt marshes on the margined of the plains and playas

It is possible to have these three types of saline deposits and salt layers in Iran; the first example is Lake Urmia. The second type of lakes can be seen in some dry salt lakes that are spread all over Iran, such as Qom Salt Lake, Great Kavir, Gavkhuni Marsh, and Abarago playas. The 3rd type salty aquifers are spread on the margines of the plains and playas of Iran.

Commercial production of salt is usually done from 5 sources:

- Layered-sedimentary deposits
- Surface brines
- Sea waters
- Salt pans
- Salt domes

1-3-1- Extraction of salt in the world

Salt extraction in the world was done for the first time in 3000 BC in China. Real salt deposits are made by underground, room and foundation and drilling, blasting and extraction methods and are crushed before reaching to the surface. Extraction is done by dissolution method with a single well and circles for injection or two connected wells that create a large underground hole (hydraulic fracturing method).

There are three ways to recycle salt, two of which are common mining methods. The third method is the evaporation method using the energy of the sun, which can separate the salt from nature and man-made salt water. The choice of method basically depends on the type of salt deposits that are exploited and the type of climate and type of land, as well as the skill and efficiency of the technology that is available to the producers.

There are several type of methods used to extract salt. For example, in West Africa, in Capcross reserves, the evaporation method using solar energy is mainly used, but rock salt is also exploited both by vertical well drilling and dissolution methods. In vacuum salt extraction method, saltwater is turned into a series of vertical evaporators connected to each other with multiple suction pumps. Sea brines coastal ponds, evaporated by sunlight and periodically crystallized salt is extracted.

The technique of evaporating saltwater in order to obtain salt is one of the oldest methods. This method, while being old, is also the easiest. In this way, the saltwater is collected in a small lake and the heat of the sun and the action of the wind causes the water to evaporate. Therefore, the salt settles, which is easily collected.

Solar evaporation has three main conditions:

- Access to saltwater source
- Hot and dry weather
- A suitable smooth and level area for making pits that are exposed to the sun's energy.

For this reason, these places are basically limited to the coastal areas of countries with hot climate. It is worth nothing that this method can be done in other areas along the sea coast. For example, in some parts of Ethiopia, many salt springs that originate from dissolved rock salt evaporate as local salt sources. Another example is extracted from saltwater lakes in Uganda. Anyway, the best place is near the sea.

Some inappropriate methods of salt recovery technology are very common in local markets, which basically include salt recovery from coasts, sabkhas, deltas and playas.

Salt is also present in evaporating minerals, such as sylvinite, which is a combination of halite and sylvite, which is potassium chloride. Many Canadian potash mines prepare salt in this way.

The Mediterranean Sea is also an example of evaporate mineral formation basins. About 16 million years ago, the Mediterranean Sea completely dried up, depositing thick, gypsum and salt that is now exploited in southern Spain and elsewhere.

If a large volume of salt reaches to a depth of about 600 to 1000 meters, the movement of the flow starts upwards, and this is because of its lesser volume compared to the rocks above it. This movement creates a salt dome known as diaper, which is chain-like in nature and can extend for several kilometers. Oil exploration often leads to the discovery of new salt deposits (National Geoscience Database of Iran).

The coasts of Louisiana-Texas in the Gulf of Mexico in America have the highest amount of salt domes in the world. The volume of the domes can be very large and the percentage of salt purity usually varies between 90 and 99 percent. Known salt domes contain about 100 million tons of salt (National Geoscience Database of Iran).

1-3-2- Exploitation and Extraction of salt in Iran

There are many sources of halite in Iran and it has been one of the country's export goods for many years. For example, during the Qajar period, 25,000 to 30,000 tons of salt were exported from Qeshm Island.

Most of Iran's rock salt mines are open-pit and the extraction method is open-pit mining. There are only

3 rock salt mines in Iran that are extracted underground. Of these three mines, two mines are in Semnan province and one mine is in Khorasan. The extraction methods of these three mines is room and pillar method.

Halite is collected in different ways:

One of the extraction of rock layers of salt is that salt has been left in the form of sedimentary deposits from the past, such as the mines around Qom and the inner deserts of Iran, as well as the exploitation of salt domes, such as the salt domes of the Persian Gulf islands (including the mine of Hormoz and Qeshm islands) and the salt dome in Near Qom. Another method is to separate part of the water from the seas and lakes in the form of ponds and collect their salt after evaporation, such as extracting salt in the west of Lake Urmia, and also exploiting the water of springs that have a large amount of dissolved salt, such as the springs of Rudbar Alamut, Bostan, Jarquyeh in Isfahan, Bijar in Kurdistan, around Khoramabad, Shorab-e-Shahrekord, around Eshthard (Karaj) and so on.

When runnig or underground water passes through salty areas, it dissolves some salt and takes it with it. Rivers such as Talkehroud and Roudshur are among the runnig waters that carry some salt with them. Springs are among the salty underground waters that when reached to the surface of the earth, their salt will be extracted.

Karabogaz Bay in Turkmenistan contains a very high level of salinity, which has led to the production of salt formations, and this is because the entrance of the bay allows a small amount of fresh water to enter the bay, and this itself causes a small amount of water to enter the bay, and result will be deposit on salt. When salt enters the water, because it is heavier than water, it deposits at the bottom of the water. This means that the sea does not need to dry up for salt extraction.

Soil salt occurs as a surface crust in dry areas in ponds and dry lakes, which is known as Playas. This type of salt is located in the vicinity of a salt marsh or a shallow sea, where these areas are covered with a layer of salt and other evaporating minerals. The examples of this type of salt are along the coast of the Persian Gulf (National Geoscience Database of Iran).

To extract salt from the bed of salt deposits, the methods are not very different, only the use of machines and human power will be different. In the past, salt harvesting from the margins of Lake Urmia was mostly done using hand shovels. After the salt depot, the collected product was transferred to a van or a dump truck and was transported to the markets. Of course, at present, local people who have limited consumption also use this method, which is also called the traditional method.

In many salty lakes, especially in Lake Urmia, salt was not extracted from the lake bed under normal conditions. Rather, there were bays along the margin of this lake that were extracted naturally by the local people. When the lake was drained in winter and spring, the water level of the lake rose and more surface of the margin of the lake was covered by water, so the marginal ponds were filled with saltwater. After the end of the summer season and the evaporation of the water, which leads to a decrease in the height of the water, the connection of these ponds with the lake water is cut off, and finally, salt deposits are left behind, which has been the traditional method of extracting salt. This method of extraction has continued for many years when the level of the lake was in a normal state, but after the occurrence of the water shortage crisis in the lake and the continuous decrease of the level of the lake, this method is no longer possible to do it. An example of this type of extracting was the Qalgachi and Anganeh mines on the western margin of the lake and the evaporation ponds of the Kaveh Soda factory in the southeast of the lake.

During the last decade, with the regression of the lake's water and the presence of salty sediments, salt producers have been forced to go into the lake and harvest the sediments directly. In these mines, in some places, the salt is collected using human power and hand shovels, and then loaded with loaders or shovels that are attached to tractors. Also, in some salt mines, for more extraction, salt has been harvested directly from the lake bed using a loader.

While the collected salt contains a large amount of water, it is stored in the lake bed for at least one day and night, and after reducing the amount of salt water, it is loaded and transported to the places of consumption (Sajadi & Hashemian, 2001). It should have pointed out that salt have important role in drilling, tanneries, textiles, acid production and serum production, pharmaceuticals, water filtration, etc.

Also, ice factories, food producers and packaging factories, health and cosmetics factories, detergent factories, fast food factories, confectioneries, bakeries, and all kinds of canned goods are among the major users of salt.

Fisheries are also among the important consumers of salt to the extent that fishing salt, is known by this name due to the high consumption of fisheries for its disinfection (Esm Hosseini Solatifar, 2009).

To get wetting and drying of the lake causes a change in the texture of the salts of the lake bed and creates the potential for the salt to be blown by the wind and finally a salt storm. Examining the results obtained from the studies of the optical depth of the atmosphere and aerial images show that in the summer season, there is the highest level with the potential to create fine dust.

But in early autumn, despite the increase of the water level, due to the rise of the underground water level and the wetting of the salt after the rains, drying again and the wind blowing can cause the dispersion of fine dust. During the extraction of salt, the movement of loaders, bulldozers, and transportation by trucks destroys the cohesive texture of the salt deposit and turns it into a powder, which will probably cause the intensification of salt pollution. Also, removing salt from the dried bed of the lake changes the texture of the deposited salt and increases the potential of creating fine dust.

2- Pollution modelling of salt recovery

In order to investigate the environmental effects and determine the amount of pollution caused by the activities related to the recovering of salt from Lake Urmia, it is necessary to do an accurate modelling of the amount and distribution of suspended particles caused by these activities. In this regard and according to the available physical models, appropriate models should be used to provide a proper analysis of the obtained results. In order to investigate the effects of wind on air pollution, first, the manner of particle diffusion should be investigated. The transfer of particles includes three mechanisms: erosion, atmospheric dispersion and redeposition on the surface. The spreading and dispersion of dust particles will endanger human health and destroy the ecosystem.

For this purpose, it is very important to check and control the dispersion of particles. In this part, ANSYSFLUENT and ADMS software's will be used and the output of these models will be evaluated.

2-1- Pollutant generation sources

Here it is assumed that salt extraction takes place in a mine with a capacity of 1250 tons per day, which is equivalent to the traffic of about 50 eighteen-wheel trailers with an average load of 25 tons.

2-2- Trucks traffic

To determine the emission coefficient of particles from the surface of unasphalted roads, with respect to the average volume of materials that are dispersed by trucks in one day, and taking into account the average weight of the trucks that are moving, by using the following formula, the emission coefficient it is calculated for each meter of roads: (EPA, Section 13.2.2, 2006)

$$E = k\left(\frac{s}{12}\right)^{a}\left(\frac{W}{3}\right)^{b}$$

E: Emission coefficient in pounds per mile traveled

W: average weight of trucks

S: the amount of silt load on the road surface in terms of percentage

k, a, b, experimental constants according to the relevant tables.

Also based on the tables in the reference (EPA, Section 13.2.2, 2006), the following values are considered in the calculations:

k: is equal to 1.5

a: is equal to 0.9

b: is equal to 0.45

s: silt percentage equal to 10% (Arizona Department of Environmental Quality, 2004)

The following equation is used to convert the diffusion coefficient obtained from the above equation into metric units:

$$1\ lb/VMT = 281.9\ g/VKT$$

In other words, each pound per mile is equal to 281.9 grams per kilometer. The calculations related to determining the emission coefficient of particles resulting from the traffic of trailers in the assumed salt mine are given in the Table 1. Here, it is assumed that an eighteen-wheel trailer is used to transport materials, so that the weight of the trailer with the load is 40 tons and without the load is 15 tons. The average of these two values based on the frequentation of loaded and unloaded trailer is calculated as 27.5 tons. (Fariborzi Araqi & Salari, 2009)

For further comparison, two other types of transport vehicles, i.e. three-axle truck and dump truck, have also been investigated and the emission coefficient related to the traffic of these vehicles has also been calculated.

It can be seen that 18-wheel trailer to compare with two other type of vehicles has a lower emission rate.

Also, based on the type of dust control method, the obtained emission coefficient can be reduced based on the Table 2 (Department of Environmental Quality, State of Utah, 2015).

Table 1: Efficiency of control methods

checking methods	**checking method efficiency (%)**
sprinkling	70
Watering and improving the road surface	75
Use of chemical stabilizers	85

Table 2: The emission coefficient resulting from the traffic of trailers carrying salt

Type of salt transporter	Eighteen wheel trailer	Three-axle truck	Dump truck
Average weight of trucks (loaded and unloaded) (ton)	27.5	18.5	6.5
Length of roads (m)	1500	1500	1500
Amount of displaced material (tons)	1250	1250	1250
The number of traffics	50	83.3	312.5
Average number of trucks per hour	2.08	3.47	13.2
Distance of traffic per day (km)	150	250	937.5
Emission coefficient (g/VKT)	973	814	508
Emission coefficient assuming no watering (g/s/m)	0.0005628	0.0007848	0.0018381
Emission coefficient from the whole road (g/s)	0.84424	1.17718	2.75713
Emission coefficient assuming watering (g/s)	0.25327	0.35315	0.82714
Diffusion coefficient assuming the use of chemical stabilizer (g/s)	0.12664	0.17658	0.41357

2-3- Accumulation and extraction

The production of dust particles can happen in different stages of the material storage cycle, such as material spillage during pile formation and removal from the pile and unloading in the material transport vehicle. The amount of dust emission in the storage cycle of materials depends on the amount of volume of displaced materials, also parameters such as pile life, humidity level and the amount of fine particles present in the materials play an important role in the amount of particle emission.

When fresh material is added to the pile, the potential for particle emission is the highest. Fine particles are easily released into the atmosphere and are scattered around due to air flow. Adding material to or removing material from piles results in the production of airborne particles. The unloading of materials by loaders from trucks also leads to the release of particles.

The amount of particle emission produced by the above activities can be calculated from the following empirical relationship (EPA, Section: 13,2,4, 2006)

$$E = k\ (0.0016)\,\frac{\left(\frac{U}{2.2}\right)^{1.3}}{\left(\frac{M}{2}\right)^{1.4}}$$

E: emission coefficient per kilogram per ton k: particle size correction factor equal to 0.35

U: Average speed in meters per second

M: the percentage of moisture content of the materials.

It should be noted that the load of silt is also considered in the derivation of this equation, although its effect is not directly included in the equation by considering the correction factor. But it seems that the load of silt and the diffusion coefficient are related to each other, however based on the following table's, no significant relationship can be seen between them.

Amount of displaced material per day (ton)	Average speed m/s	relative humidity %	emission factor Kg/ton	Emission coefficient g/s
1250	2.21	0.4 - 22.8	0.00282	0.0815

Also, according to the Australian Government, NPi, (2012), the value obtained from the above relationship should be increased by 5 to 10 times in order to comply with the experimental values.

2-4- Piles of salt accumulation

The distribution of particles depends on many environmental factors, among which the following can be mentioned

1) Wind speed and direction

Wind speed is the most important factor in the amount of deflation. The analyzes are based on the highest speed measured at the meteorological station. The wind direction is also one of the effective factors in the amount of deflation.

2) Accumulation particles method

There are different ways to accumulate particles for storage. But in most industrial applications, two accumulation methods are used that is, conical and linear (Figure 6 &Figure 7 &Figure 8).

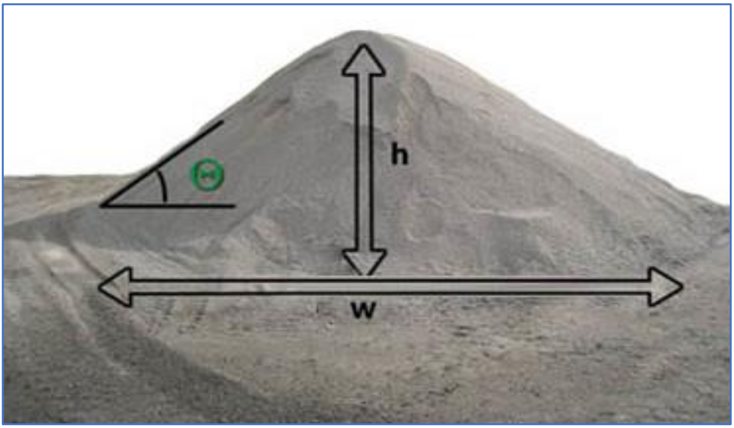

Figure 6: Conical pile dimensions

In the Figure 6, *h* is the height of the pile and *W* is the width of the maximum cross-section of the pile and θ is the angle of the external surface of the pile with the horizon.

Linear piles require special equipment's for storage and removal. In some cases, obstacles are created around the pile to reduce deflation. Also, in cases where there is a need to protect the accumulated materials against cold or moisture, covers can be used for protection.

Figure 7: How to accumulate linearly

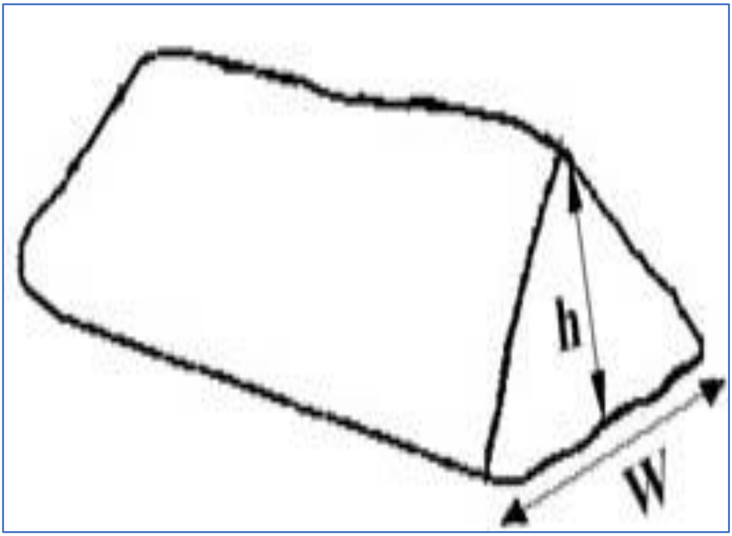

Figure 8: Linear pile dimensions

3) How to arrange the piles against the wind

There are different arrangements for placing the piles against the wind, and it is important to know which arrangement will have the least amount of deflation?

4) The size of the accumulated particles

The size and density of the particles and grain uniformity of the accumulated particles have an effect on the amount of threshold friction velocity of salt particles, which has a direct effect on the number of particles removed from the pile. The greater the relative roughness of the accumulated salt, cause more disturbances and the greater the scattering of particles.

5) The size of the barrier and how the barrier is positioned against the wind

Barrier can prevent pile erosion to a large extent. The dimensions of this barrier should be determined based on the executive decision and consumptive use.

6) The amount of surface of the pile that is against the wind

The surface of the pile that is against the wind is important for deflation factor. The lower this level is, the less deflation.

7) Velocity profile near the ground surface

The velocity near the ground surface is not uniform and has severe gradients. The speed and gradients are determined by natural roughness such as mountains, valleys and vegetation and unnatural roughness such as buildings, etc.

8) Moisture of accumulated particles

Humidity is one of the factors to reduce the erosion of materials. In some areas, in order to prevent pollution caused by the spreading of particles on the piles, liquids are used for stabilization.

2-4-1- Empirical approach for particle emission rate

For the experimental investigation of pollution and special manner of particles distribution, new parameters must be defined first (Yaping, 2000).

Threshold friction speed:

Threshold friction speed is the lowest value of the speed at which the accumulated particles are stable and do not move at all. This speed is determined based on the density, relative roughness and size of the particles. To determine the threshold friction speed, a material testing laboratory and accurate equipment's are needed. But it is possible to use approximately the available tables and relationships to obtain the threshold friction speed. The Figure 10 & Figure 11 shows two of the most famous models related to the threshold frictional speed. In these models, the threshold friction speed is only dependent on the particle size. Bagnold's the model is a linear model that introduced in 1941, and based on the theory, that the larger the particle size, the higher the threshold friction speed. Bagnold's model is far from reality, that's why Greely and Iverson (1985) introduced a new model. The Greeley and Iverson model is based on the forces between particles and the forces applied by the fluid flow. According to this model, the value of threshold friction speed is equal to:

$$u_t^* = A_1 \sqrt{\sigma_p g d}\, F(Re_t^*) G(d)$$

A_1 is a constant based on Reynolds friction threshold ***Re_t*****, ***σ_p*** is the ratio of the substance density of the under investigation to the density of the fluid that causes deflection (air). ***g*** is the value of the standard acceleration of the earth's gravity in the universal system and is equal to 9.815, ***F*** is the Reynolds threshold friction function and ***G(d)*** is a function of particle diameter and relative density. The values of these parameters are shown in the following table's.

Re_t^*	A_1	$F(Re_t^*)$
$0.03 \le Re_t^* \le 0.3$	0.2	$(1+2.5\ Re_t^*)^{-1/2}$
$0.\ 3 \le Re_t^* \le 10$	0.13	$(1.928\ Re_t^{0.09} - 1)^{-1/2}$
$Re_t^* \ge 10$	0.12	$1 - 0.0858\exp[-0.0617(Re_t^* - 10)]$

The value of ***G(d)*** can be obtained from the following equation:

$$G(d) = (1 + 0.006 / \rho_a g d^{2.5})^{1.2}$$

Of course, by replacing the density (1.229 kilograms per cubic meter) and the gravity constant, the value of ***G(d)*** can be obtained from the Figure 9.

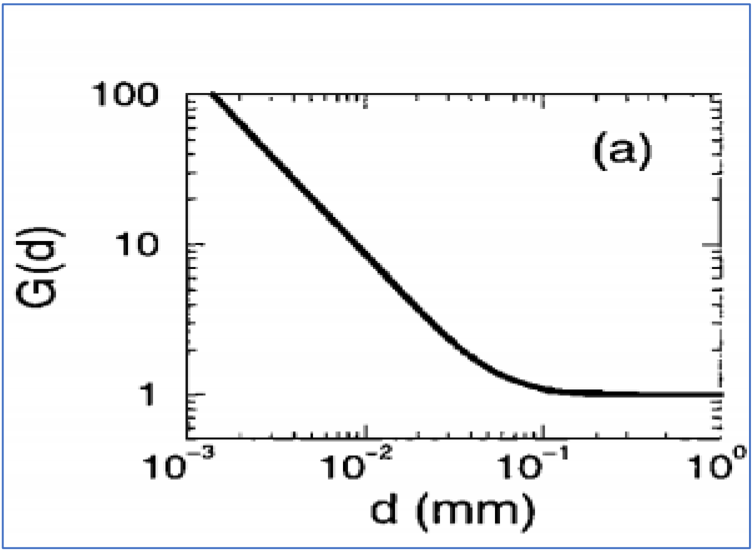

Figure 9: The value of G function as a function of particle diameter

Also, the following diagram (Figure 10) is suggested for the *F* function:

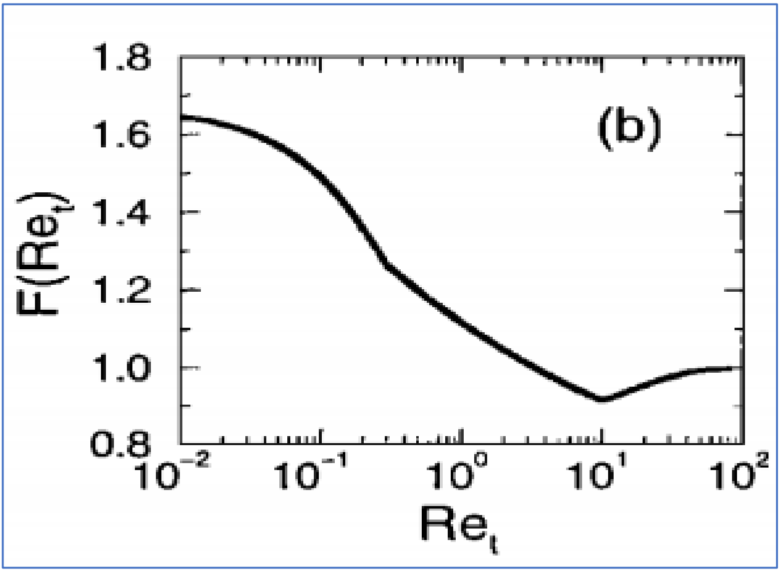

Figure 10: The value of F function according to the threshold friction Reynolds number function

According to this theory, particles with a diameter of approximately 75 micrometers have the lowest threshold frictional speed. However, in the size of more than 200 micrometers, the two models will be conforming.

On the basis of the above relationships, the value of the threshold friction speed can be obtained (Figure 11)

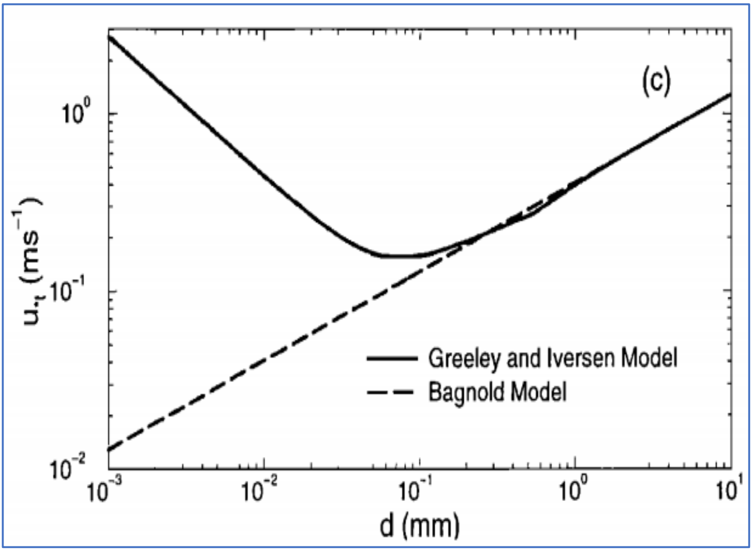

Figure 11: Frictional speed value according to particle diameter

$$\rho_{salt} = 2170\ kg/m^3 \qquad \rho_p = \frac{\rho_{salt}}{\rho_{air}} = 1765.66 \qquad d = 100\ \mu m$$

$$Re_t^* = \frac{\rho u d}{\mu} = 68.17 \quad 1 - 0.0858 \exp[-0.0617(Re_t^* - 10)] = 0.9976 \qquad A = 0.12$$

$$G(d) = (1 + 0.006 / \rho_a g d^{2.5})^{1.2} = 1.01$$

Therefore, the value of the frictional speed is equal to:

$$u_t^* = A_1 \sqrt{\sigma_p g d}\, F(Re_t^*) G(d) = 0.1591 \quad m/s$$

After obtaining $\boldsymbol{u_t^*}$, the velocities $\boldsymbol{u_{10}^+}$ and ratios $\frac{\boldsymbol{u_s}}{\boldsymbol{u_r}}$ must be extracted to calculate $\boldsymbol{u^*}$.

$\boldsymbol{u_{10}^+}$ is the speed at a distance of 10 meters from the ground surface. If we have the velocity at another distance from the earth's surface, we can convert it to $\boldsymbol{u_{10}^+}$ with the following equation:

$$u_{10}^+ = u^+ \frac{ln(10.0 / 0.005)}{ln(z / 0.005)}$$

Where $\boldsymbol{z}$ is the speed at a distance of 10 m from the ground surface. Considering that in meteorological stations, the speed is measured at a distance of 10 meters, there is no need to use the above relationship. According to (EPA Section 13.2.5, 2006), all points of the pile are not exposed in the same extent to the wind, and in some points on the pile wind speed is higher, so the deflation is naturally higher in those places. For example, a conical pile is shown in the Figure 12 & Figure 13. The Figure 13 is the result of modelling and the Figure 12 is based on the EPA Section 13,2,5, (2006).

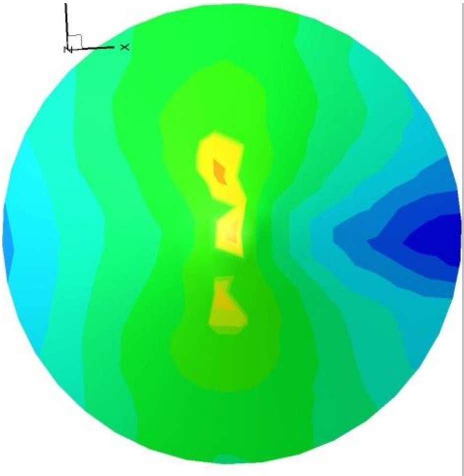

Figure 12: Velocity contour on pile based on top view

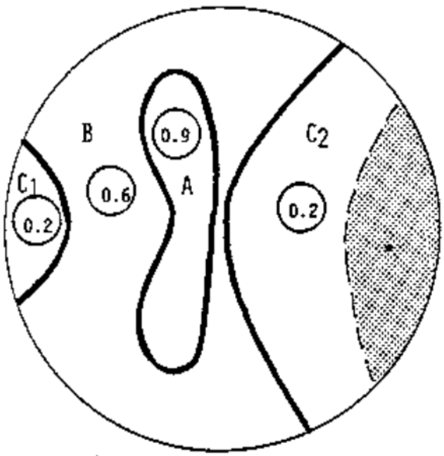

Figure 13: $\frac{u_s}{u_r}$ velocity contour at different points of the pile

As it is clear from Figure 12 & Figure 13, in most of the points of the pile, the ratio of $\frac{u_s}{u_r}$ is between 0.2 and 0.6, and in a small part that is mainly located in the highest part of the pile, the amount of $\frac{u_s}{u_r}$ reaches 0.9. In Table 3, the value of $\frac{u_s}{u_r}$ is based on the geometry of pile and wide direction.

Table 3: $\frac{u_s}{u_r}$ value based on pile geometry and wind direction

Pile shape	Area name	Portion of the total area (%)	Amount of $\frac{u_s}{u_r}$
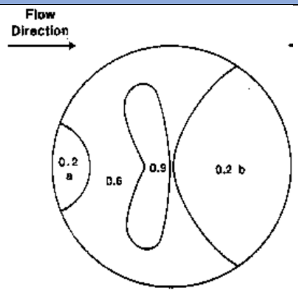 Pile A	0.2 a	5	0.2
	0.2 b	35	0.2
	0.2 c	0	0.2
	0.6 a	48	0.6
	0.6 b	0	0.6
	0.9	12	0.9
	1.1	0	1.1
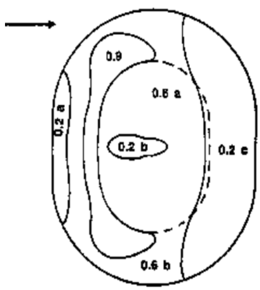 Pile B1	0.2 a	5	0.2
	0.2 b	2	0.2
	0.2 c	29	0.2
	0.6 a	26	0.6
	0.6 b	24	0.6
	0.9	14	0.9
	1.1	0	1.1

<table>
<tr><td rowspan="7">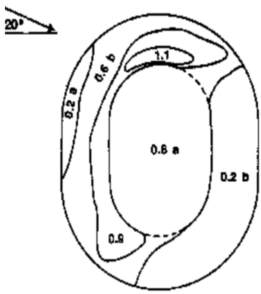Pile B2</td><td>0.2 a</td><td>2</td><td>0.2</td></tr>
<tr><td>0.2 b</td><td>28</td><td>0.2</td></tr>
<tr><td>0.2 c</td><td>0</td><td>0.2</td></tr>
<tr><td>0.6 a</td><td>29</td><td>0.6</td></tr>
<tr><td>0.6 b</td><td>22</td><td>0.6</td></tr>
<tr><td>0.9</td><td>15</td><td>0.9</td></tr>
<tr><td>1.1</td><td>3</td><td>1.1</td></tr>
<tr><td colspan="4"></td></tr>
<tr><td rowspan="7">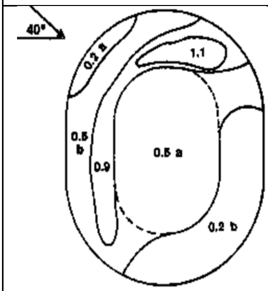Pile B3</td><td>0.2 a</td><td>3</td><td>0.2</td></tr>
<tr><td>0.2 b</td><td>25</td><td>0.2</td></tr>
<tr><td>0.2 c</td><td>0</td><td>0.2</td></tr>
<tr><td>0.6 a</td><td>28</td><td>0.6</td></tr>
<tr><td>0.6 b</td><td>26</td><td>0.6</td></tr>
<tr><td>0.9</td><td>14</td><td>0.9</td></tr>
<tr><td>1.1</td><td>4</td><td>1.1</td></tr>
<tr><td colspan="4"></td></tr>
</table>

For example, in the case of last line of Table 3, it can be said that if the shape of the pile is linear and the wind blows at an angle of 40 degrees to the pile, then 4% of the outer surface of the pile is exposed to the wind with a ratio of $\frac{u_s}{u_r} = 1.1$. The outer area of the conical pile is calculated from the following equation.

$$A_s = \pi r \sqrt{r^2 + h^2}$$

In order to compare the different types of piles, the equivalent volume should be modelled in different forms against the wind flow, and in each of the methods, that the amount of mass displaced by the wind is less, that form is more optimal. In this regard, we consider four different forms: (Figure 14).

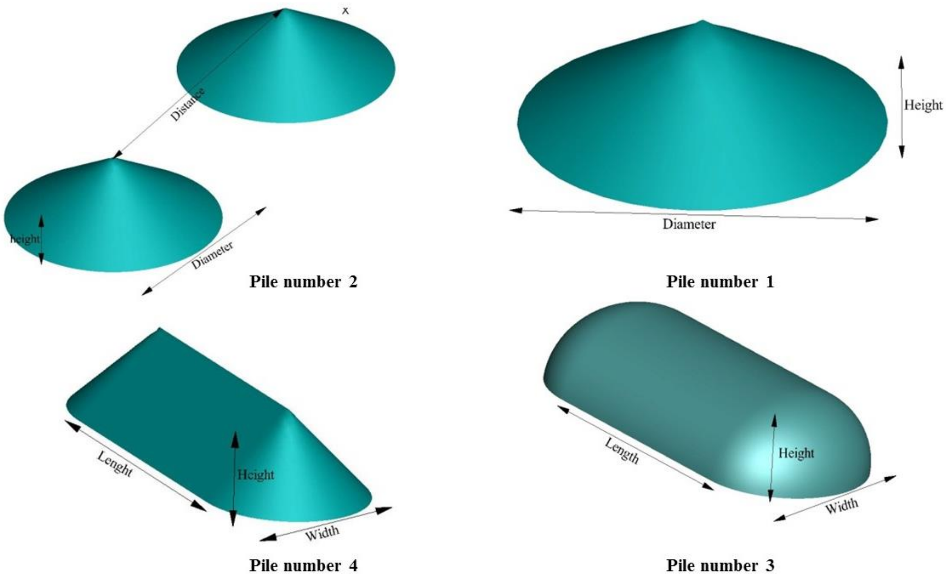

Figure 14: Shape of the studied piles

1) A conical pile with a capacity of 181.4 tons of salt, the diameter and height of this pile are 11.99 and 3.81 meters, respectively.
2) Two conical-shaped piles, each of which has a capacity of 90.7 tons. The diameter of the pile is 9.5 meters and its height is 3.05 meters.
3) A linear pile with a capacity of 181.4 tons. The length of the pile is 7 meters, the diameter of the pile is 6.7 meters, with a height of about 2.55 meters.
4) A linear pile whose upper surface is triangular instead of circular. The capacity of this pile is also 181.4 tons. Outer surface area of different piles is given in Table 4.

Table 4: External surface area of investigated piles

Pile number	**1**	**2**	**3**	**4**
External area (m^2)	133.78	168.47	115.62	138.16

In Table 5, the amount of area corresponding to different ratios of $\frac{u_s}{u_r}$ for all four types of piles is shown.

Table 5: Area corresponding to different $\frac{u_s}{u_r}$ ratios for piles

Pile number	$\frac{u_s}{u_r} = 0.2$	$\frac{u_s}{u_r} = 0.6$	$\frac{u_s}{u_r} = 0.9$	$\frac{u_s}{u_r} = 1.1$	**The total area of different areas (m^2)**
1	53.51	64.21	16.05	0.0	133.78
2	67.38	80.86	20.21	0.0	168.47
3	41.62	57.81	16.18	0.0	115.62
4	49.73	69.08	19.34	0.0	138.16

According to Table 4 &Table 5, it can be seen that the outer surface of conical piles is more, but on the other hand, there are areas in linear piles where the speed is high, while these areas are less in linear piles. It is possible to compare the dispersion and pollution of these piles by numerical fluids methods.

Now we can calculate the value of $\boldsymbol{u_s}^{+}$ using the following relationship. Also, based on the meteorological information, the rate of $\boldsymbol{u_{10}}^{+}$ is around 11 meters per second.

$$u_s^+ = \frac{u_s}{u_r}\, u_{10}^+$$

Then, the following relationship can be used to obtain the friction speed in each sub-region.

$$u^* = \frac{0.4\, u_s^+}{\frac{25}{\ln 0.5}} = 0.1\, u_s^+$$

In the next step, the deflation potential that is $\boldsymbol{P}$, must be calculated, and value of this variable is equal to:

$$P = 58\,(u^* - u_t^*)^2 + 25\,(u^* - u_t^*)$$

Table 6 showing the calculation of frictional speed and deflation potential

Table 6: Calculation of frictional speed and wind potential

$\boldsymbol{u^* = 0.1u_s^+ (\frac{m}{s})}$			
$\boldsymbol{\frac{u_s}{u_r} = 0.2}$	$\boldsymbol{\frac{u_s}{u_r} = 0.6}$	$\boldsymbol{\frac{u_s}{u_r} = 0.9}$	$\boldsymbol{\frac{u_s}{u_r} = 1.1}$
0.22	0.66	0.99	1.21
1.73	27.07	60.81	90.32

No movement occurs at frictional speeds lower than the threshold frictional speed. But at higher speeds, some salt particles will move. If we multiply the value of P by its corresponding level, then the total amount of pollution produced by the deflation will be obtained (Table 7).

Table 7: Calculation of the amount of wind diffusion coefficient

Pile number	$\frac{u_s}{u_r} = 0.2$	$\frac{u_s}{u_r} = 0.6$	$\frac{u_s}{u_r} = 0.9$	$\frac{u_s}{u_r} = 1.1$	**Total (gr)**
1	92.57	1738.16	976.00	0.0	2806.73
2	116.56	2188.88	1228.98	0.0	3534.41
3	72.00	1564.91	983.90	0.0	2620.81
4	86.03	1870.13	1176.06	0.0	3132.22

Based on the Table 7, it can be seen that linear piles totally produce less pollution in total. Also, if the top surface of the pile is closer to the circle form, then the surface exposed to wind will decrease and as a result, the amount of deflation will be less.

Considering the above instances, $\frac{u_s}{u_r}$ values have been investigated by changing the wind direction from perpendicular to the pile to a state with different angles, and taking into account the equations related to the frictional speed and the threshold frictional speed, as well as the calculations related to the wind blowing potential, it can be concluded that any amount of wind blowing on the pile from vertical to parallel, the amount of deflation and as a result the pollution caused by the emission of particles is reduced. It is worth mentioning that in general, it is not possible to consider a direction where the winds of that area are always parallel to the desired pile, but by taking into account the dominant and semi-dominant wind direction, one can choose a direction for the pile that has the least deviation from the different winds during the day and night. By considering different shapes of piles (four types of arrangement) and also by considering the calculations made in Table 7, it can be seen that the more piles are accumulated, the amount of deflation will decrease. For example, it instead of two conical pile if a larger conical pile is used, the amount of particles emitted from the surface of the pile will be less. Also, if the materials are piled in a linear way so the amount of deflation will reach its lowest value. It is also worth noting that the creation of sharp corners in pile increasing the amount of deflation. Therefore, the extraction area should have the smallest dimensions in the direction of the prevailing wind.

2-4-2. CFD dynamic fluids analysis

For analysis with the help of computational fluid dynamics software, gridding must be done on the entire geometry. This type of gridding is very important and can reduce the analysis time and greatly increase the accuracy of the solution. A good network refers to a network that fosses the following two features at the same time:

1) At the points where the changes of the problem variables are large, the grid should be finer so that it can record all the changes of the problem well.
2) It is preferable that the lines of the grid both inside and in the surfaces of the grid to be perpendicular to each other. In this case, the errors are reduced by smoothness.

In places where the geometry is irregular, regular gridding cannot be used and we must use triangular elements. There are different methods for problem gridding algorithm. In these problems, the Delaware algorithm has been used. The advantage of using the Delaware algorithm is that it reduces the number of networks compared to other methods (Figure 15 & Figure 16 & Figure 17 & Figure 18).

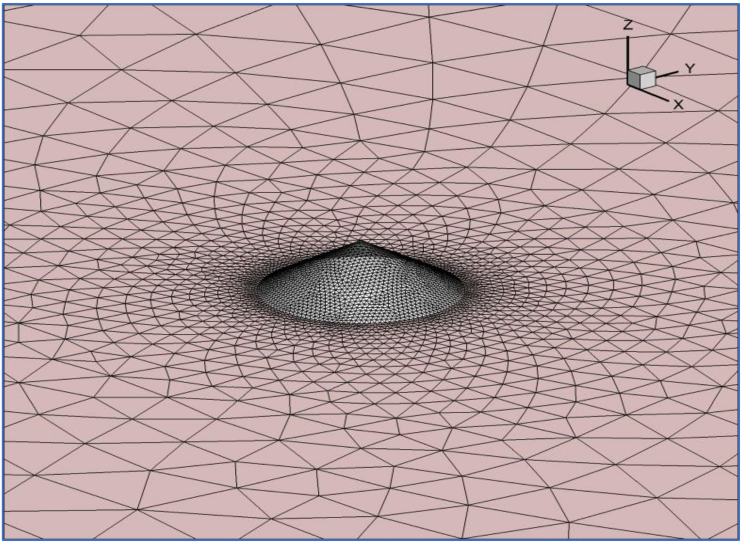

Figure 15: Gridding around pile number 1

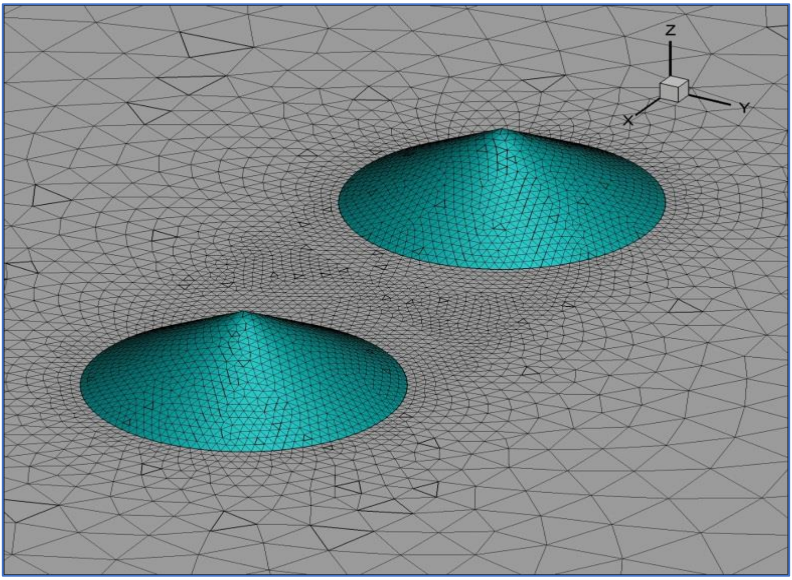

Figure 16: Gridding around pile number 2

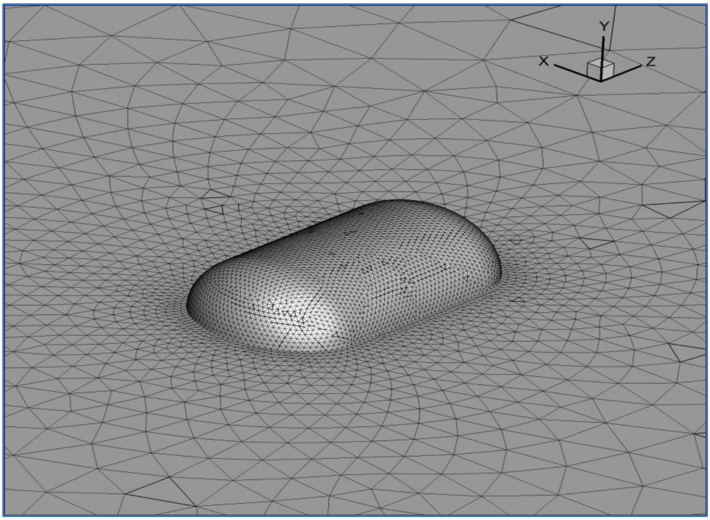

Figure 17: Gridding around pile number 3

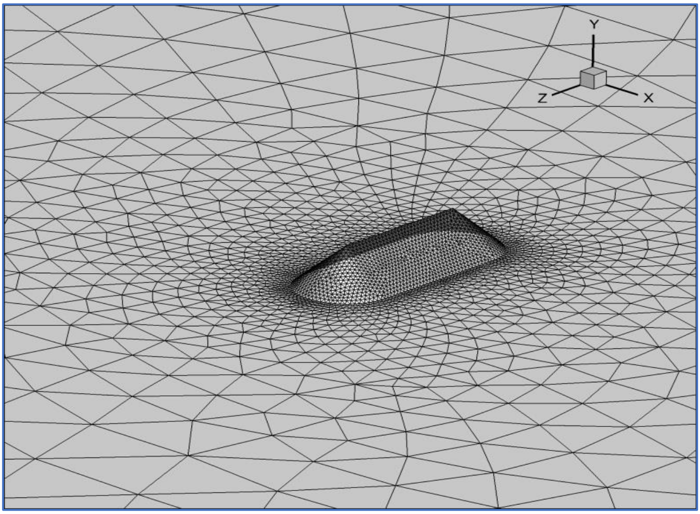

Figure 18: Gridding around pile number 4

In the gridding of the above geometries, it has been tried to make the smaller gridding around the pile wall in order to model the main factor of deflation, correctly. For the upper and side walls, square grids, and for the lower wall, triangular elements have been used. The gridding inside the geometry is done by quadrilateral and hybrid elements. The quality of gridding has been checked by Gambit software for all geometries and the skewness value and the aspect ratio are suitable for most of the cells (Table 8).

Table 8: The number of cells in the modelling network

Pile number	1	2	3	4
The number of cells	42472	63682	66745	49379

After gridding the geometry, we need to set the solution parameters, which include boundary conditions, initial conditions, solvent type, discretization order, turbulence model, solvent accuracy, etc.

The boundary conditions of the problem are assigned for all geometries based on Figure 19. Also, the dimensions of the solution domain are also shown in Figure 19. These dimensions should be chosen in a way that has the least impact on the flow. Of course, increasing details too much also increases the computational cost and processor time, which is not desirable.

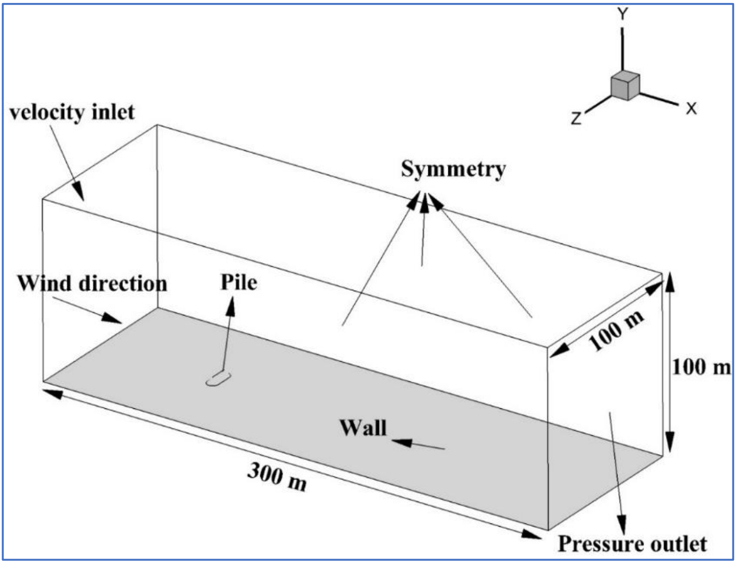

Figure 19: Boundary conditions used to solve the problem

The problem is defined as stable and invariant with time. Because the velocity in the solution field is much lower than 0.3 Mach, and there is no need to consider the variable density. For turbulence modelling, there are different models, each of which has a specific application based on the type of geometry.

Turbulent flow [Wilcox, Turbulence Modelling for CFD]

This flow has a very random and disorganized behavior. In this flow, due to intense mixing processes, (except in the areas very close to the wall), the shape of the flow layers is not easily recognizable and the fluid molecules do not follow a specific path. In other words, turbulent flow is a type of fluid flow in which the fluid is subjected to flow fluctuations and intense mixing processes. This behavior is contrary to the behavior of smooth flow in which the fluid flow moves under certain layers and paths. In a turbulent flow, the measure of the velocity at any point is constantly, both in magnitude and in the direction of motion under fluctuation and variation, so that the detection of the position of each particle within the field of flow and also at every moment is difficult.

The same situation of permanent and unspecified fluctuations in the speed can be seen in the pressure, temperature and density of any point. Of course, the measure of density fluctuations is only observed in compressible flows or flows involved in free displacement heat transfer.

The turbulent flow of a roaring river or turbulent wind currents are clear examples of turbulent flows, although the average velocity may be low in these flows. Most of the flows that we deal with in engineering problems are considered turbulent flows, except for flows with very small Reynolds numbers, or flows very close to the edge of objects, or layers very close to the solid surfaces of objects, or fluids with high viscosity. In general, characteristics of a turbulent are as follow:

1) spatio-temporal irregularity;
2) spatial and temporal continuous spectrum;
3) high Reynolds numbers;
4) Increased decay of energy and size of movement;
5) Mixing and increased heat transfer and increased shell drag coefficient;
6) Being three-dimensional even in flows that are apparently two-dimensional;
7) Dominant rotational movements;
8) Periodicity

Direct examination of disturbance:

If we want to examine the turbulence completely, we must make the grid fine enough to be able to examine all the vortices and eddies. This work is not possible in practice because, despite this number of networks, the calculation time for an advanced home computer needs at least 15 years. This method is called direct numerical simulation and is possible through supercomputers. For this reason, the importance of turbulence modelling becomes clear.

Turbulence modelling:

Dominant equations:

In order to investigate the flow field on the pile, since the type of flow is turbulent flow, time-dependent Navier-Stokes equations must be solved. But for the simplicity of solving the equations, the time averaged equations are solved first and then the turbulence equations are added to them. Then all these equations are solved together. Momentum and mass conservation equations are as follows:

$$\frac{\partial \rho}{\partial t} + \frac{\partial}{\partial x_i}(\rho u_i) = 0 \cdot 0$$

The above equation is the continuity equation. x_i are the dimensional parameters of the question, also because the problem is incompressible, the above equation becomes as follows:

$$\frac{\partial}{\partial x_i}\,(u_i) = 0 \cdot 0$$

The second equation that is discussed in all fluid problems is the momentum equation:

$$\frac{\partial}{\partial t}\left(\rho u_i + \frac{\partial}{\partial x_i}\,(\rho u_i u_j)\right) = -\frac{\partial p}{\partial x_i} + \frac{\partial \tau_{ij}}{\partial x_i}$$

In the above equations, ρ is fluid density, u_i is the velocity component in the x_i direction and τ_{ij} is the shear stress in the xy plane.

Time-averaged Navier-Stokes equations

Navier-Stokes equations are actually an important part of hydrodynamic equations to describe the velocity in the flow field. Of course, the continuity equation is also very fundamental for satisfying the continuity in the flow field. Navier-Stokes equations and its different components in tensor form are explained first. These equations are the result of force balance based on Newton's second law. The velocity field at a point of turbulent flow is usually as follows (Figure 20).

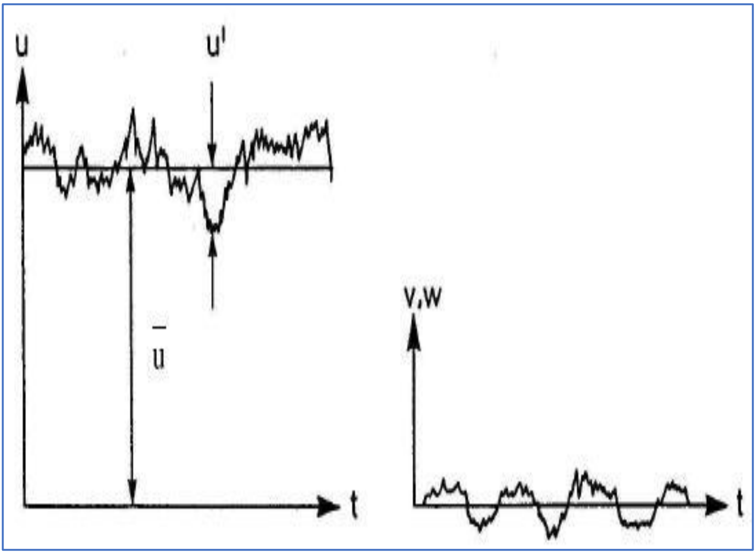

Figure 20: Velocity value at a specific point of the velocity field

The flow is always unstable because the velocity inside the field never has a specific value and change every moment. But the turbulent flow can be considered constant, that is, approximately these speed values will be repeated. But in processes that are accompanied by disturbances, stability means that the amount of disturbance production is equal to the amount of overthrow. In order to simplify the momentum equation, the first speed will be divided into two oscillating and non-oscillating parts, which is shown in the Figure 20, and then averaging on the equation.

This method is called Reynolds averaging, which is the basis of almost all turbulence equations.

$$U = u + \overline{U}$$

After replacing the speed with an average and oscillatory value and applying averaging on the equations, we get the following relationship:

$$\frac{\partial \overline{U}}{\partial t} + \overline{U}_j \frac{\partial \overline{U}}{\partial x_j} = \frac{1}{\rho} \frac{\partial}{\partial x_j} \left(-P\delta_{ij} - \rho \overline{u_i u_j}\right)$$

In the above equation, $\boldsymbol{\delta_{ij}}$ is known as Kronecker's delta, which is the same as the matrix, and all members of the main diameter are equal to 1 and the rest of the members are zero.

Relations to find the velocity dependence:

To have a look at the above equation, we will notice that all the terms except $\overline{u_i u_j}$ are known. This term is known as the velocity dependence, which is the main factor in creating disturbances, and the main purpose of modelling is to obtain this value. However, other equations such as energy and concentration equations, etc., other correlations such as velocity-temperature correlation, pressure-velocity correlation, and velocity-concentration dependence is obtained, which is the main goal of modelling, but since we do not need the equation of energy and concentration in the salt pile modelling, the only existing correlation will be $\overline{u_i u_j}$.

There are various relationships to determine the value of this term. Some of these relationships are as follow:

Buzinsk relationship:

This equation is the main relationship for determining $\overline{u_\iota u_J}$ and is expressed as follows**:**

$$\overline{u_\iota u_J} = -v_t \left(\frac{\partial v_i}{\partial x_j} + \frac{\partial u_j}{\partial x_i}\right) - \frac{2}{3} k\delta_{ij}$$

V_t is the value of turbulent viscosity, which is obtained based on the modeling method. By inserting and rewriting the equation, we have:

$$\frac{\partial \overline{U}}{\partial t} + \overline{U_J} \frac{\partial \overline{U}}{\partial x_i} = \frac{1}{\rho} \frac{\partial}{\partial x_i} \left(-p\delta_{ij} + \rho v_t \left(\frac{\partial v_i}{\partial x_j} + \frac{\partial u_j}{\partial x_i}\right) + \frac{2}{3} \rho k\delta\right)$$

The goal of modelling is to find the value of V_t, and then by putting the value of V_t[1] in the Buzinsk equation, the velocity correlation value is obtained. The characteristic of the simplicity of the relation is easy to apply it to all equations. The main problem of this relationship is in the modelling of strongly rotating flows.

Speziale **relationship:**

This model was presented by a German scientist and has the ability to solve non-isotropic flows. Non-isotropic flows are flows that do not have the same value in different directions at a point of disturbance.

$$-\rho\overline{u_i u_j} = 2\mu_t S_{ij} - \frac{2}{3}\rho k\delta_{ij} + 4C_{sp}C\mu\frac{k}{\varepsilon}\mu_t[S_{ik}S_{kj} + \bar{S}_{ij} - \frac{1}{3}(S_{mn}S_{mn} + \bar{S}_{mn})\delta_{ij}]$$

C and C_{sp} are two specific constants, *k* is the kinematic energy of the flow, ε is the value of the flow overthrow, and $\boldsymbol{\bar{S}_{ij}}$ is defined as follows:

$$\bar{S}_{ij} = -\frac{\partial u_i}{\partial x_k}S_{kj} - -\frac{\partial u_j}{\partial x_k}S_{ki}$$

The main weakness of speziale relation is in predicting secondary flows. They are secondary currents that are created due to non-isotropic stresses in the sections of Poiseville currents. One of the examples of this type of flow is the flow due to pressure difference in circular sections.

Launder relationship

This relation is a very complex relation that has the ability to solve eddy and non-isotropic flows completely, but it takes a long time. While the equations of this method are very long therefore, are beyond the scope of this topic.

After equating the velocity correlations with the flow parameters, it is necessary to find the value of turbulent viscosity or V_t. Various models have been introduced for this purpose. Each of these equations solves a number of equations to obtain the value of V_t. For example, the $k - \varepsilon$ model solves two equations to obtain the turbulent viscosity, therefore it is a two-equation model (Table 9).

Table 9: Modelling base on Reynolds Average Navier-Stokes

<table>
<tr><th>Basic relations</th><th colspan="3">Models based on Eddy viscosity (Vt)</th><th colspan="3">More accurate methods</th></tr>
<tr><td>Buzinsk</td><td>Zero equation</td><td>One equation</td><td>Two equation</td><td rowspan="4">Large eddy simulation</td><td rowspan="4">Reynolds stress modelling</td><td rowspan="4">Direct Numerical simulation</td></tr>
<tr><td>Speziale</td><td rowspan="3">Mixing length and algebraic models</td><td>Sparat Almaras</td><td>k - ε</td></tr>
<tr><td rowspan="2">Launder</td><td>Baldwin & Lomax</td><td>k - ω</td></tr>
<tr><td>k</td><td>SST k - ω</td></tr>
</table>

Accordingly, the smaller the grid and the number of solved equations, the higher the accuracy of turbulence modelling.

<u>Wilcox disturbance model k-ω:</u>

The general mode of *k-ω* models uses the turbulence frequency *ω* instead of the viscous decay rate

ε to specify the turbulence. Such models are more related to *k*-ε model. In *Wilcox k*-ω model, relation between longitudinal and velocity disturbance, that is, δt and μ_t with k (kinematic energy) and disturbance frequency ω are established as follows:

$$\delta_t \propto \frac{\sqrt{k}}{\omega}$$

$$u_t \propto \sqrt{k}$$

The disturbance frequency ω can be related to the values of k and ω by the expression $\omega = \varepsilon k$. In the mentioned relationship, ε represents the dissipation of turbulence and the viscosity of turbulence μ_t is obtained by the following equation:

$$\mu_t = C_\mu \rho \frac{k}{\omega}$$

The transfer equations for k and ω in *Wilcox* model are as follows:

$$\rho \frac{\partial k}{\partial t} + \rho u_j k_j = [\mu + \frac{\mu_t}{\sigma_k} k_j]_j + G + B - \rho \omega k$$

$$\rho \frac{\partial \omega}{\partial t} + \rho u_j \omega_j = [\mu + \frac{\mu_t}{\sigma_\varepsilon} \omega_j]_j + C_1 \frac{\omega}{k} G + C_1(1 - C_3) \frac{\omega}{k} B - C_2 \rho \omega^2$$

In the above equations *r* = density, *k* = kinematic energy, time, μ_j = velocity component, *G* = shear generation, *B* = Buoyancy wastage. Generation coefficiency of *Wilcox* model can be determined by using Table 10.

Table 10: Wilcox model disturbance coefficients

σ_k	σ_ε	C_μ	C_1	C_2
2	2	0.09	0.555	0.8333

Characteristics of Wilcox model k-ω:

The *Wilcox k-ω* model performs better than the standard *k-Ɛ* model in flows that include deceleration and separation due to reverse pressure gradient. Since k-Ɛ models belong to the category of Reynolds models (that is, they provide good results only in regions with high Reynolds number), in order to solve the equations in the regions near the wall, which are locally considered as regions with low Reynolds number, encounter with many problems. But the *Wilcox k-ω* model can be used to predict the changes of turbulent variables up to the edge of solid walls (and of course by using dense elements near the wall).

The *Wilcox* model that predicts the values for the dispersion rate of free shear flows, is in close agreement with the measured values for distant eddies, mixing layers, planar, circular and radial directions, and therefore, this model can be used for wall-enclosed flows and to some extent for free shear flows.

Shear stress transfer model k-ω**:**

The ***SST.k-ω*** model was presented by Mentz in order to combine the accurate and powerful formulation of the ***k-ω*** model in the areas near the wall, with the independent ***k-Ɛ*** model of the free flow in the areas far from the wall. This means that the resulting model simultaneously has the high capability of the ***k-ω*** model in the regions with low Reynolds number and the high capability of the ***k-Ɛ*** model in the regions with the high Reynolds number.

The ***SST. k-ω*** model is very similar to the standard ***k-ω*** model, but includes the following optimizations: (It should be noted that the standard ***k-ω*** model was developed on the basis of the ***Wilcox k-ω*** model, which contains improvement for the effects of low Reynolds number, compressibility and dispersion of shear flow).

a) The standard ***k-ω*** model and the transformed form of the ***k-Ɛ*** model are both multiplied by a fusion function and then the two models are added together.

In fusion function the value of one is in the areas near the wall (which activates the ***k-ω*** model in those areas) and a value of zero in the areas far from the wall (which activates the transformed form of the model).

It should be noted that although this method can significantly increase the capabilities of both models, but due to the conversion process from one model to another, this model often faces unstable behaviors or weak convergences.

b) b) The SST model has a cross diffusion derivative term in the ***ω*** equation.

c) c) The definition of turbulence viscosity μ_t in order to account for the effects of the transfer of the main shear stresses of the turbulent flow, has been changed.

d) d) The constants of the model have been changed compared to the standard ***k-ω*** model.

These characteristics have made the ***SSTk-ω*** model much stronger and more reliable than the standard ***k-ω*** model for a wide range of flows (such as flows containing reverse pressure gradients, airfoils, and shock waves). In order to compare the turbulence intensity of each flow, the dimensionless and time-uniformized value of the square of velocity fluctuations is used:

$$ב = \frac{[(u^{t2})]^{\frac{1}{2}}}{\bar{u}} = \frac{[\frac{1}{T}\int_0^T u^{t2} dt]^{\frac{1}{2}}}{\bar{u}}$$

The usual values of turbulence intensity are:

1) For completely calm flow $ב = 0$
2) For a well-designed wind tunnel, $ב \approx 0.01$
3) For river currents or atmospheric currents, $ב > 0.1$
4) For very turbulent flows, such as the flow in roaring rivers or the flow behind fast moving objects, $ב \gg 1.0$

To measure the perturbation length near the solid surface, due to the comforting nature of the flow, $\boldsymbol{l_m}$ must go to zero faster than y. Therefore, a correction coefficient named "Van Drist damping coefficient" should be used:

$$l_m = ky\,(1 - e^{-\,y^+ / A_1^+})$$

In the above equation, k is Carmen's constant and its value is approximately equal to 4.0 and A_1^+ is equal to 26.

According to the correction term in the above relation, it can be shown by using the mathematical expansion of the part related to the corrected term that whenever $y \rightarrow 0$ goes, then becomes $l_m\ \mu\ y^2$. The correction factor l_m should always be chosen so that when $y \rightarrow 0$, l_m tends to zero faster than y, that is, $l_m \mu y^n$, so that it is $n>1$.

Turbulence model k – ε:

This model is the most famous and widely used turbulence model, and due to a large number of corrections on this model, it has more accurate results than other models. The main application of this model in geometrical factors are as follows:

1) The dissolution of eddies in the combustion phenomenon
2) Buoyant currents in buildings or on structures
3) Flow in pipes with sudden contraction
4) Modelling of the ignition phenomenon
5) Flow inside a bunch of heat exchanger tubes
6) Flow inside pipes with circular sections and intermittent pressure changes
7) Modelling dispersion of pollution in the atmosphere and water
8) Studying the expansion of jets in a stationary environment
9) Flow in vessels and pressure waves inside oil and gas transmission pipes
10) The flow inside the manifold of internal combustion engines

Of course, this model faces problems in modelling of strongly rotating flows and modelling of the boundary layer. The main reason is the existence of many sources terms inside the boundary layer and rotational currents, which creates problems for the stability of this method.

2-4-3. CFD Analyzes

Speed investigation on the pile:

The input speed is 11 meters per second. But the maximum speed on the pile is higher than the input speed. Usually, the highest speed occurs on the highest level of the pile.

Next, we will draw the speed contour together with the speed vectors to display the speed field more clear (Figure 21 & Figure 22 & Figure 23 & Figure 24).

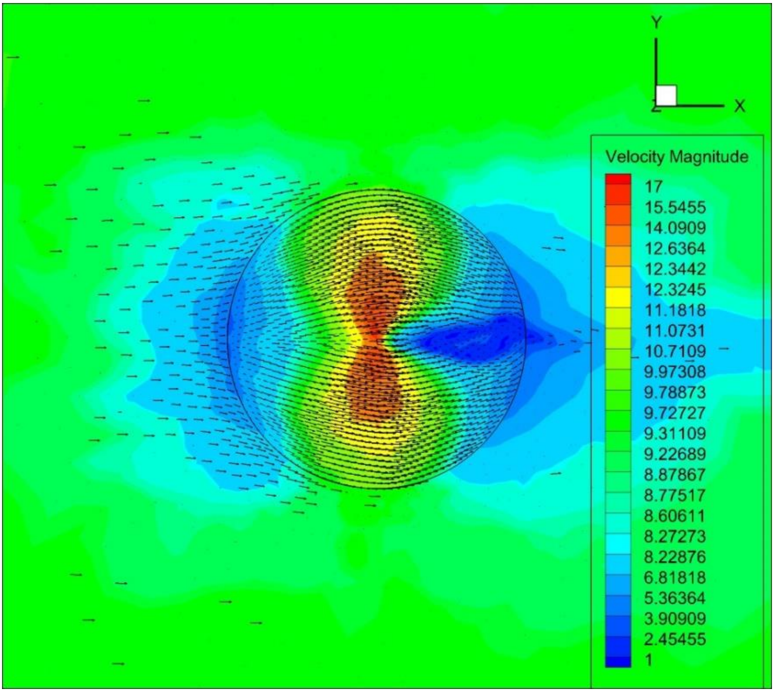

Figure 21: Speed distribution together with speed vectors on pile number 1

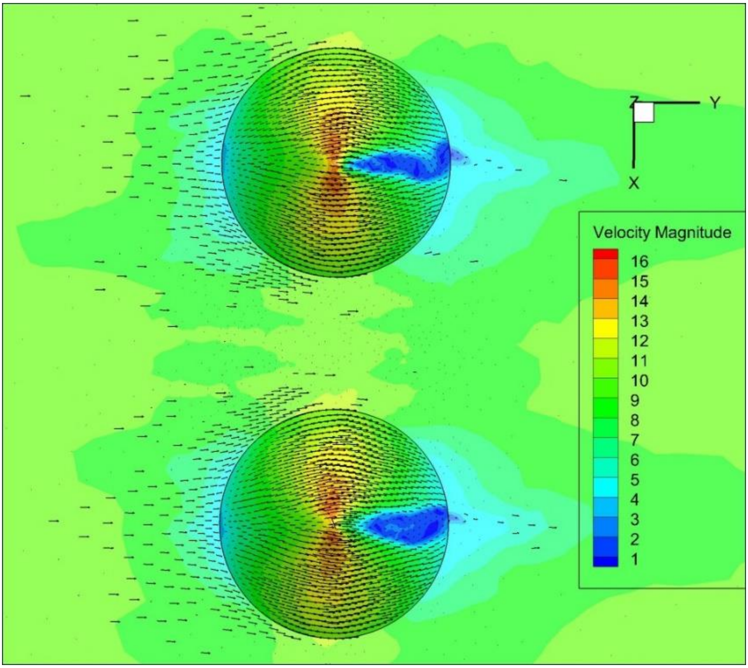

Figure 22: Velocity distribution together with velocity vectors on pile number 2

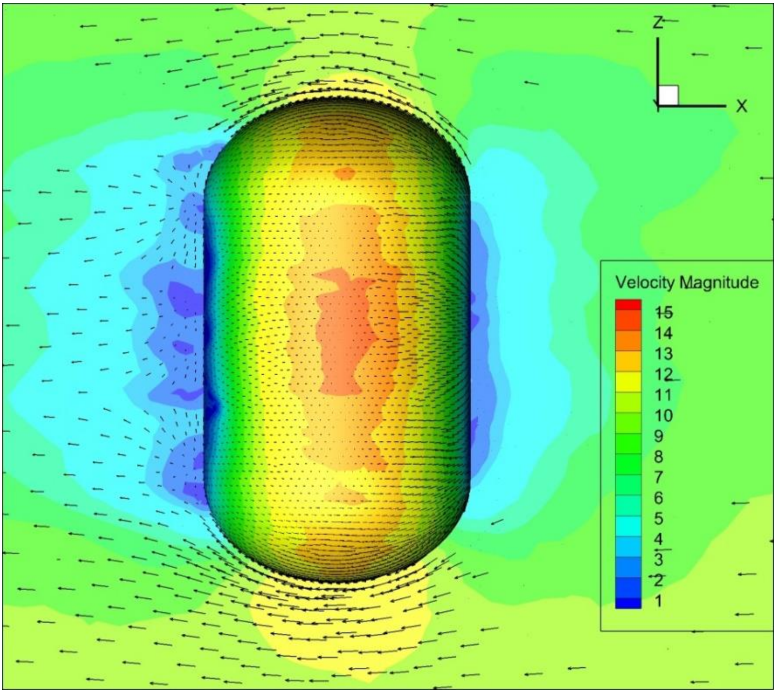

Figure 23: Speed distribution together with speed vectors on pile number 3

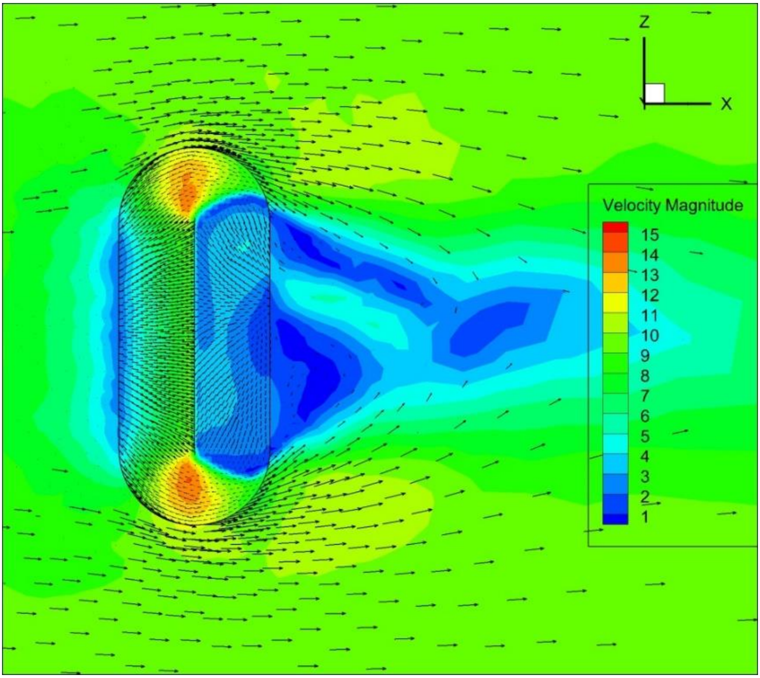

Figure 24: Speed distribution together with speed vectors on pile number 4

The maximum speed for each pile is listed in Table 11.

Table 11: Maximum speed on the pile

Pile number	1	2	3	4
Maximum speed on the pile (m/s)	17.74	16.61	16.19	15.61

It is worth noting that, the above criteria cannot be used as a measure of deflation. But the heterogeneity of the speed makes the amount of deflation from all points of the pile not the same and deflation from some points is more. In other words, as can be seen from the contours drawn for the speed distribution on the pile surface, the amount of the wind speed is not the same in different parts of the pile surface, that is, for some parts there is the lowest wind speed and for others the highest flow speed. This subject causes the wind to be waried from different parts of the pile. Only for some points where the maximum speed of the flow occurs, the highest deflation is observed.

Flow lines are those lines that are tangent to the velocity vector at any moment. Also, the direction of the velocity indicates the movement path of a particle in the physical field. Therefore, the flow lines approximately indicate the movement path of very light particles. If the mass of the particle and other volumetric forces are considered in the field, then the trajectory of some of the particles will change (Figure 25 & Figure 26 & Figure 27 & Figure 28).

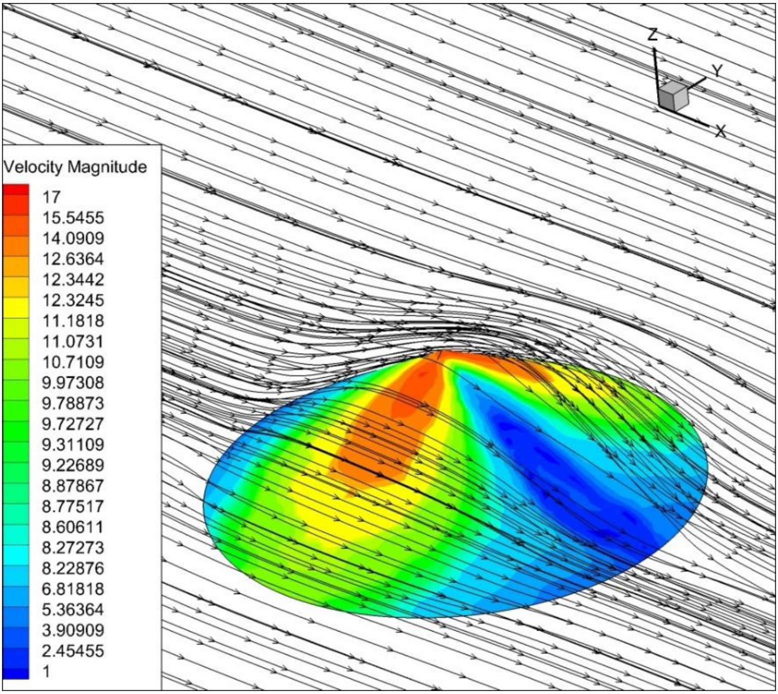

Figure 25: Transient flow lines on pile number 1

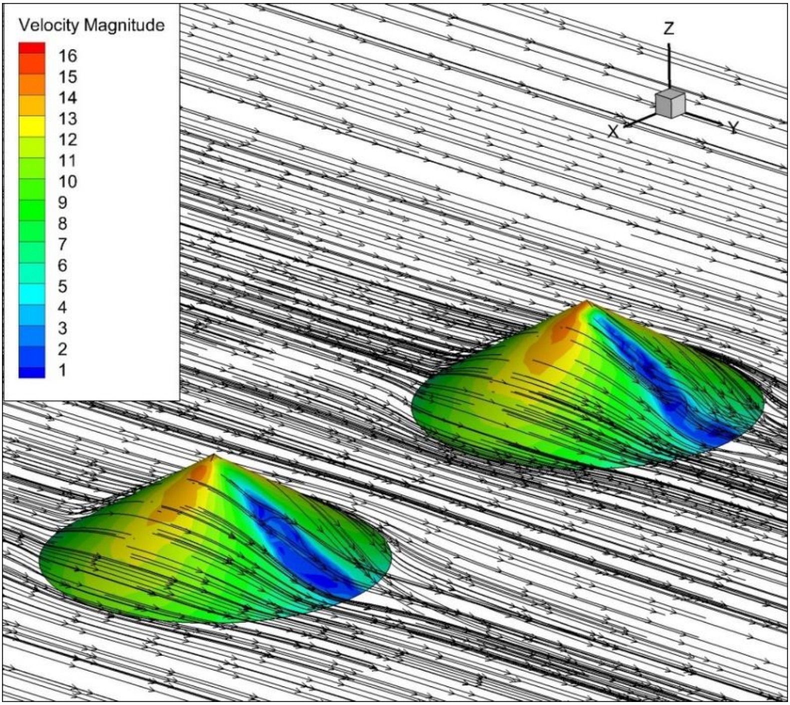

Figure 26: Transient flow lines on pile number 2

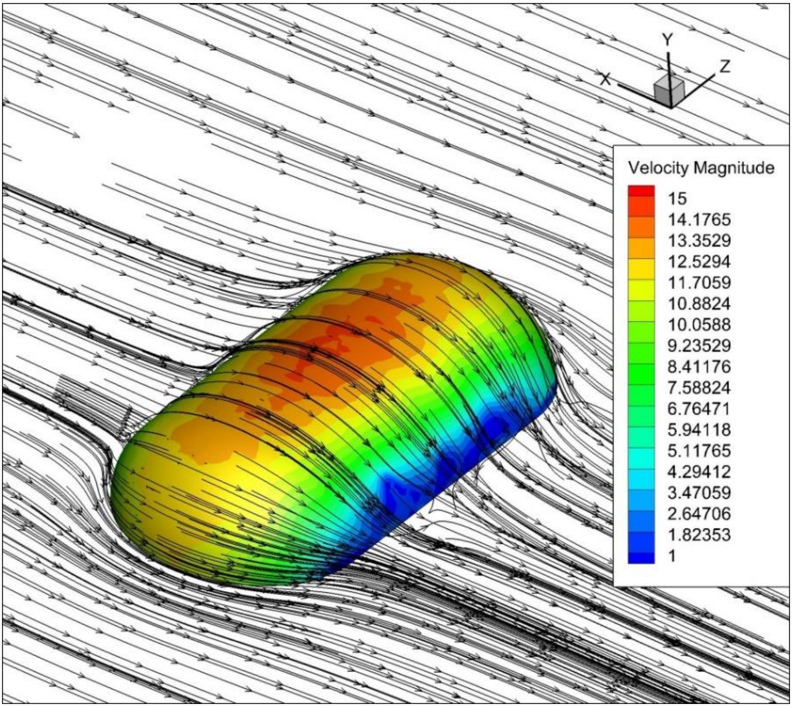

Figure 27: Transient flow lines on pile number 3

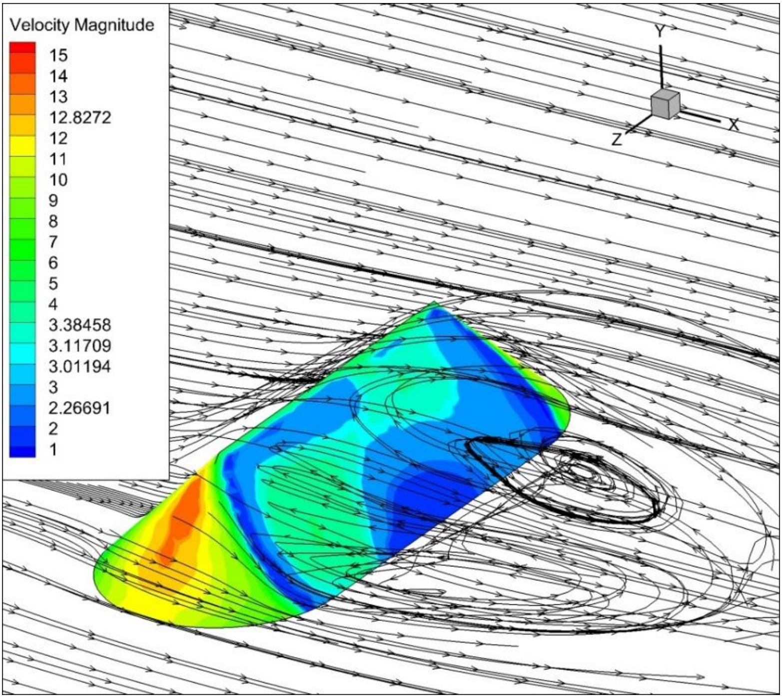

Figure 28: Transient flow lines on pile number 4

Due to the higher height of this particular type of pile, eddy currents are formed behind this pile. The difference between the front and back speeds of this type of pile is more than other piles.

Now, the pressure distribution is examined. The pressure distribution on the pile can be related to the flow direction in the pressure field. In the pressure field, the direction of fluid movement is from the side of higher pressure to the side of lower pressure (Figure 29 & Figure 30 & Figure 31 & Figure 32).

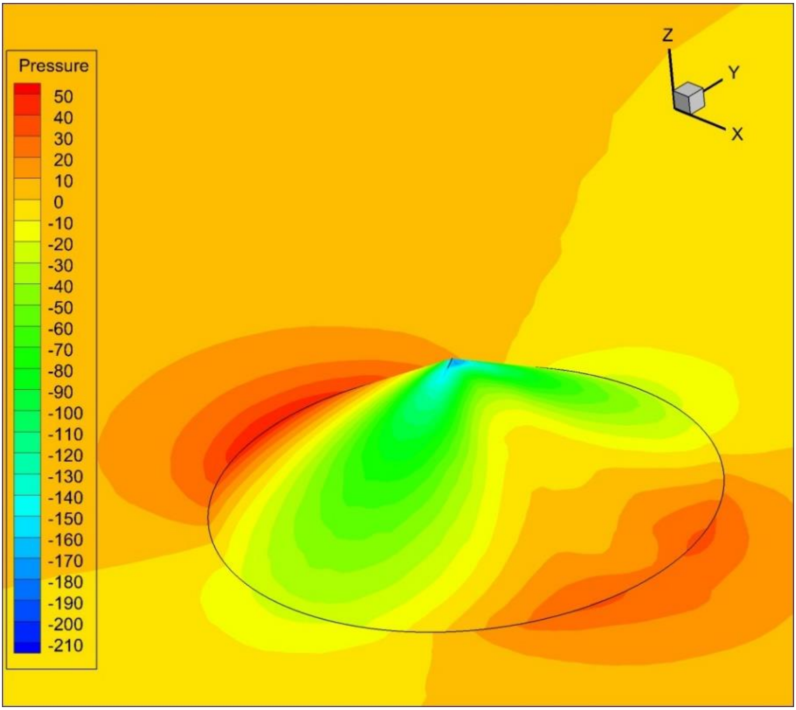

Figure 29: Pressure distribution on pile number 1 and around the pile

It is clear from Figure 29 that the lowest amount of pressure occurs in the place that has the highest speed. Also, the highest pressure occurs at low speed points.

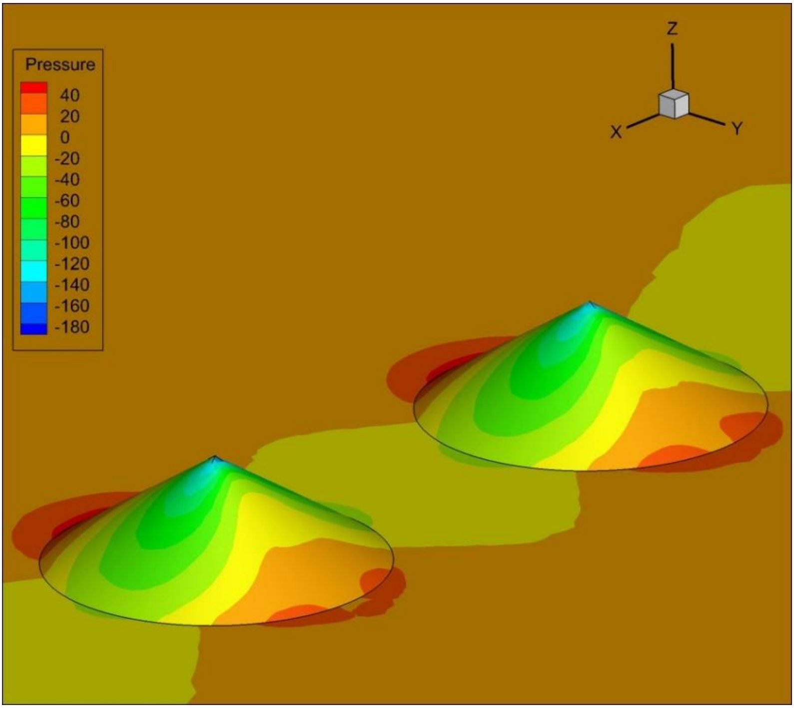

Figure 30: Pressure distribution on pile number 2 and around the pile

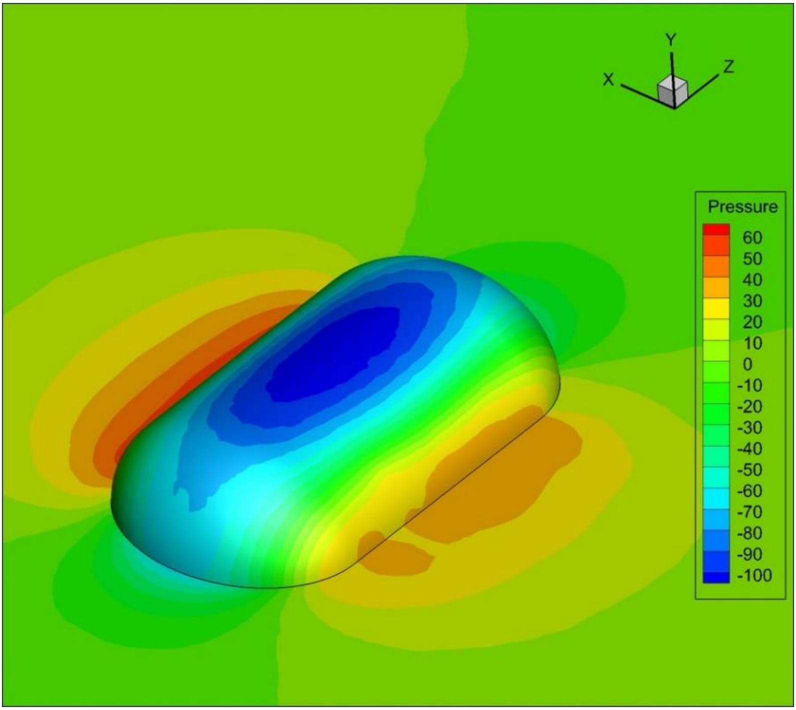

Figure 31: Pressure distribution on pile No. 3 and around the pile

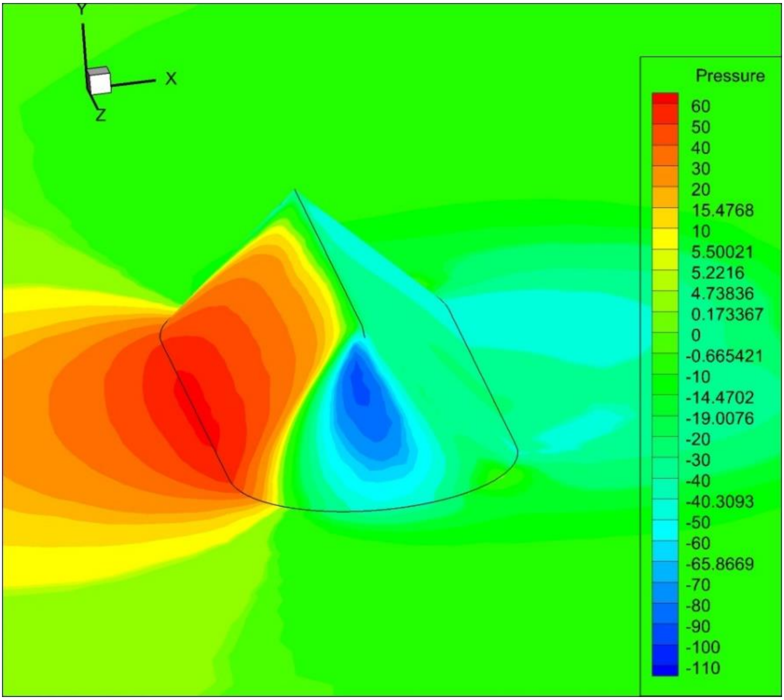

Figure 32: Pressure distribution on pile number 4 and around the pile

In order to better investigate the phenomenon of deflation, it is better to plot the speed and pressure at different sections of the pile to get a better understanding of the speed around the pile. For this purpose, the velocity and pressure have been drawn on the middle surface of the pile (Figure 33 to Figure 49)

The location of these plains is shown in the Figure 33.

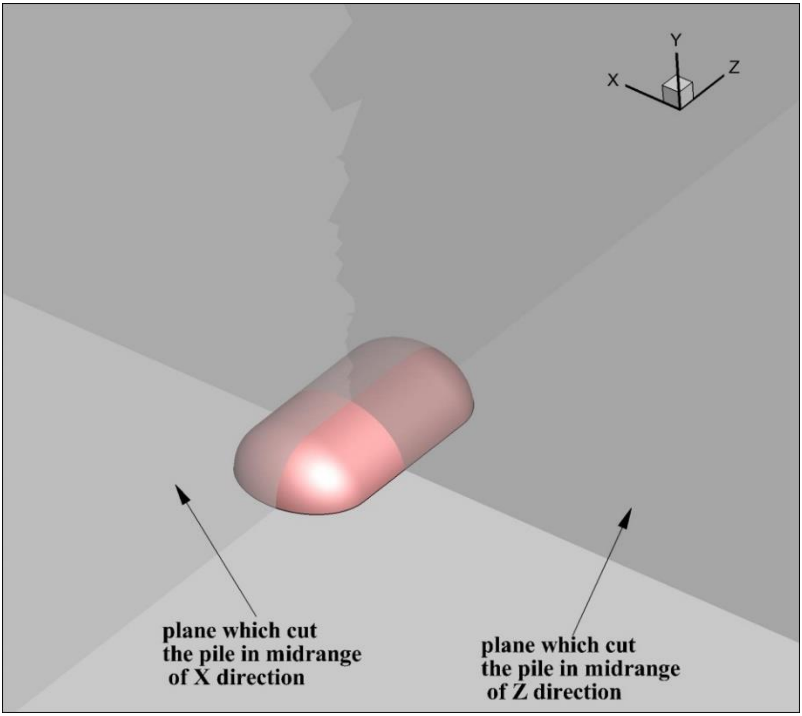

Figure 33: Layout of transmissive planes from the middle of the pile

Velocity and pressure distribution on the plane passing through the middle of the piles in the x direction

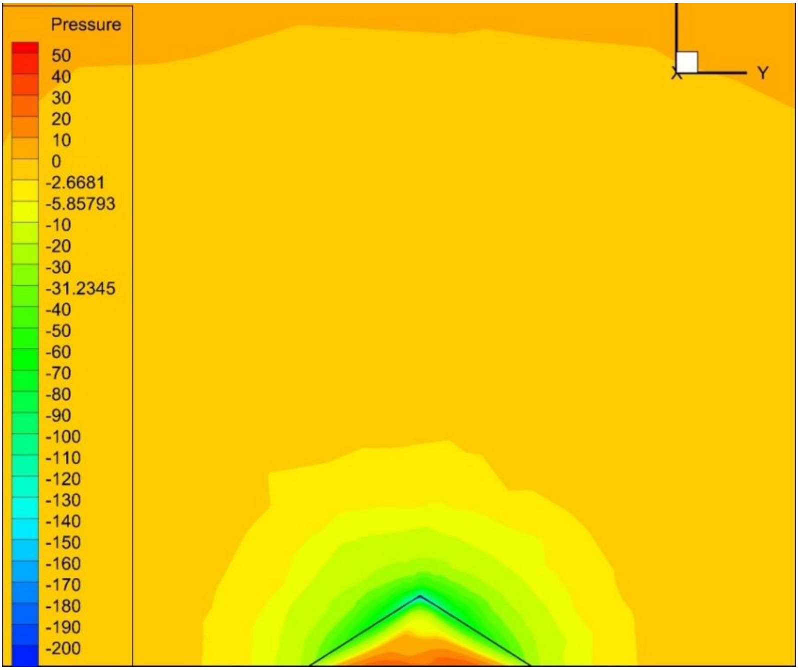

Figure 34: Pressure field distribution on pile number 1 on the plane passing through the middle of the pile in the x direction

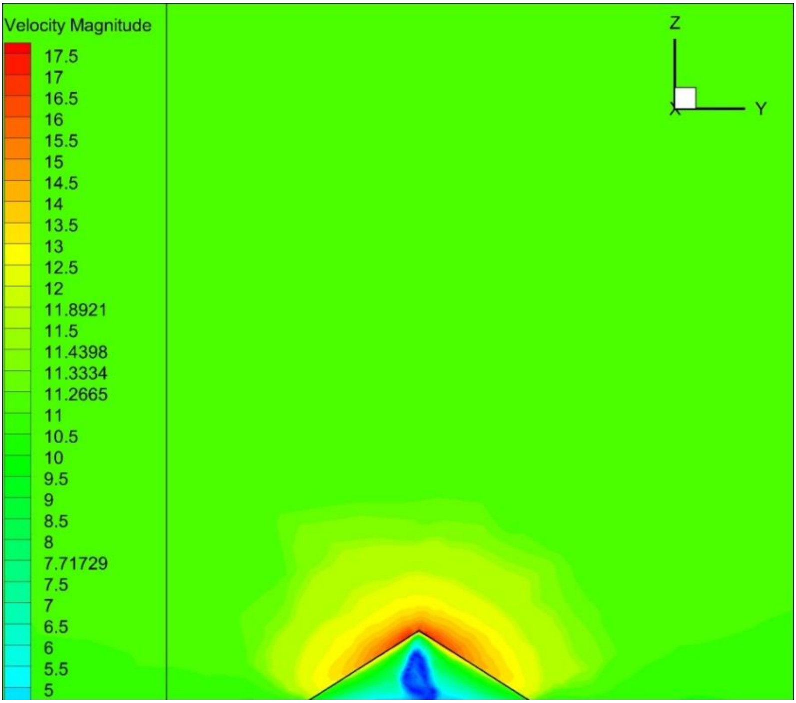

Figure 35: Velocity field distribution on pile number 1 on the plane passing through the middle of the pile in the x direction

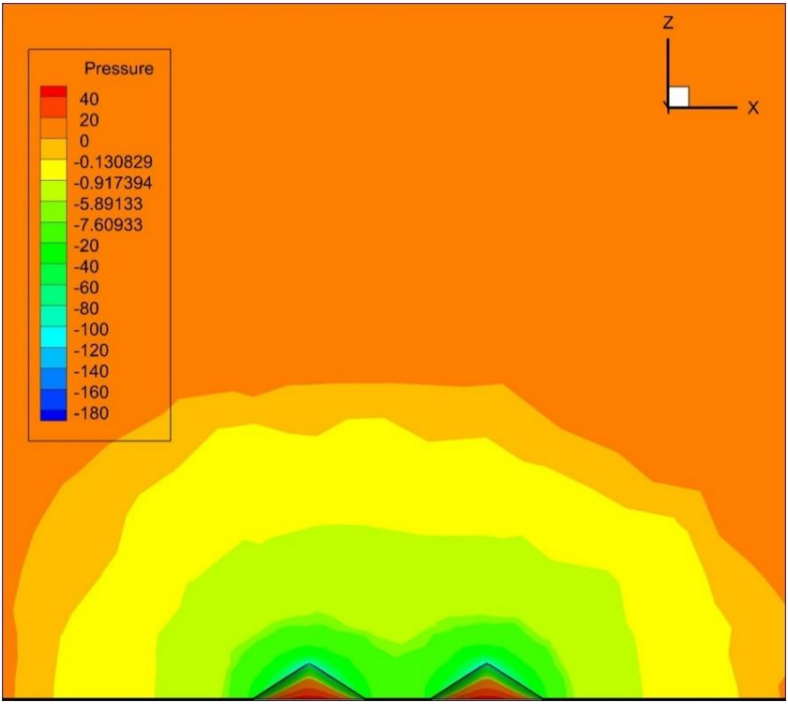

Figure 36: Pressure field distribution on pile number 2 on the plane passing through the middle of the pile in the x direction

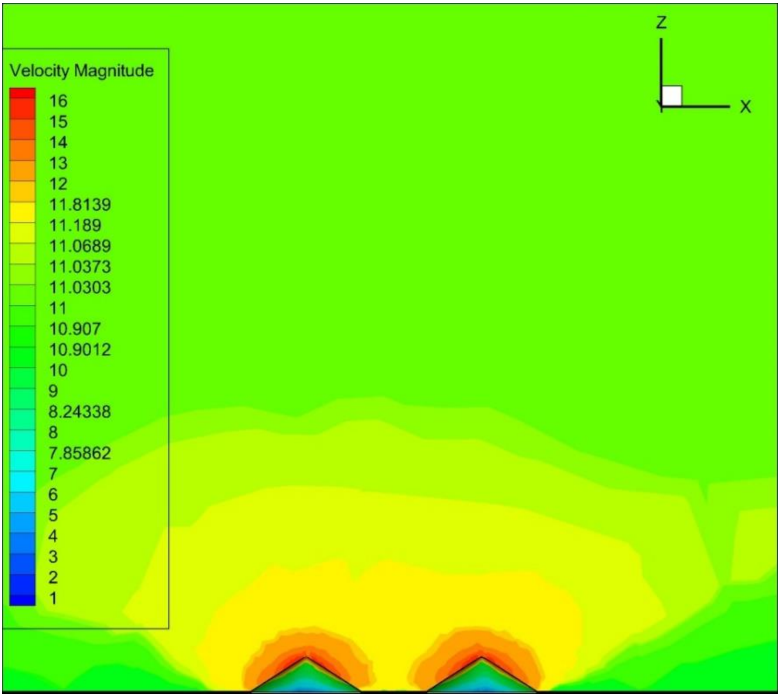

Figure 37: Velocity field distribution on pile number 2 on the plane passing through the middle of the pile in the x direction

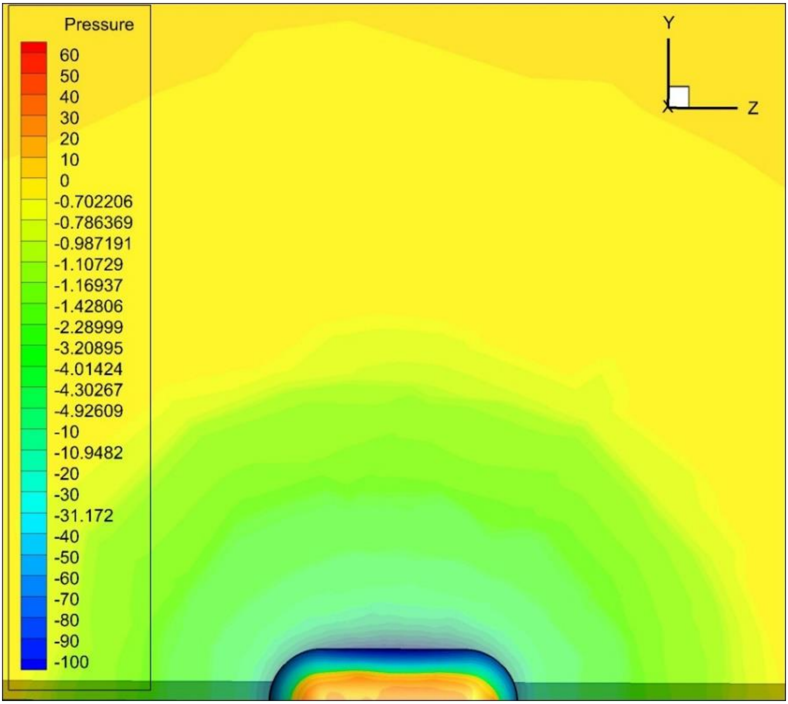

Figure 38: Pressure field distribution on pile No. 3 on the plane passing through the middle of the pile in the x direction

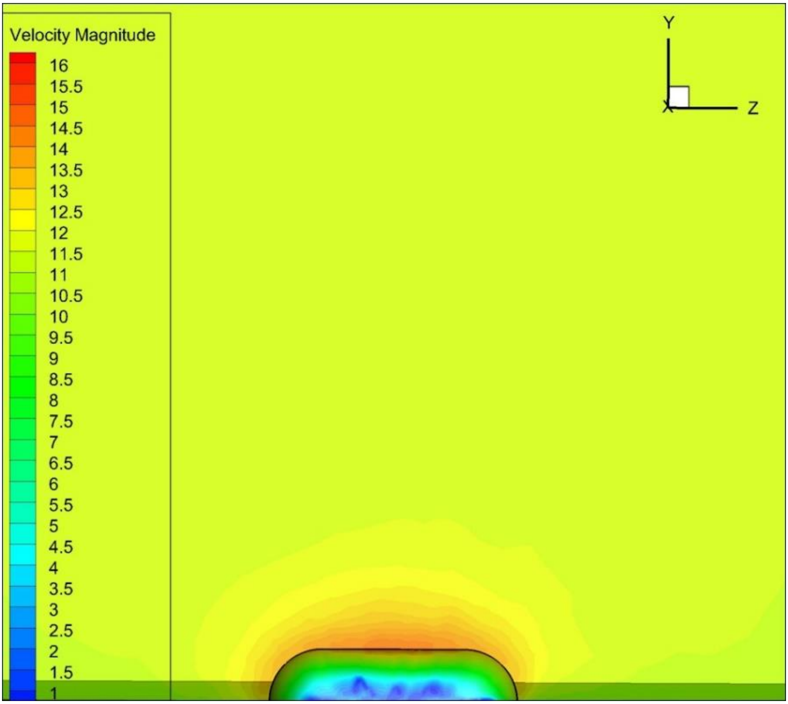

Figure 39: Velocity field distribution on pile No. 3 on the plane passing through the middle of the pile in the x direction

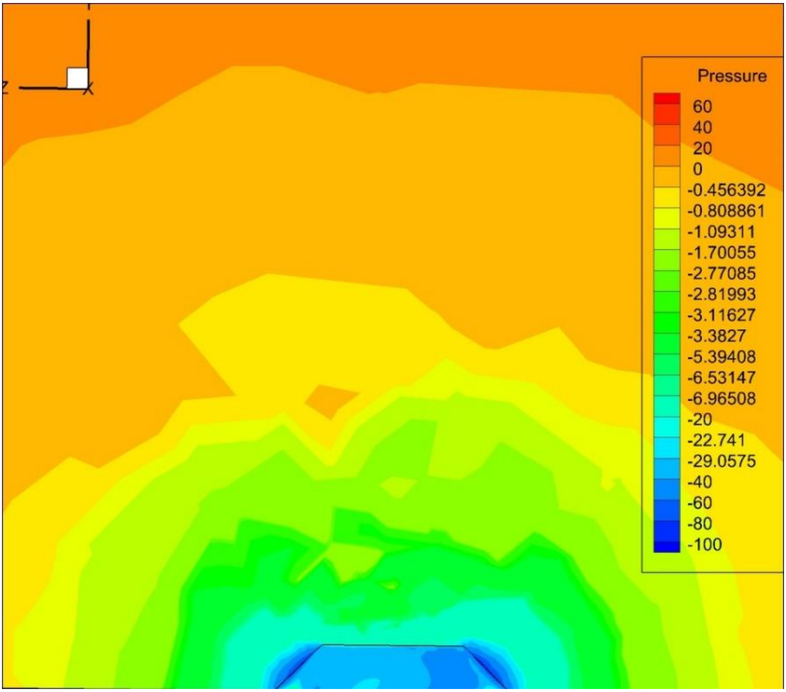

Figure 40: Distribution of the pressure field on pile number 4 on the plane passing through the middle of the pile in the x direction

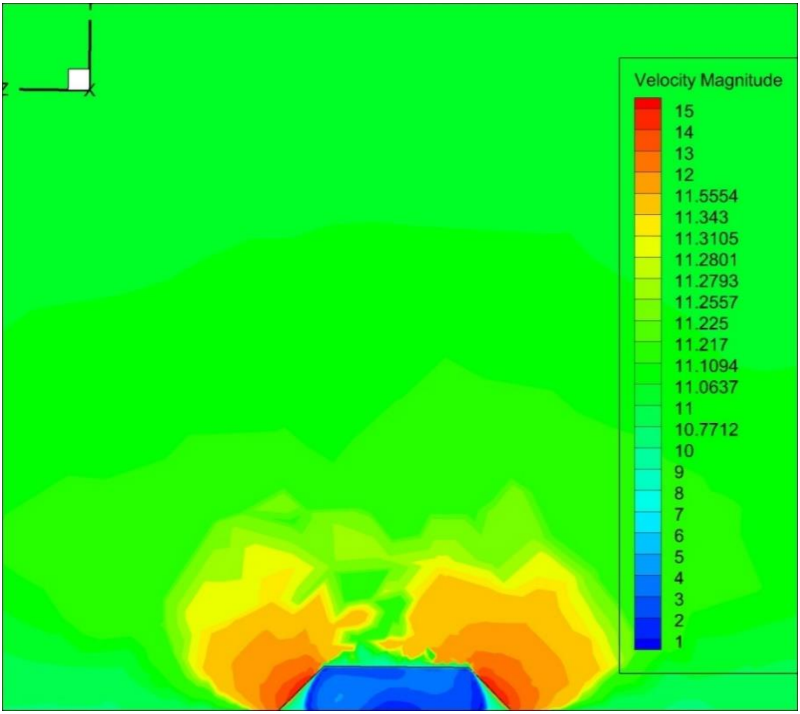

Figure 41: Velocity field distribution on pile number 4 on the plane passing through the middle of the pile in the x direction

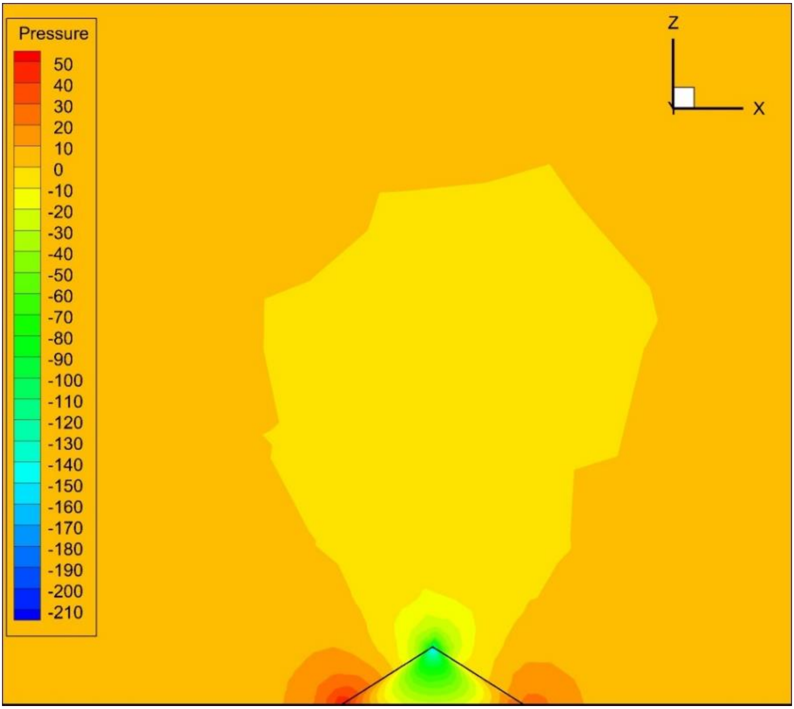

Figure 42: Pressure field distribution on pile number 1 on the plane passing through the middle of the pile in the z direction

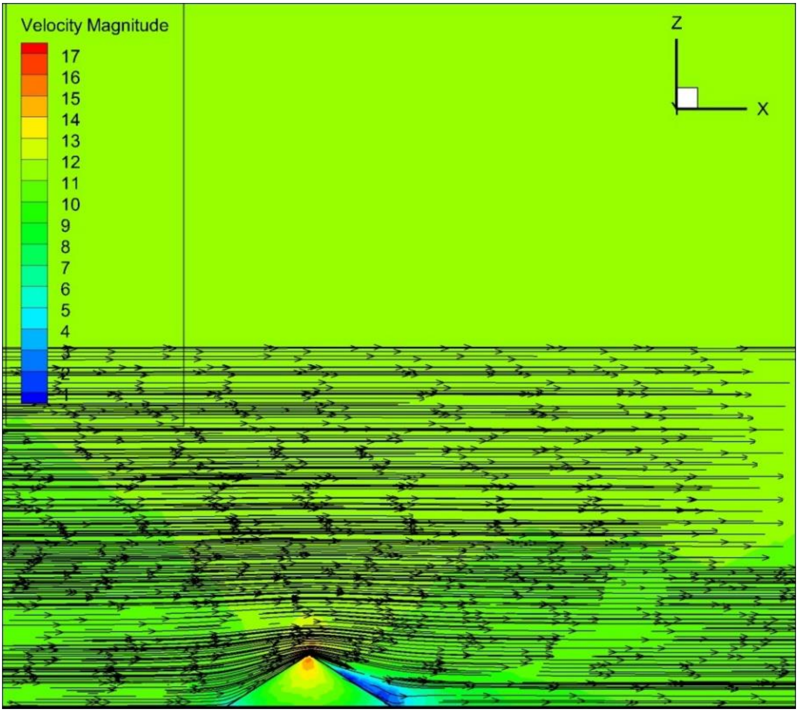

Figure 43: Velocity field distribution on pile number 1 on the plane passing through the middle of the pile in the z direction

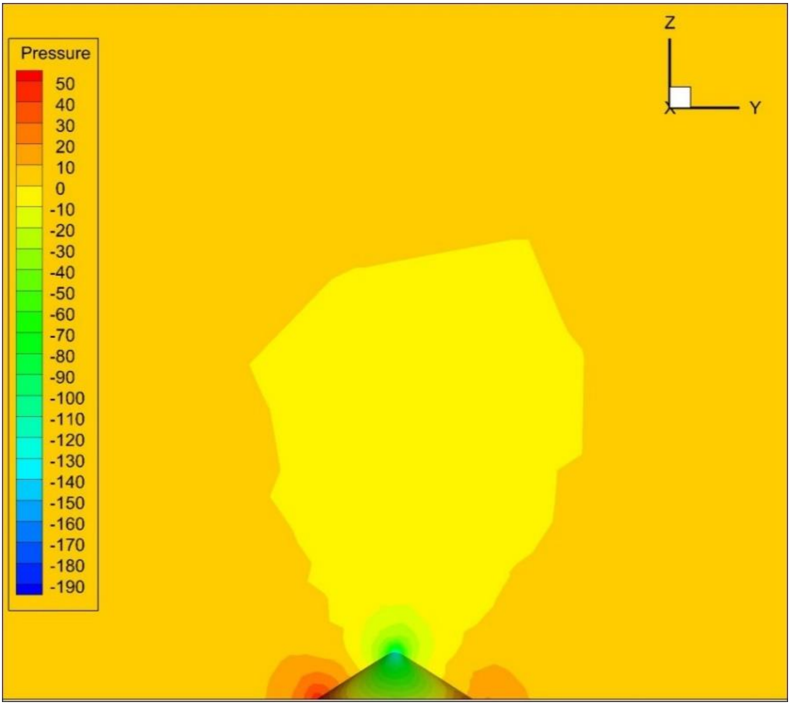

Figure 44: Pressure field distribution on pile number 2 on the plane passing through the middle of the pile in z direction

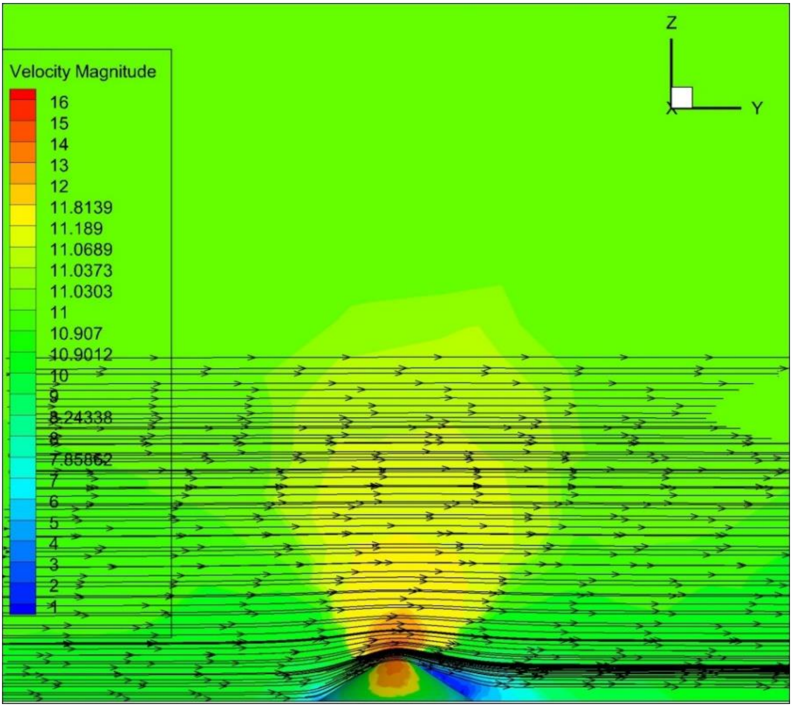

Figure 45: Velocity field distribution on pile number 2 on the plane passing through the middle of the pile in z direction

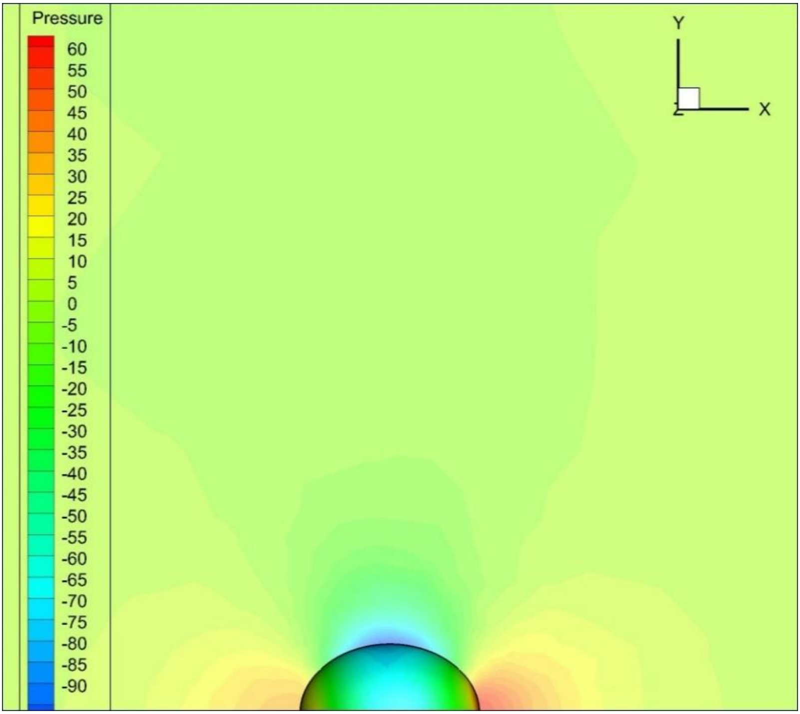

Figure 46: Pressure field distribution on pile No. 3 on the plane passing through the middle of the pile in z direction

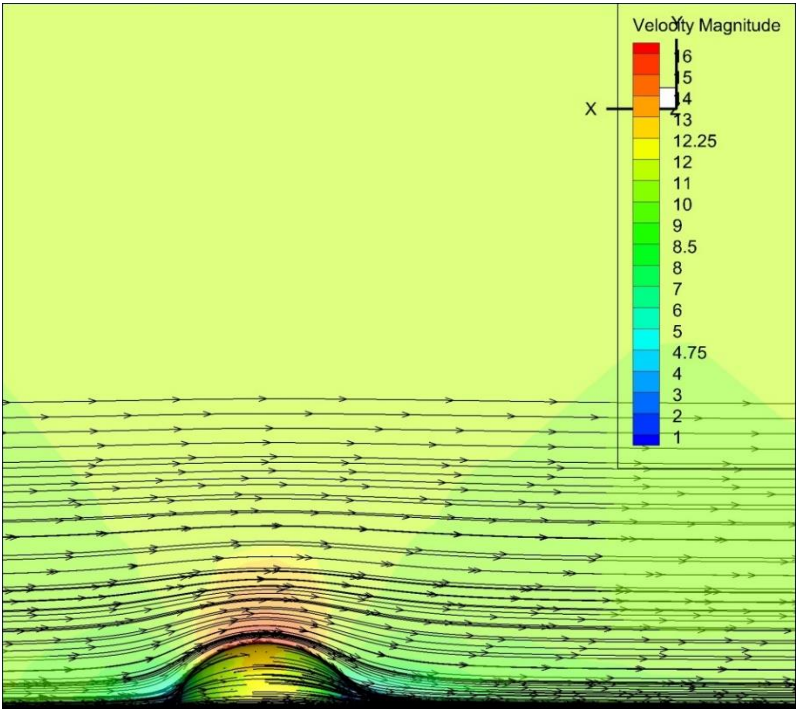

Figure 47: Velocity field distribution on pile number 3 on the plane passing through the middle of the pile in z direction

As can be seen in the Figure 33 to Figure 47, the distribution of speed and pressure in the pile 47 is more uniform than other piles, which makes the amount of deflation from this pile less than other piles.

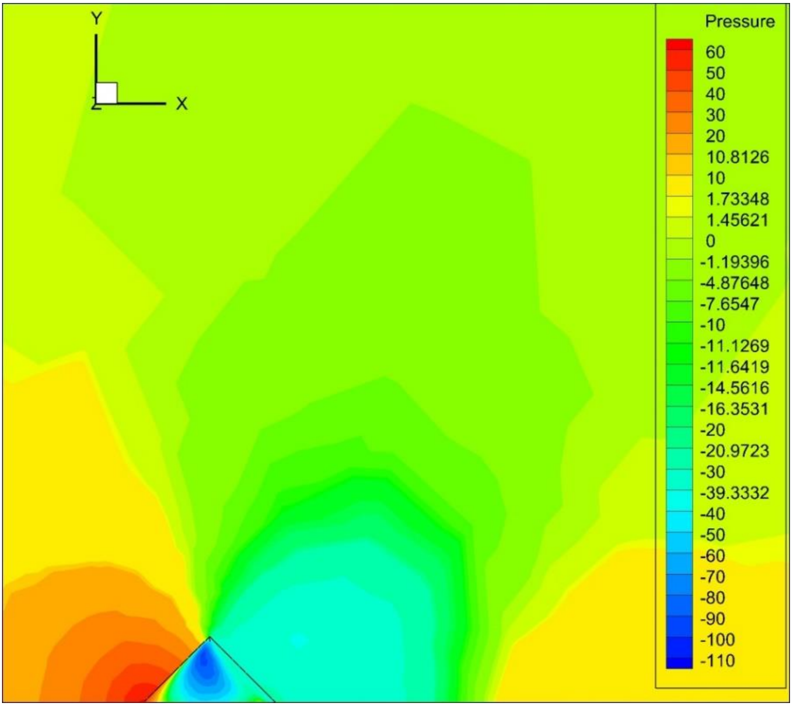

Figure 48: Pressure field distribution on pile number 4 on the plane passing through the middle of the pile in z direction

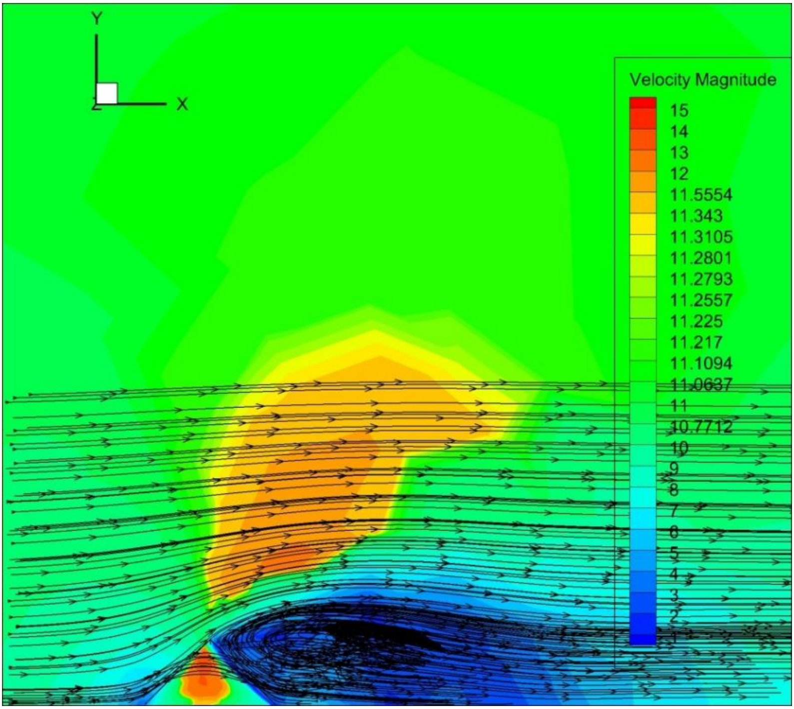

Figure 49: Velocity field distribution on pile number 4 on the plane passing through the middle of the pile in z direction

In this pile, due to the presence of walls facing the wind, there is a strong front against the wind, which results in the formation of an eddy flow behind the pile.

<u>2-4-4- Investigating the effects of creating a barrier in front of the pile</u>

In order to investigate the effects of the presence of a barrier in front of the salt piles, another modelling has been done by creating a barrier with a height of one meter and at a distance of one meter from the four mentioned piles. The geometry and meshing related to pile number one is shown in Figure 50.

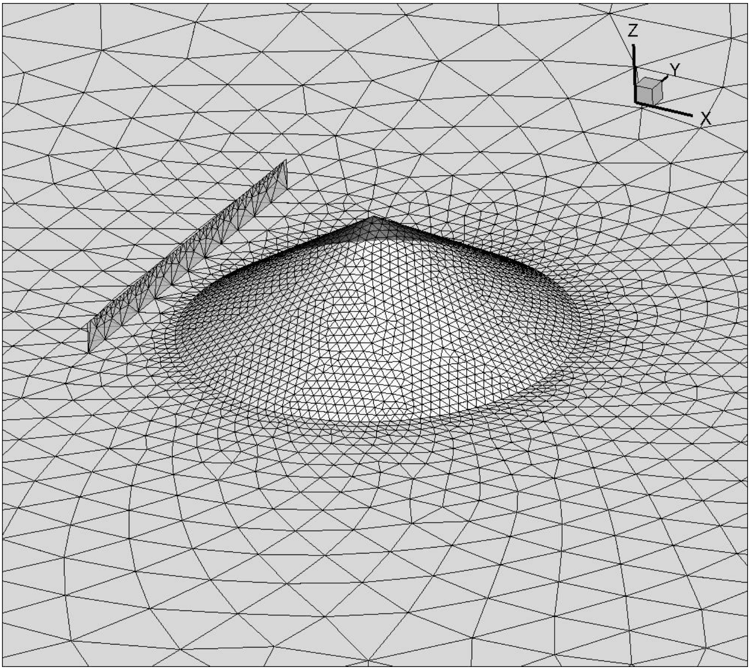

Figure 50: Meshwork of the model created for the barrier in front of pile number 1

For a better comparison, the velocity contour on the surface of the piles in two cases without obstacles and with obstacles are placed next to each other, which are presented in Figure 51 to Figure 58. Also, the average speed on each of these levels has been compared with each other in Table 12. According to the following figures, it can be seen that due to the installation of the barrier in front of the pile, the range of the contours where the speed value is high is reduced compared to the case where the barrier is not used, and as a result, the speed on the surface of the pile with the barrier reduced to an unobstructed level.

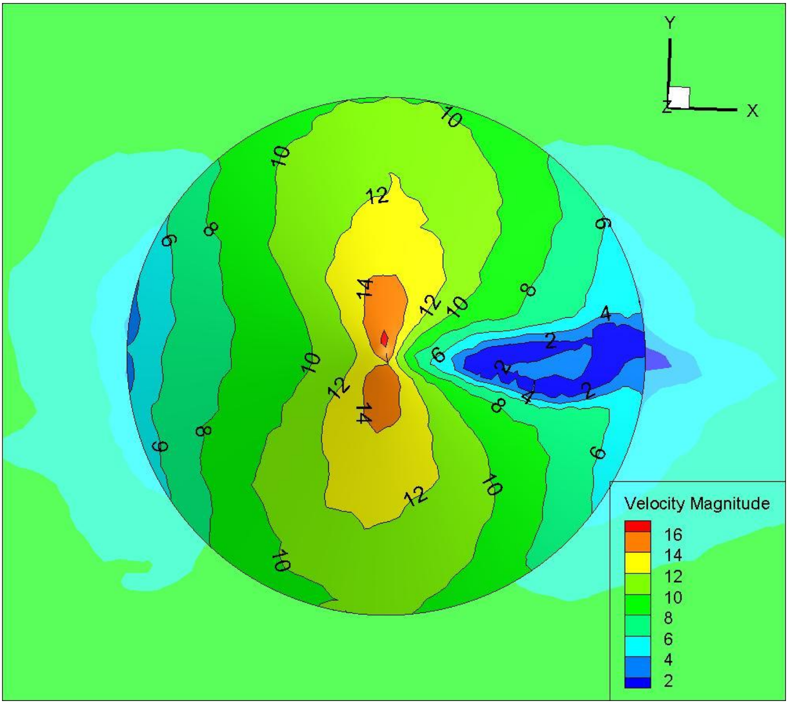

Figure 51: Speed contour on file number 1 (without barrier)

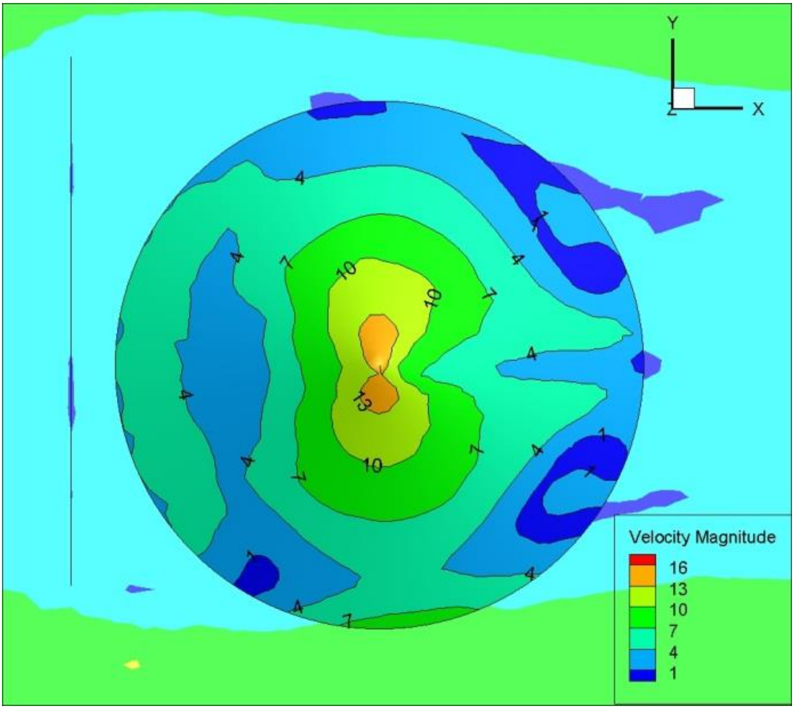

Figure 52: Speed contour on file number 1 (with barrier)

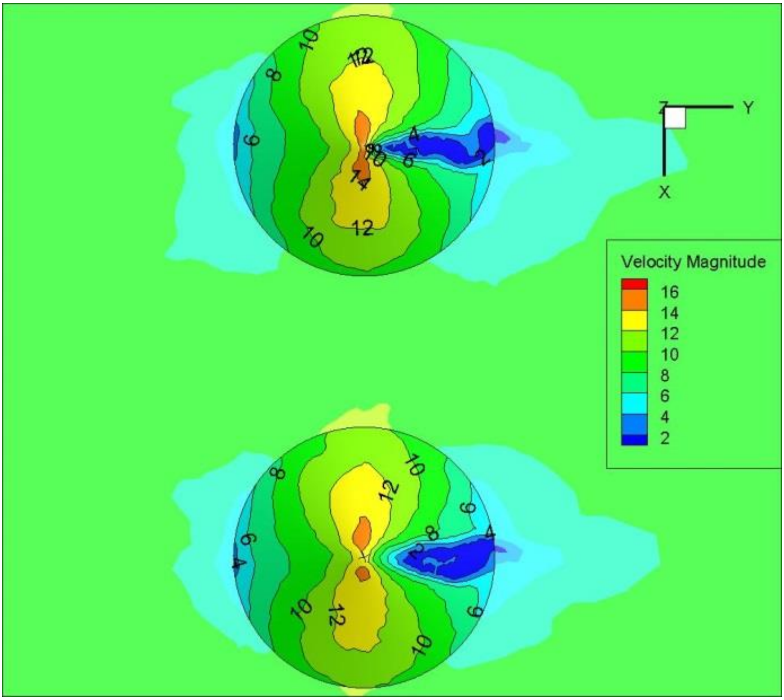

Figure 53: Speed contour on file number 2 (without barrier)

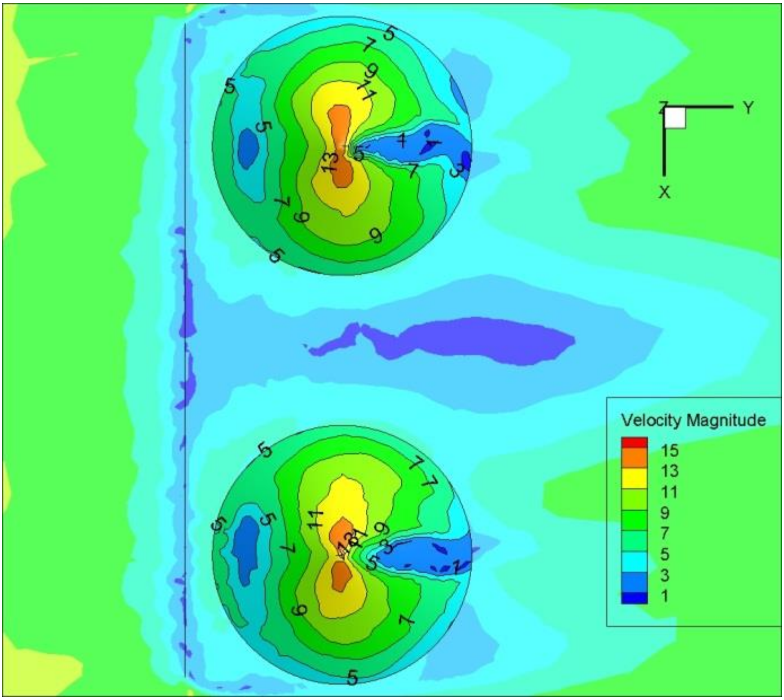

Figure 54: Speed contour on file number 2 (with barrier)

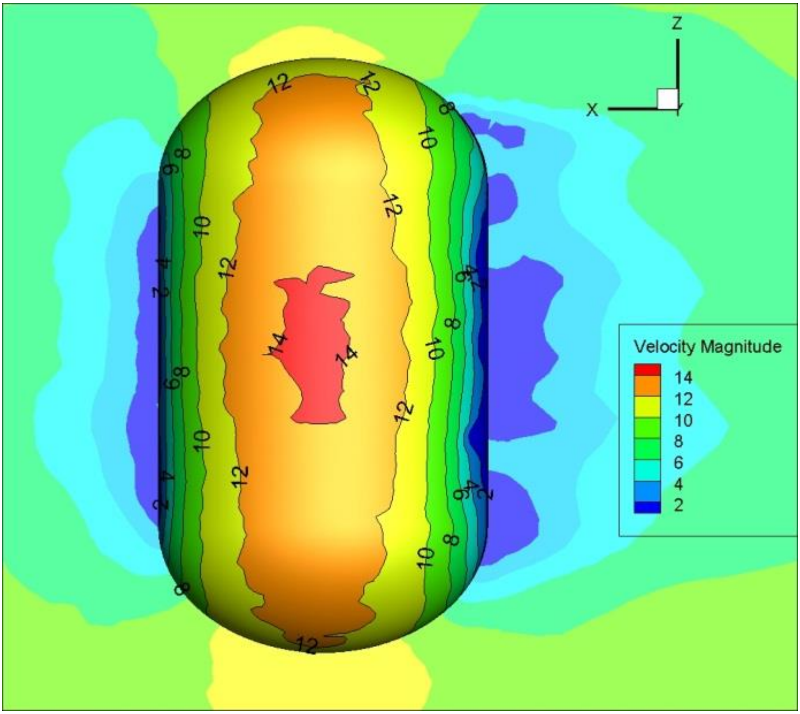

Figure 55: Speed contour on file number 3 (without barrier)

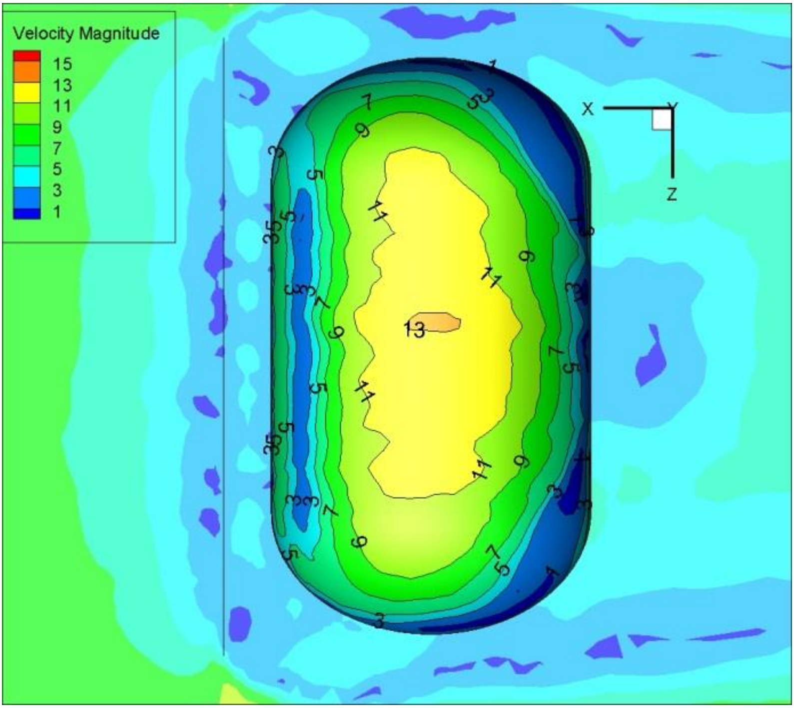

Figure 56: Speed contour on file number 3 (with barrier)

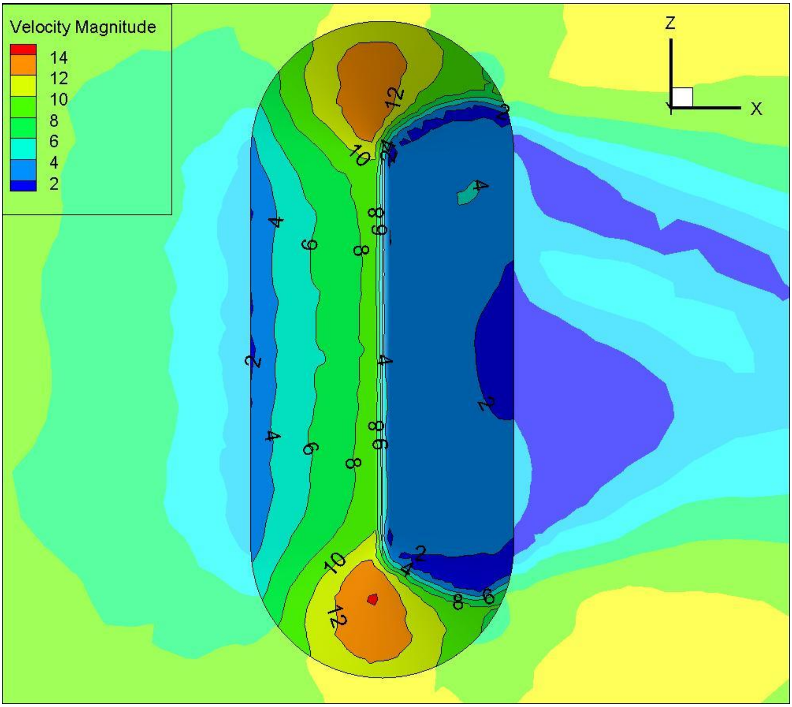

Figure 57: Speed contour on file number 4 (without barrier)

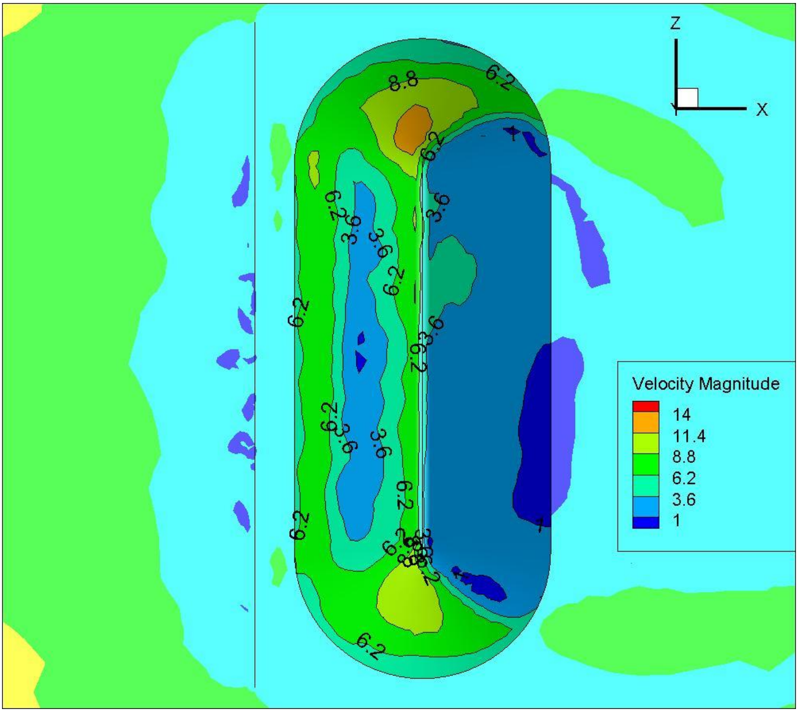

Figure 58: Speed contour on file number 4 (with barrier)

Table 12: Comparison of the speed on the surface of the piles in the state without obstacles and with obstacles

Pile number	Average speed (m/s)		Percentage difference
	without obstacles	with obstacles	
1	9.690	5.0466	44
2	9.1141	6.9996	23
3	9.4715	6.1582	35
4	5.8909	4.6534	20

As can be seen Table 12, the average speed on the surfaces of the piles that are directly exposed to the wind is much lower than the piles that have a one-meter-high barrier in front of them. This indicates the reduction of wind speed on the surface of piles with obstacles, and as a result, it will reduce the amount of deflation.

Accordingly, the areas of the pile surface on which the air flow has the maximum speed will decrease when a barrier is used in front of the pile. Obviously, considering the definition related to the threshold frictional speed, by reducing the speed on the pile, the amount of dispersing of particles in the air also decreases. Therefore, it is suggested to create obstacles in the wind direction to prevent the diffusion of particles.

2-4-5. Investigating the effect of using a fence instead of an obstacle

In this part, the use of a fence instead of an integrated metal barrier is examined in terms of the amount of changes of speed of the surface of pile. The speed on the pile has a direct relationship with the amount of deflation, so by checking the average speed on the pile, it can get the approximate amount of the pile's pollution emission. In practice, it is almost impossible to model fences and nets and sharp edges in fluid analysis software due to the existence of singular points, but this problem has been solved to some extent in the latest editions of Fluent commercial software. However, the geometry with very sharp angles causes very acute or obtuse angles to be created in a cell, which reduces the quality of the network, resulting in late convergence and in some cases it causes non-convergence of the solution. Therefore, to solve a geometry like a fence which consists of sharp surfaces, an alternative option should be used to analyze the desired surfaces. In this regard, they can be defined as a kind of porous body, and porosity coefficient for a porous body is considered as follows.

$$\varepsilon = \frac{V_v}{V_T}$$

that $\boldsymbol{V_v}$ represents the amount of empty space in the geometry and $\boldsymbol{V_T}$ indicates the total volume.

Therefore, the value of coefficient porosity of one represents a solid objector a rigid barrier and coefficient of zero indicates the absence of obstacles.

For normal fances, the porosity coefficient is around 0.3. To determine the type of porous medium in FLUENT software, the pressure drop parameters on the sides of the fence, the pressure drop coefficient (C_2) and the thickness of the porous material must be determined.

There are different types of fences to control deflation. A type of wind control fence is shown in Figure 59. This type of fence is made of a kind of resistant plastic fabric with many small holes. Also, this type of fence it has the ability of replacement. But the value of the porosity coefficient for this type of fence is high, which will reduce the resistance of the fence against the wind, and it is more suitable for areas with low wind speed.

Figure 59: A view of a type of fence with low porosity

There are other types of fences that have a lower porosity coefficient. These fences, which are often non-fabric, have a higher porosity coefficient than fabric fences. Therefore, these fences are used in cases where the wind speed is higher. In the Figure 60, one of the types of these fences is shown along with the required connections. These fences are simply not movable.

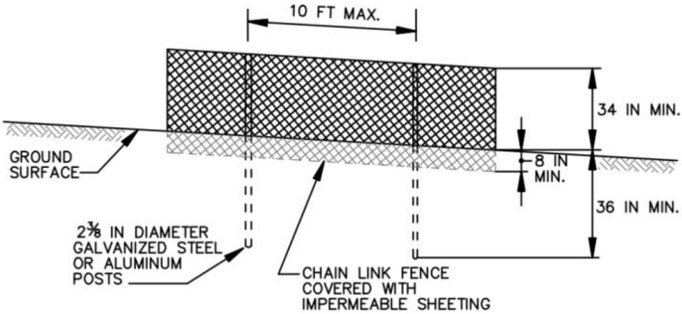

Figure 60: A view of a type of fence with high porosity

The important parameters for selecting fence are as follows:

height, type and size of netting, fence thickness, together with environmental conditions such as, wind speed, pile dimensions and threshold friction speed of the pile. The standard thickness of specific fences in order to prevent deflation, is 0.75 inches (about 1.9 cm). To obtain the value of the pressure drop coefficient (C_2), we use the empirical relationship suggested by WANG and TAKE. According to this relationship, the value of the porosity coefficient is related to the pressure drop coefficient with the following relationship:

$$\varepsilon = 1.0422 \times C_2^{-0.4289} \rightarrow C_2 = 18.2376$$

The amount of pressure drop for this type of mesh will be obtained based on Darcy's relations or experimental tests. According to Darcy's relation, the amount of air pressure drop when passing through the wall is equal to:

$$\Delta p_s = (-\frac{\mu}{\alpha}\, u + \ C_2\left(\frac{1}{2}\,\rho u^2\right))$$

The C_2 coefficient has already been calculated, also $\boldsymbol{\mu}$ is the viscosity value and $\boldsymbol{\alpha}$ is the permeability coefficient, which has a direct relationship with the porosity coefficient value, and $\boldsymbol{u}$ is the velocity value perpendicular to the barrier. To calculate $\boldsymbol{\alpha}$, there are different models for modelling the penetration coefficient. But the general definition of penetration coefficient is as follows:

$$a = \frac{\varepsilon}{k_z S_{pv}^2}$$

In the above relationship, $\boldsymbol{k_z}$ is Kozeny's constant and $\boldsymbol{S_{pv}}$ is the surface area per unit volume of the porous material, which is equal to ***2/R*** for cylindrical pores. But the value of Kozeny's constant coefficient is equal to:

$$k_z = \ k_0 \ \times \ \tau$$

In this regard, $\boldsymbol{k_0}$ is the shape coefficient and for square and cylindrical pores, it is 2 and 1.78, respectively. $\boldsymbol{\tau}$ is the torsion coefficient, which is equal to one if the pores are straight. Therefore, for cylindrical porosity without bends, we have:

$$k_0 = 2$$

The amount of surface to volume for a fence to prevent deflation is high, which increases the power of the fence to prevent wind. This coefficient for commercial fences is something between 80 and 200. For a normal fence, this value can be considered 150. With this description, the value of the permeability coefficient is equal to:

$$s_{p_v} = 150 \;\rightarrow\; \alpha = \frac{\varepsilon}{k_2 S_{p_v}^2} = \frac{0.3}{2 \times 150^2} = 0.66 \times 10^{-6}$$

Therefore, the amount of pressure drop due to the presence of a fence with a porosity coefficient of 0.3 is equal to:

$$\Delta\rho_s = \left(-\frac{\mu}{\alpha}\,\mu + C_2\,\frac{1}{2}\,\rho u^2\right) = 1385.77\,p_a$$

In the Table 13, you can see the values of the maximum speed and the average speed for the case where we use a fence-like barrier. See also Figure 61 to Figure 68.

Table 13: Comparison of the speed on the surface of the piles in the state without obstacle and with the fence obstacle

Pile number	Average speed (m/s)		Percentage difference
	without obstacles	with obstacles	
1	9.0690	4.6873	48
2	9.1141	7.1126	22
3	9.475	6.3336	33
4	5.8009	4.5436	23

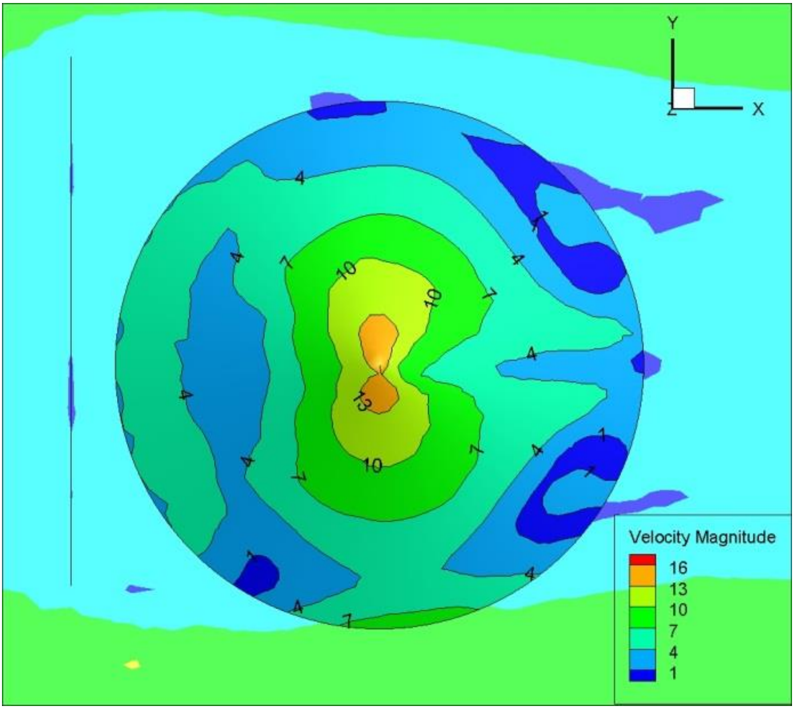

Figure 61: Speed contour on file number 1 (with solid barrier)

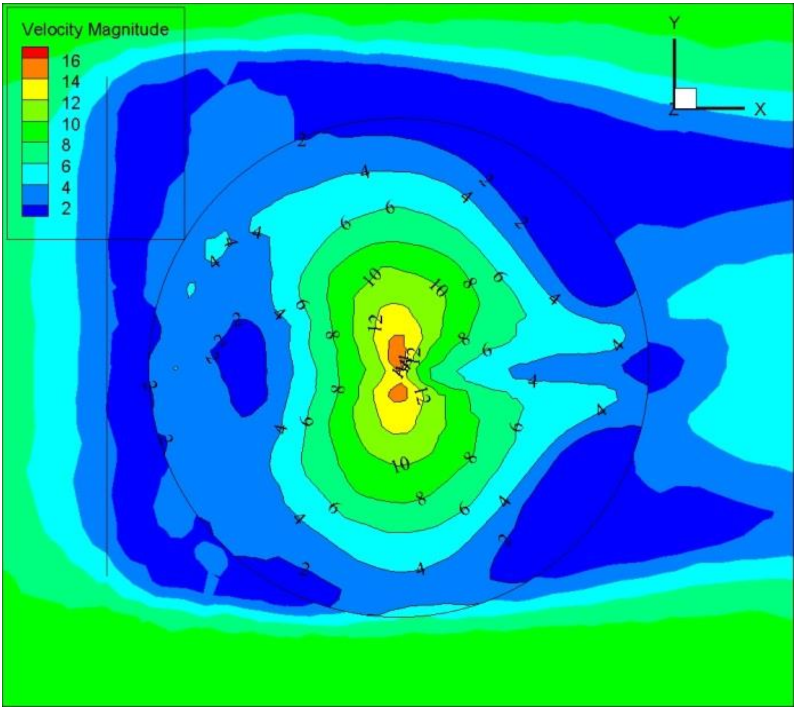

Figure 62: Speed contour on pile No. 1 (with fence barrier)

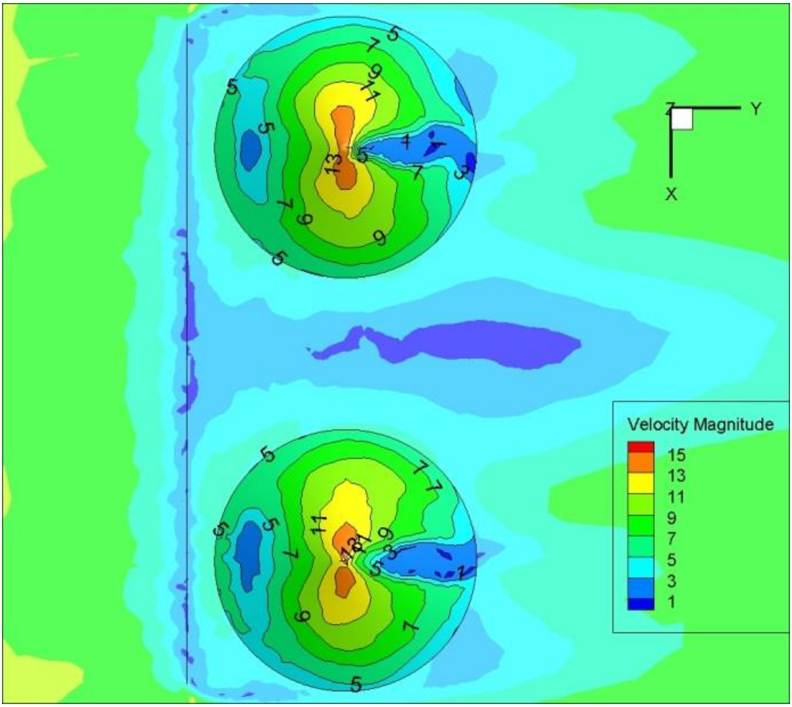

Figure 63: Speed contour on file number 2 (with solid barrier)

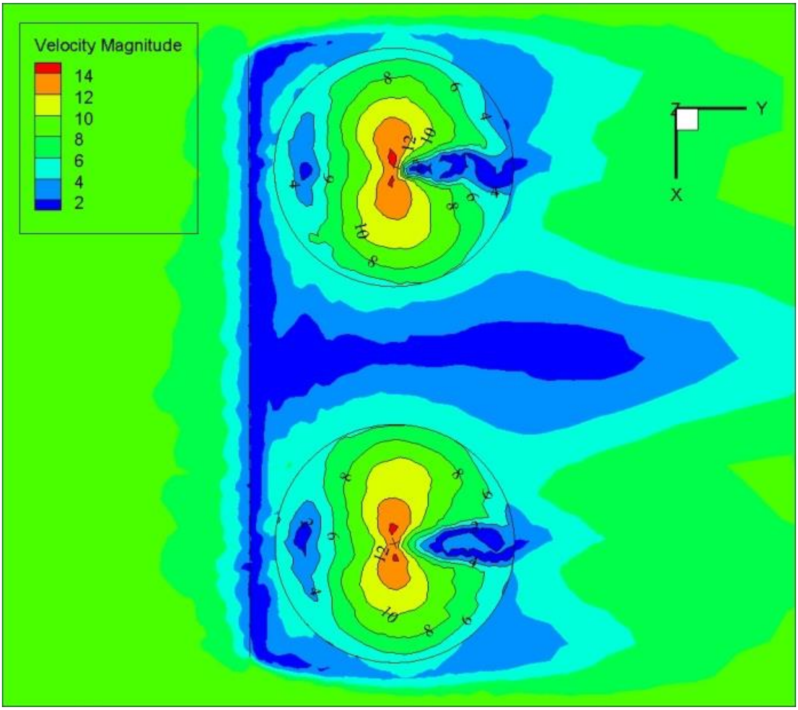

Figure 64: Speed contour on pile number 2 (with fence barrier)

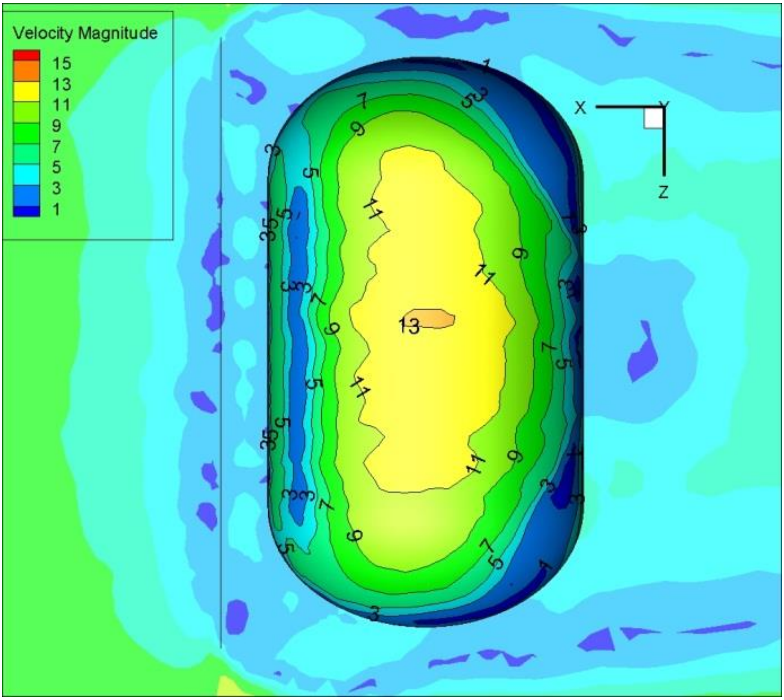

Figure 65: Speed contour on file number 3 (with solid barrier)

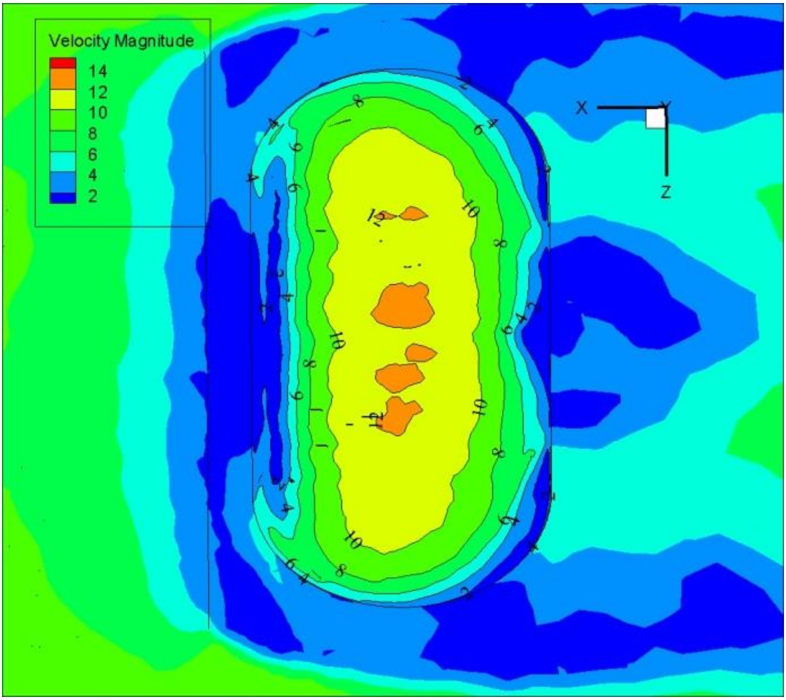

Figure 66: Speed contour on pile No. 3 (with fence barrier)

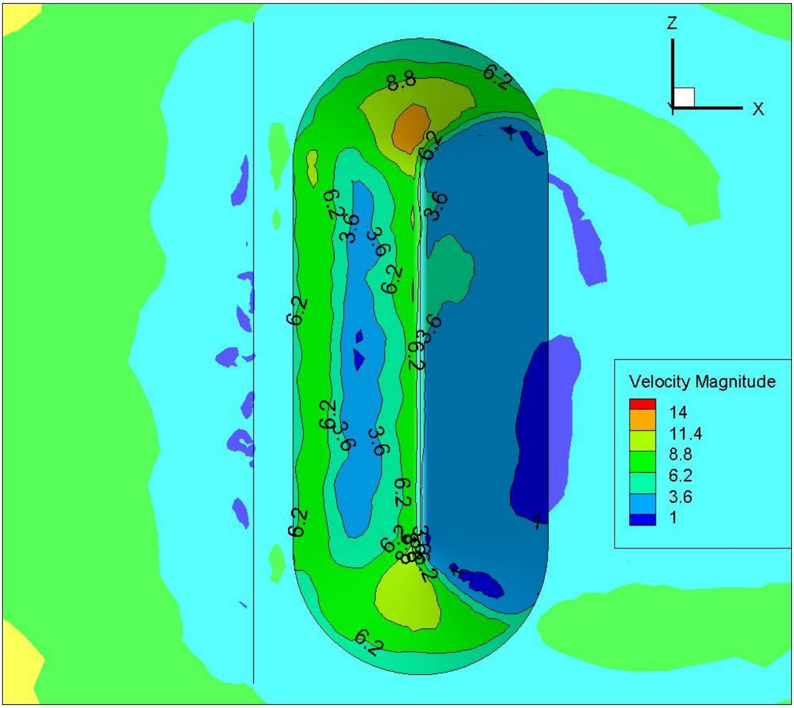

Figure 67: Speed contour on file number 4 (with solid barrier)

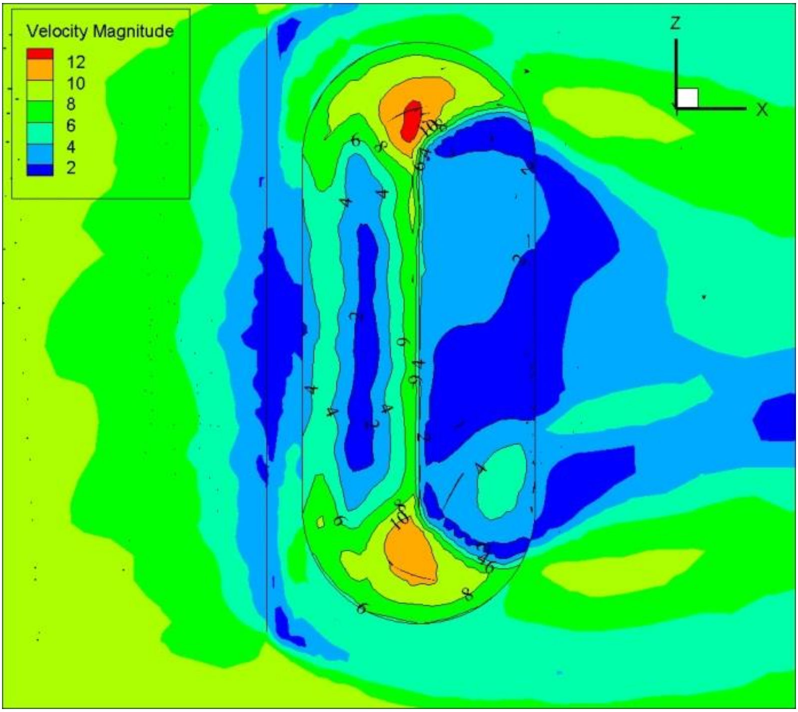

Figure 68: Speed contour on pile number 4 (with fence barrier)

In the previous section, an integrated rigid barrier was used to prevent deflation. This rigid barrier creates a high-pressure area behind the barrier, and while the velocity behind the barrier is zero and on top of the pile, the flow is flowing at a speed of about 11 meters per second, strong vortices will form in the distance between the barrier and the pile, which is the factor of scattering of particles. Another problem with these types of barriers is that due to their high surface and integrity, they create a high drag against the wind, and a very strong support must be installed to keep such barriers against the wind. The third problem of this type of obstacles is their weight. To solve these problems, it is suggested to use fences. Fences are more convenient to move because they weigh less than solid barriers. Also, due to the presence of holes on the surface of the fences, the pressure difference between the back and front of the barrier is reduced, which reduces the drag force on the barrier and reduces the possibility of its failure. The most important point in using fences is their better performance against the wind to compare to the normal barriers. The reason is, the wind flow that passes through the fence, neutralizes the eddy currents behind the barrier and weakens and makes them smaller, but the air passing through the fence depends on the wind speed and the porosity of the fence. This is shown in Figure 69 & Figure 70.

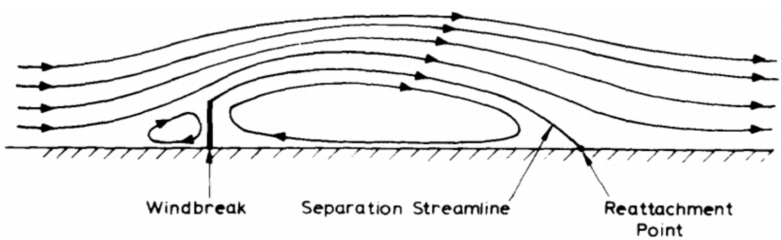

Figure 69: Flow behind an obstacle without porosity

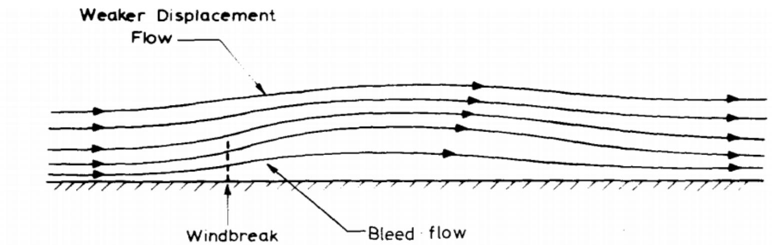

Figure 70: Flow behind a fence

Therefore, the flow behind a fence has a lower speed than the flow behind an integrated barrier. To prove this claim, one of the results of one of the researches conducted in this field is presented. In Figure 71 &Figure 72, the velocity in a plane in the direction of the wind flow with obstacle are shown. In Figure 71, the barrier is completely without the porosity, and in Figure 72, the porosity value is 0.34, and the wind speed is 11 meters per second and the height of the obstacle is 1 meter.

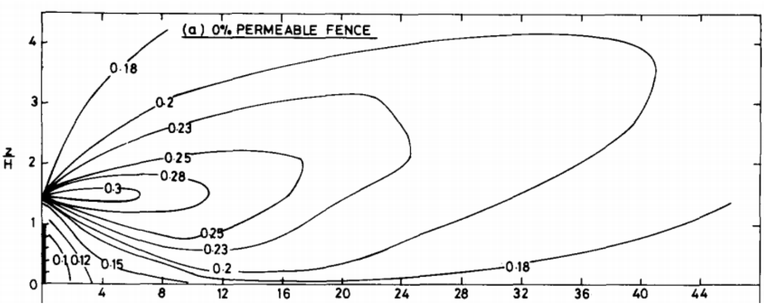

Figure 71: Dimensionless velocity for a unified barrier without porosity

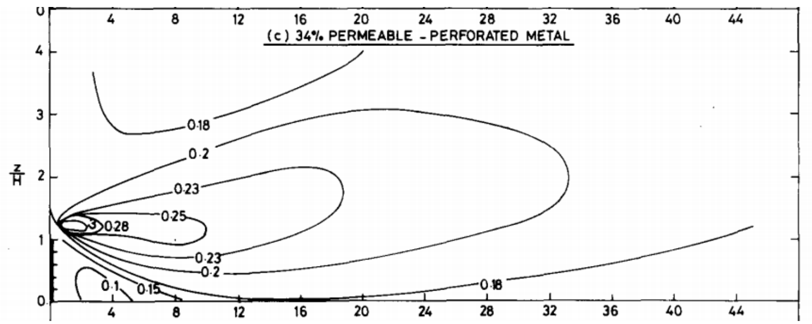

Figure 72: Dimensionless speed for the fence

As can be seen, in the case where the fence is used, the dimensionless speed, especially behind the barrier, is much lower than the barrier without porosity.

2-4-6. Determining the particles tracking from the file

After the investigations on the way of the particle tracking on the pile, we are now going to model the tracking of particles on the pile. It should be noted that this simulation was done in stable mode. In this section, a comparison has been made between different piles.

From the experimental results of Shao's research, the diameter of salt particles ranges from about 10 microns to about 200 microns. For particle distribution, we use the famous Rosin-Remler 3 distribution, which is available in the AnsysFluent software package. In Figure 73, you can see the mass of the particles.

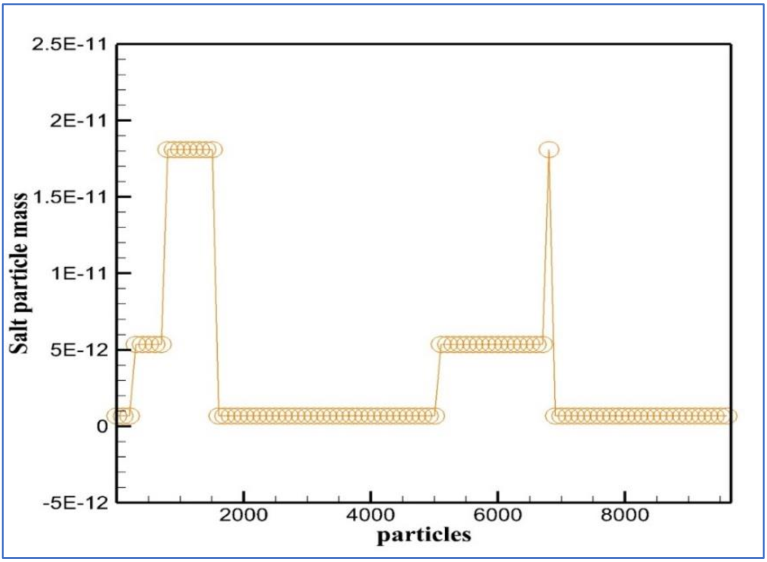

Figure 73: Distribution of particles considered for modelling based on Rosin-Remler distribution.

For each of the considered walls in the control volume of the model, particle diffusion must be defined with boundary conditions. That is, what is the behavior of the particle with the wall due to the impact of the particle with the wall. In Figure 74, the type of behavior of each wall with particles is specified, and spreading manner of particles on salt piles showing in Figure 75.

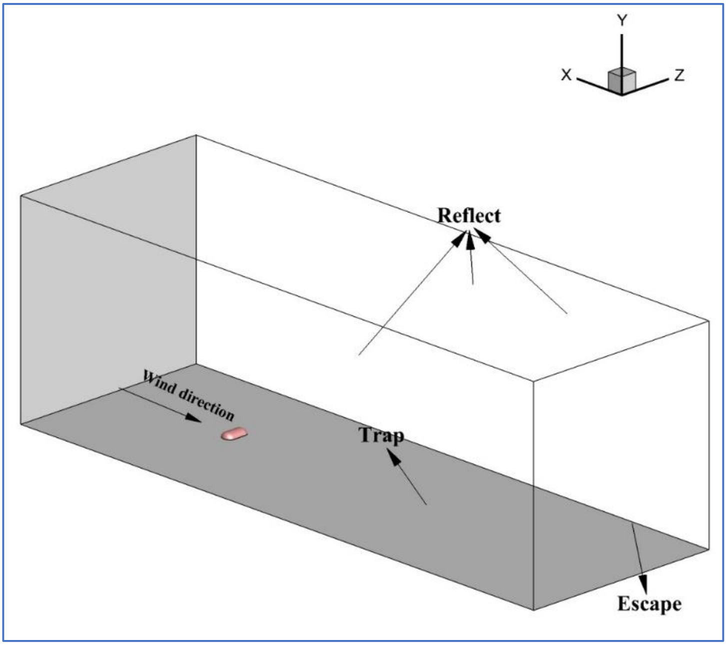

Figure 74: Boundary conditions of different walls in collision with particles

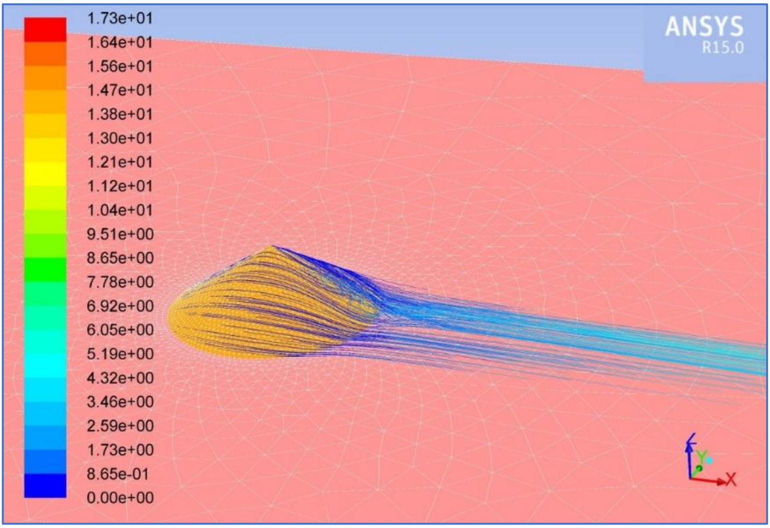

Figure 75: The spreading manner of salt particles from file number 1

In Figure 75, the color of the particles indicates the time that the particle was in the air and after this time the particle either left the end of the border or got stuck on the ground. In Table 14, a number of particles have been randomly selected and it has been checked in which part these particles are placed.

Table 14: State of particles after modeling (Pile 1)

	Out of the end of the border	Stuck on the ground	Suspended in the air	total
The number of sample particles	152	7.84	3	939
10^{-5} kg/s Mass of sample particles	1.654	7.431	0.005086	9.094

One of the most important factors that affect the amount of pollution is the length of time that the particle is suspended in the air. Table 15 shows this time on the base of statistical parameters.

Table 15: Duration of suspended particles in the air (Pile 1)

	number	**Minimum time (s)**	**Maximum time (s)**	**Average time (s)**	**Variance**
Out of the end of the border	152	14.00	21.44	15.47	1.031
Stuck on the ground	748	0.45	16.81	3.30	3.74
Suspended in the air	3	99.79	153.55	118.20	24.98

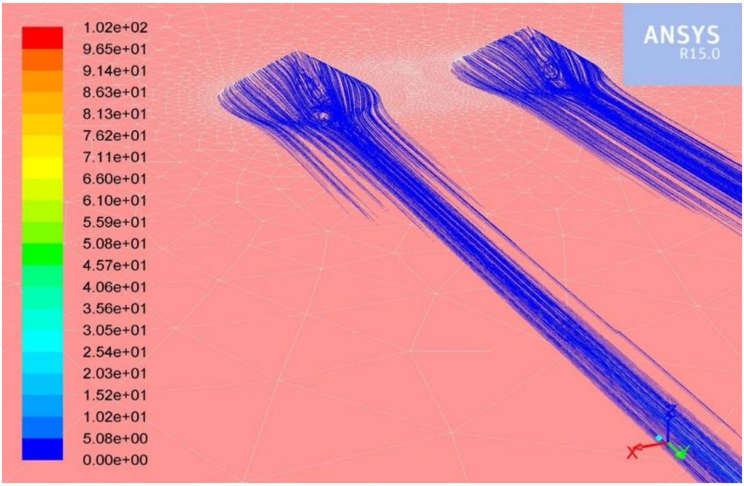

Figure 76: The manner of salt particles spreading from file number 2

Table 16: Situation of particles after modelling (Pile 2)

	Out of the end of the border	**Stuck on the ground**	**Suspended in the air**	**total**
The number of sample particles	135	1035	0	1270
10^{-5} kg/s Mass of sample particles	1.81	7.94	0	9.12

Table 17 shows the duration of the particles suspended in the air.

Table 17: Duration of suspended particles in the air (Pile 2)

Situation of particles	number	Minimum time (s)	Maximum time (s)	Average time (s)	Variance
Out of the end of the border	135	23.96	26.61	24.92	0.05
Stuck on the ground	1035	0.032	101.6	61.13	76.68

Based on the empirical relationships, pile number 3 has the lowest amount of pollution spreading among the piles (Figure 77).

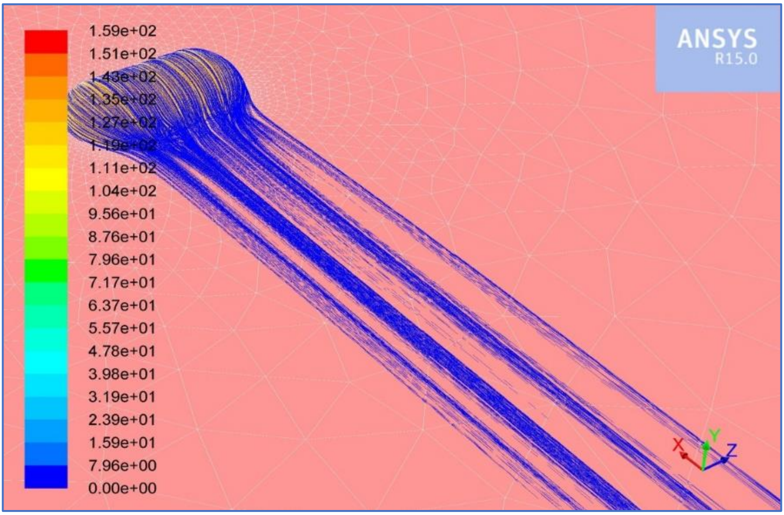

Figure 77: The manner of spreading salt particles from file number 3

The color of the particles in Figure 77 indicates the amount of time that the particles are suspended in the air. As it is clear in Figure 77, many particles get stuck on the ground while tracking and are imprisoned in the same place.

Table 18: Condition of particles after modelling (Pile 3)

	Out of the end of the border	**Stuck on the ground**	**Suspended in the air**	**total**
The number of sample particles	1	1686	1	1688
10^{-5} kg/s Mass of sample particles	0.15	9.088	0.00028	9.104

Table 19: Duration of suspended particles in the air (pile 3)

Situation of particles	number	Minimum time (s)	Maximum time (s)	Average time (s)	Variance
Out of the end of the border	1	37.12	37.12	37.12	0
Stuck on the ground	1686	0.107	25.45	5.71	5.89
Suspended in the air	1	24.15	24.15	24.15	0

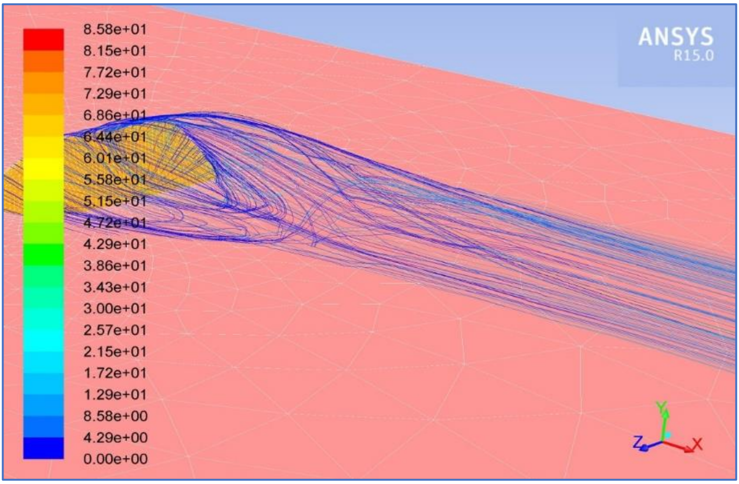

Figure 78: The manner of salt particles spreading from file number 4

In this model, the number of particles that are suspended in the air for a long time is more than other piles, and the reason for this must be presence the of eddy current behind the pile. This eddy current causes the particles move randomly in the air and causing of increasing the turbulence of the flow.

Table 20: Situation of particles after modeling (Pile 4)

	Out of the end of the border	**Stuck on the ground**	**Suspended in the air**	**total**
The number of sample particles	714	218	34	966
10^{-5} kg/s Mass of sample particles	6.75	2.12	0.22	9.106

Table 21: Duration of suspended particles in the air (Pile 4)

Situation of particles	number	Minimum time (s)	Maximum time (s)	Average time (s)	Variance
Out of the end of the border	714	24.72	62.67	28.76	4.98
Stuck on the ground	218	0.038	12.91	1.21	1.71
Suspended in the air	34	14.53	108.80	37.29	26.30

2-4-7. Investigating the effect of the shape of dust particles on their pollution level

To investigate the effect of the shape of the particles, one must first define a parameter that differentiates between different shapes of the particles. This parameter is called shape factor and will be defined as follows.

$$a = \frac{S'}{S}$$

In this relation, S' indicates the outer surface of the particle and S indicates the surface of a spherical particle with the same volume. Among the volumes with a specific volume, the circle has the least amount of surface, therefore S is always smaller than S' and the value of the shape coefficient will always be greater than one. The value of the shape coefficient for a spherical object will be 1. To compare the shape coefficient, several different shapes are listed in the Table 22.

Table 22: Values related to particle shape coefficient

Shape of particles	**Shape coefficient**
Spherical	1
Regular tetragonal	1.49
Regular hexagonal	1.24
Regular octahedral	1.18
Disc shape	> 1.15

To investigate the effect of the shape of the particles, Pile No. 4 is modeled with particles with a shape coefficient of 1.24. In this modelling, it is assumed that the salt particles are not spherical but regular hexagonal (Table 23).

Table 23: Examining the effect of particle shape on emission rate

Situation of particles	**Spherical particles**	**Hexagonal particles (a=1.24)**
Out of the end of the border	714	715
Stuck on the ground	218	218
Suspended in the air	34	33

2-4-8. Investigating the effect of increasing humidity on the amount of deflation

In this section, the effects of particle moisture on the threshold friction speed will be investigated. An increase in humidity causes an increase in density and, as a result, a decrease in buoyancy, and on the other hand, when the humidity of salt minerals increases, it will cause changes in the morphology of the particle and, as a result, it will become loose, which the second factor acts against the previous factor. Now, the effect of each of the above factors will be examined. Clay-sized sedimentary particles, which exist mainly as interlayers within salt layers, are effective in this subject.

Ravi et al., (2006) investigated the effect of increasing humidity on friction speed in a wind tunnel. It is worth noting that as the fluid humidity increases, the surface humidity also increases.

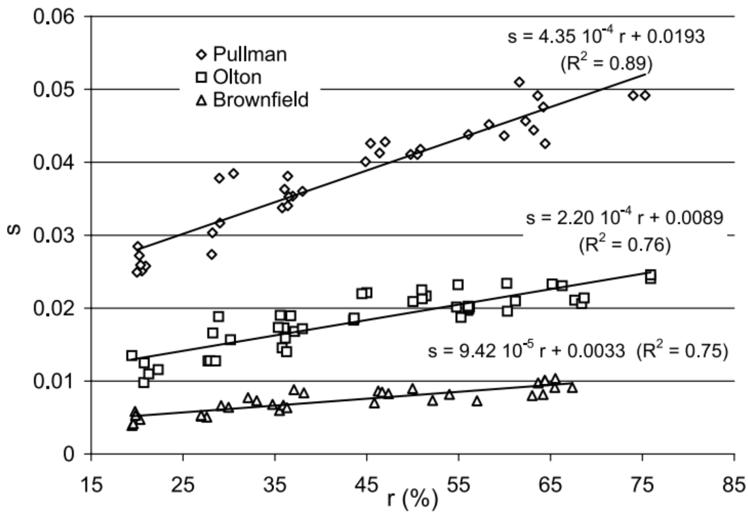

Figure 79: Surface humidity (S) based on relative air humidity (r)

Figure 79 shows that with the increase of the relative humidity of the air, the amount of surface humidity increases almost linearly for different compositions. The studied material consists of different percentages of clay, mud, sand, and results of tests are values shown in Table 24, and Figure 80 & Figure 81 & Figure 82.

Table 24: Compounds used in investigating the effects of humidity

Clay %	Mud %	Sand %	Compound
31	26	43	Pullman
17	13	10	Olton
8	0	92	Brown field

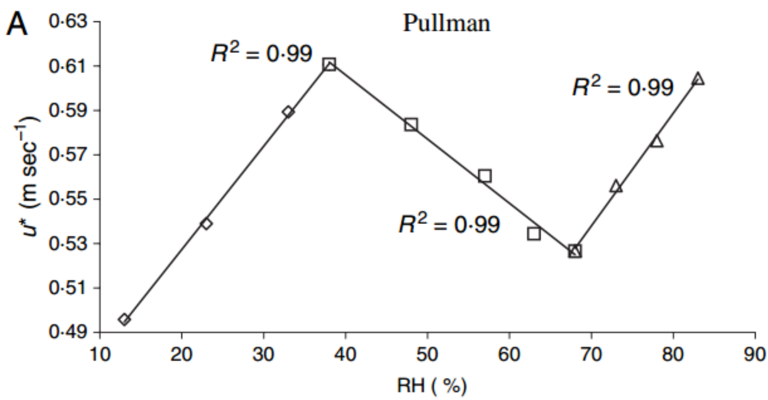

Figure 80: Experimental results of threshold friction speed for Pullman

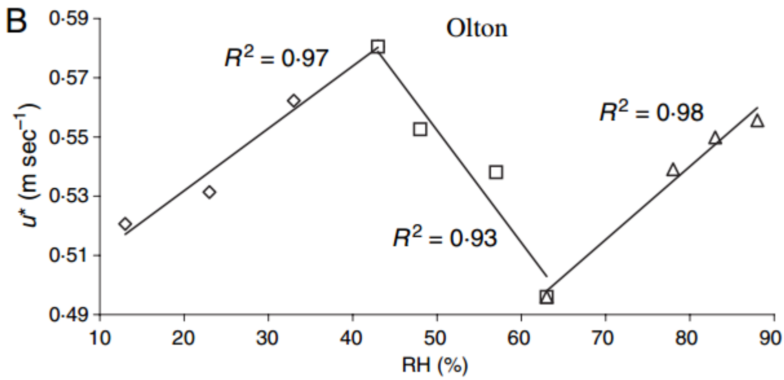

Figure 81: Experimental results of threshold friction speed for Olton

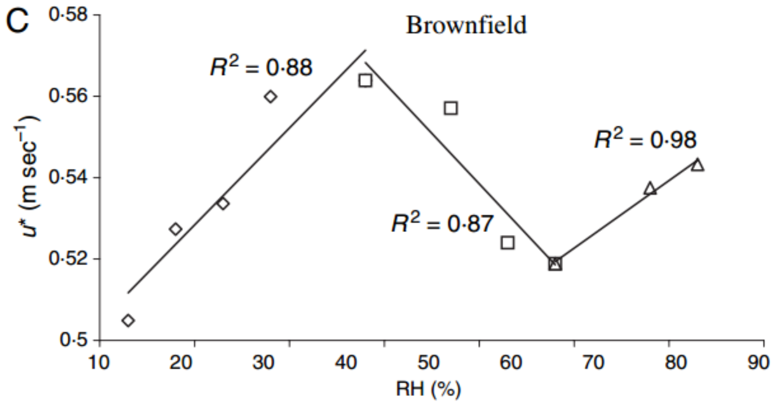

Figure 82: Experimental results of threshold friction speed for Brownfield

These results show that with the increase of relative humidity between 40 and 65 percent, the value of the threshold friction speed decreases. This phenomenon is the result of the loosening of the surface grafting between the molecules of the surface particles, but in the rest of the values, the value of the threshold friction speed increases with the increase of the relative humidity. This theory shows that in the relative humidity between 40 and 65 percent, the effect of particle swelling is more than the increase of its density, but for dry particles (relative humidity less than 3 percent), F increasing of moisture causes an increase in the frictional speed of the threshold, and as a result, it causes more stability.

2-5- ADMS software

This software is one of the most powerful software available for modelling air pollution. This software is designed based on the Gaussian model, which can be considered both Eulerian and Lagrangian.

The stages of model preparation and implementation include activating a number of algorithms required in the model, entering information on pollutant sources, meteorological and topographical data, as well as calibrating the model. The output of the model also includes the short-term or long-term average concentration of the desired pollutants. In the following section, there are explanations related to each of the stages of model preparation and implementation.

The ADMS model includes following algorithms:

- ✓ Topographic relief;
- ✓ Wet sedimentation;
- ✓ Gravitational and dry sedimentation;
- ✓ Short-term fluctuations in concentration;
- ✓ Spreading from directed sources;
- ✓ Time averages from very small time intervals (seconds) to yearly;
- ✓ Chemical reactions;
- ✓ Radioactive decays and gamma ray dose;

It is worth noting that the mentioned algorithms will be activated only if needed.

2-6- Meteorological Information

The most important meteorological information used for modelling are speed and wind directions, together with additional data, such as rate of precipitation, humidity, temperature and amount of cloudy days. These data must be prepared in order to use in software.

Due to the expansiveness of the study area, only meteorological informations of Ajabshir, Urmia and Salmas cities analyzed and used for particles dispersion modelling.

Figure 83 &Figure 84 & Figure 85 indicating the rose-wind of Ajabshir, Urmia and Salmas cities. It can be seen that prevailing wind for Salmas (NW of lake) is north to west, semi-prevailing wind is west to east, for Ajabshir (SE lake) prevailing wind is west to east and semi-prevailing is southeast to northwest, and finally for Urmia (west of lake) prevailing wind is west to east.

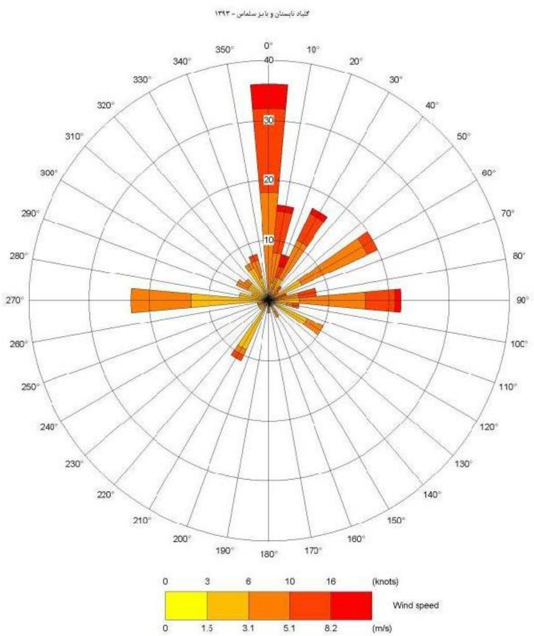

Figure 83: Selmas wind rose (summer and autumn 2014)

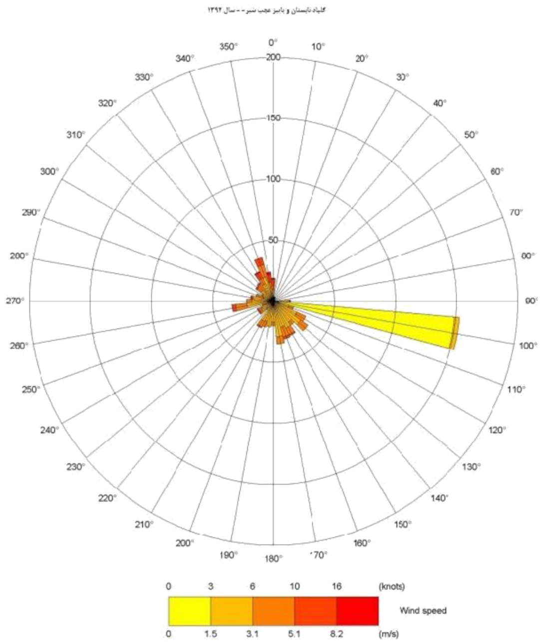

Figure 84: Ajab Shir wind rose (summer and autumn 2014)

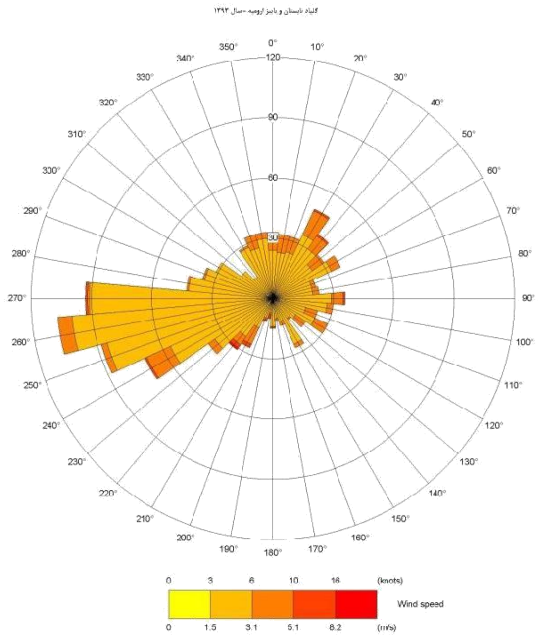

Figure 85: Urmia wind rose (summer and autumn 2014)

As a result, it can be observed that prevailing wind in Summer and Autumn is from land towards the lake (Figure 86).

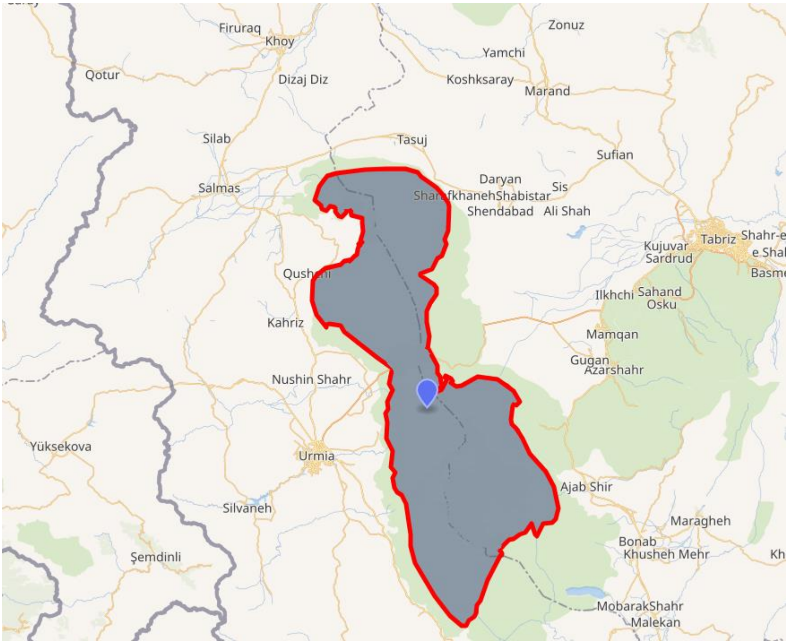

Figure 86: The location of Urmia Lake and its surrounding cities

2-7- Topographical Data

Topographical data taken from **srtm.esi.cqiar.org site**. Topographic relief and area of study show in (Figure 87). The input file model consists of 4 columns, including series number, longitude, latitude and altitude, based on the UTM geographical coordinates. For this purpose, user should select **complex terrain** in this page (Figure 88). The page of entering information related to topography of the region in the ADMS software.

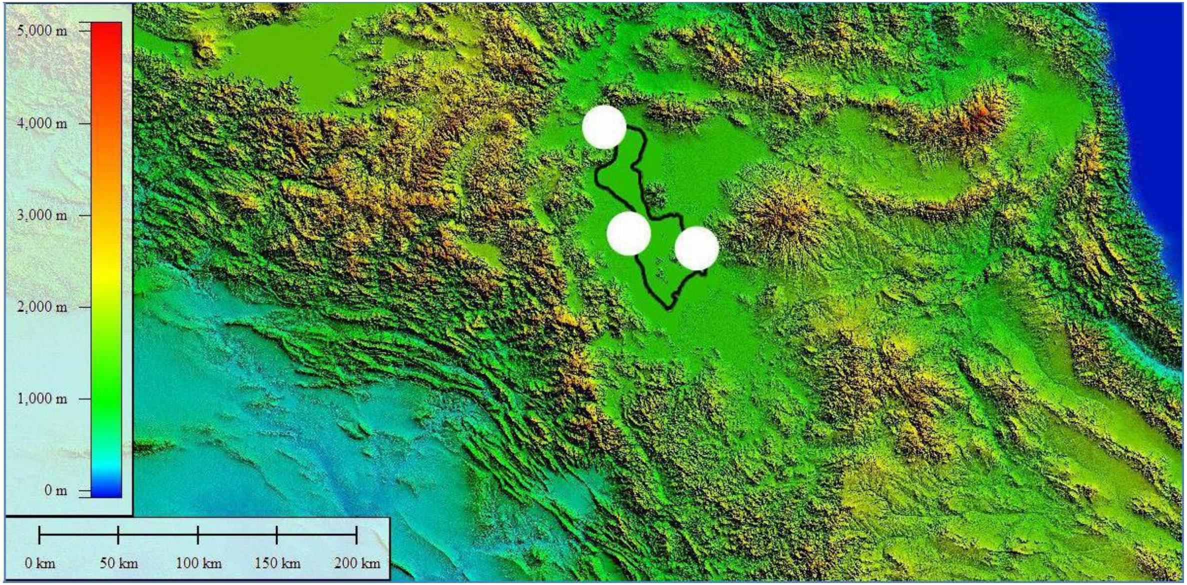

Figure 87: Tif file of land features around Lake Urmia (the studied areas are marked with white circles)

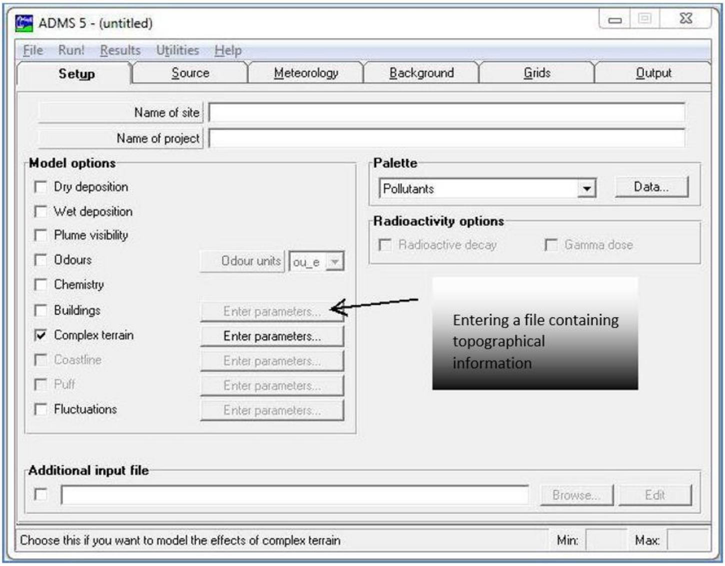

Figure 88: The page of entering information related to the topography of the region in the ADMS software

As mentioned earlier, three area selected around the Urmia Lake, for particles dispersion modelling. For all three areas, one supposed salt recovery zone selected with the specifications. Then based on the topographical data and information of nearest meteorological station, particles dispersion modelling accomplished.

The obtained results of modelling, based on the ADMS software, by using surfer software, shown under the circumstance of particles distribution. In this part of the studied area we also used the Google Earth software and Google Map site.

2-8- Qobadlu Coast Modelling

The nearest meteorological station to this area, located in Ajabshir city. This area is one of the locations for salt recovery (Figure 89). Coordinates of a supposed mine in Qobadlu coast shown in Table 25. The, coordinates considered for the supposed mining area have been shown in Table 26. The results of particles spreading modelling and related wind-rose are presented in Figure 99 to Figure 103.

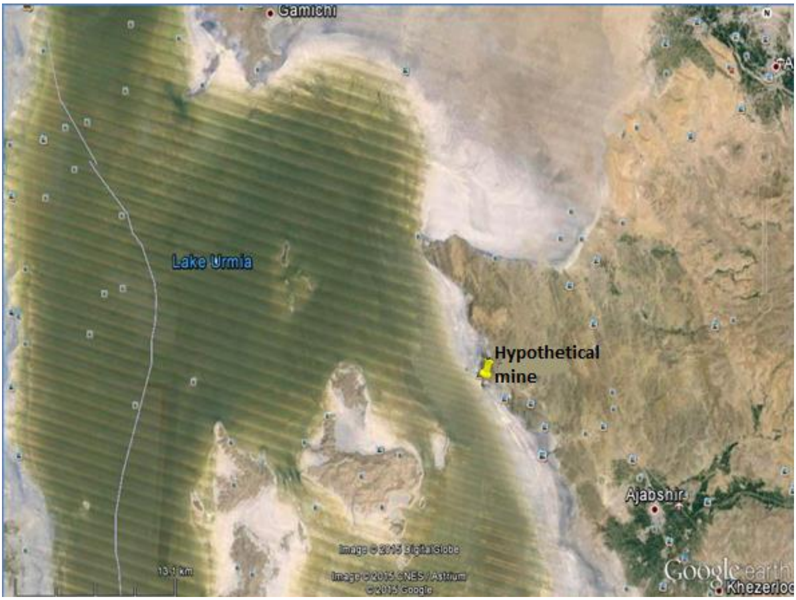

Figure 89: The studied area in the southeast of Urmia Lake (Qobodlu beach)

Table 25: Hypothetical base coordinates of salt extraction in Qobodlu beach

Coordinates	Head number				Area (District)
	1	2	3	4	
X	564232	564240	564270	564261	38S
Y	4155585	4155593	4155560	4155552	

Table 26: Coordinates of the desired area in the modelling of Qobodlu beach

Coordinates	min	max	Area (District)
X	562908	565908	38S
Y	4156955	4153955	

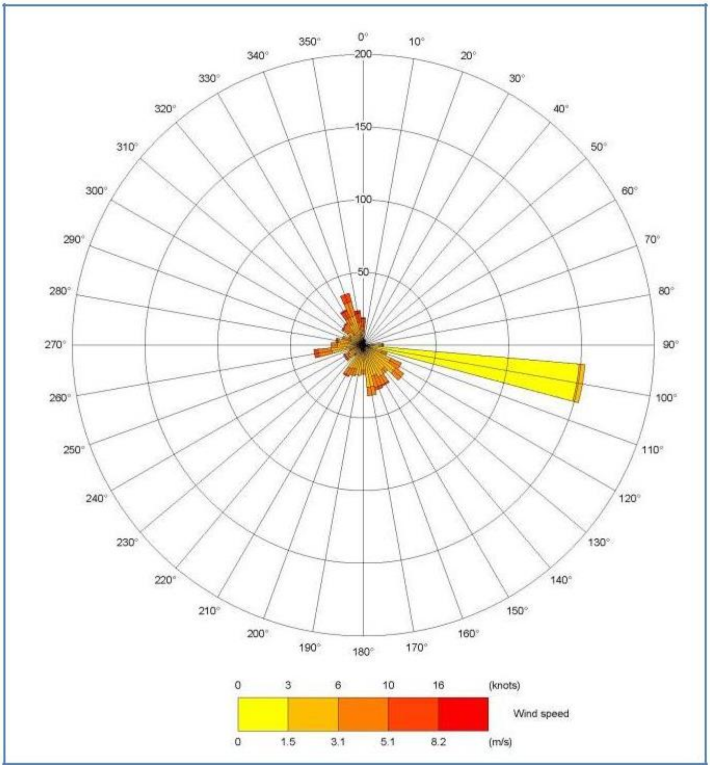

Figure 90: Ajab Shir wind rose (summer and autumn 2014)

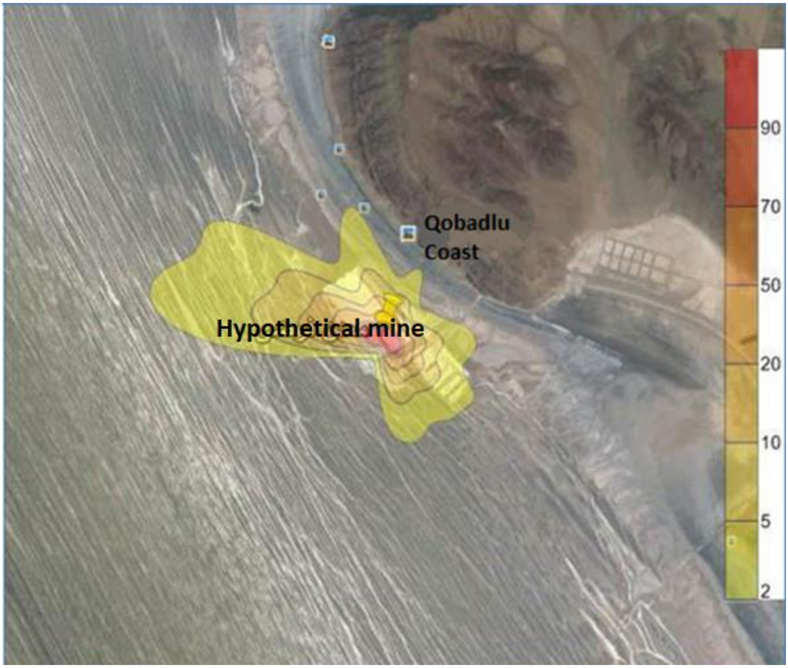

Figure 91: The distribution of particles in Qobadlu coast (summer and autumn 2014)

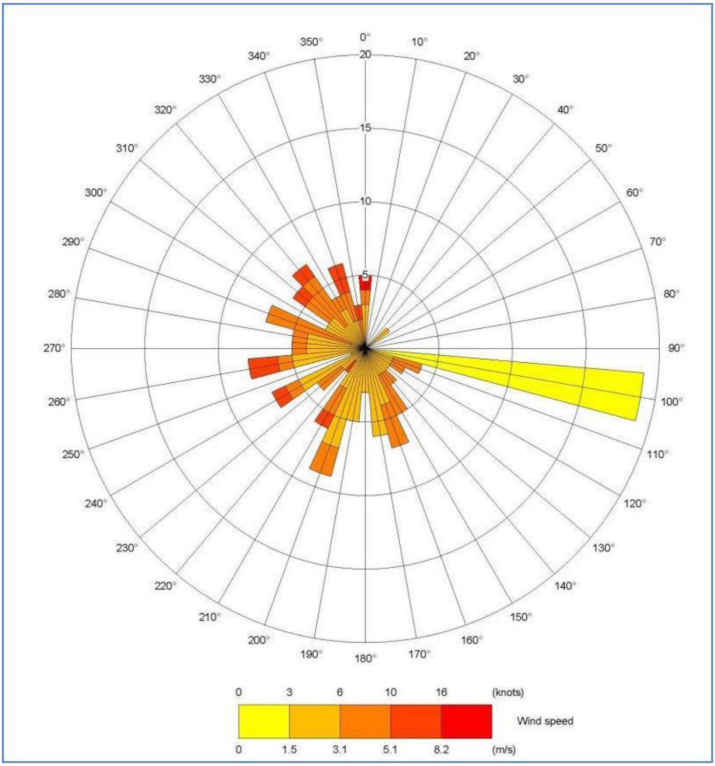

Figure 92: Ajab Shir wind rose (July 2014)

Figure 93: How particles are distributed in Qobadlu coast (July 2014)

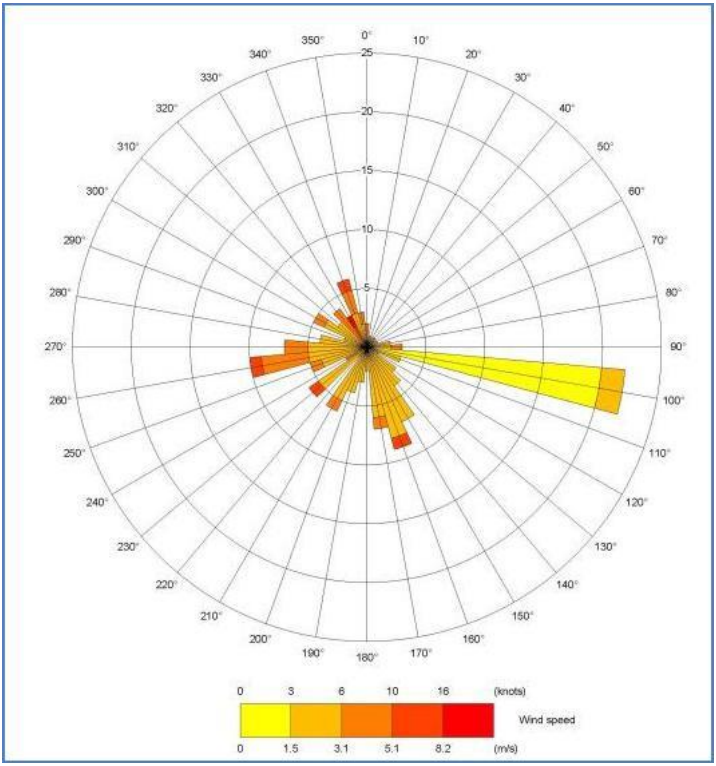

Figure 94: Ajab Shir wind rose (August 2014)

Figure 95: How particles are distributed in Qobadlu coast (August 2014)

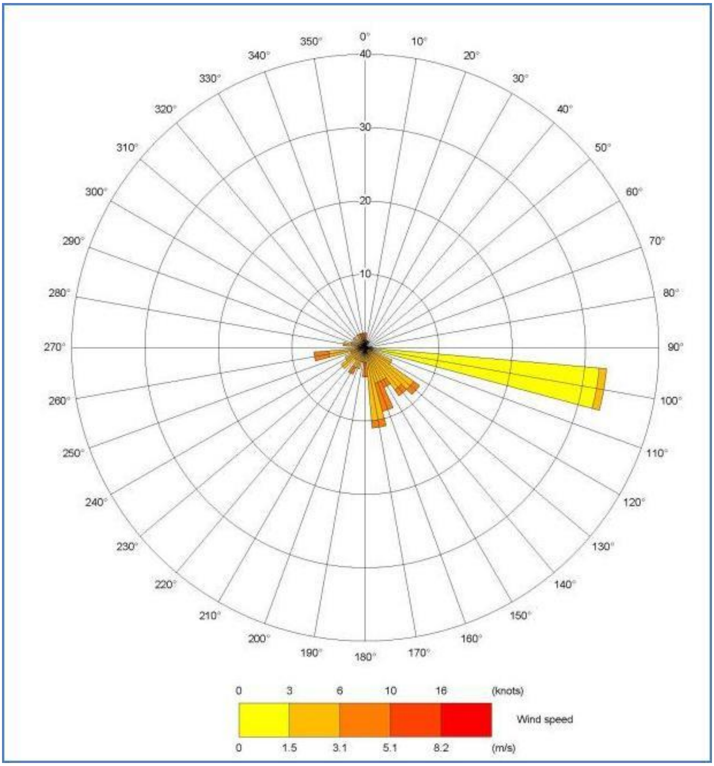

Figure 96: Ajab Shir wind rose (September 2014)

Figure 97: The distribution of particles in Qobadlu coast (September 2014)

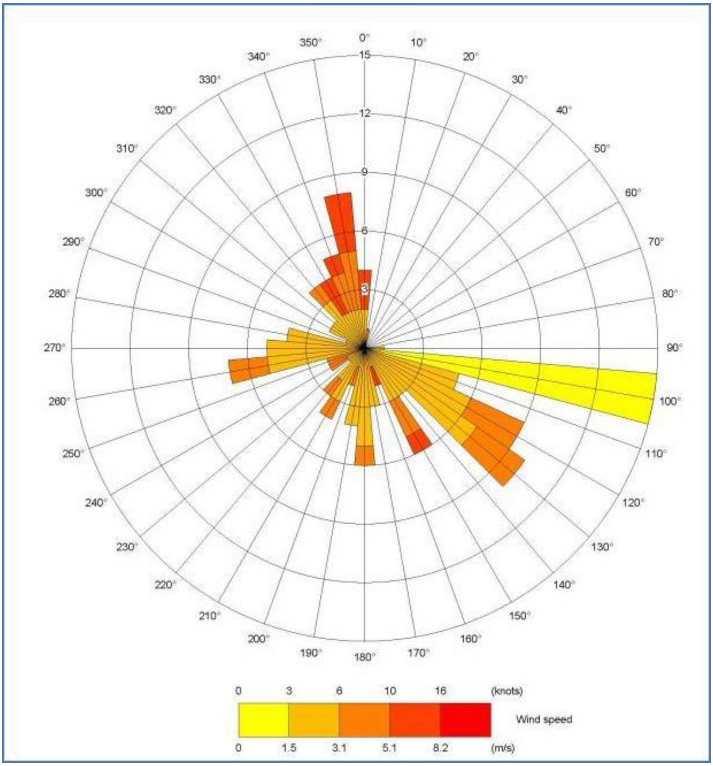

Figure 98: Ajab Shir wind rose (October 2014)

Figure 99: How particles are distributed in Qobadlu coast (October 2014)

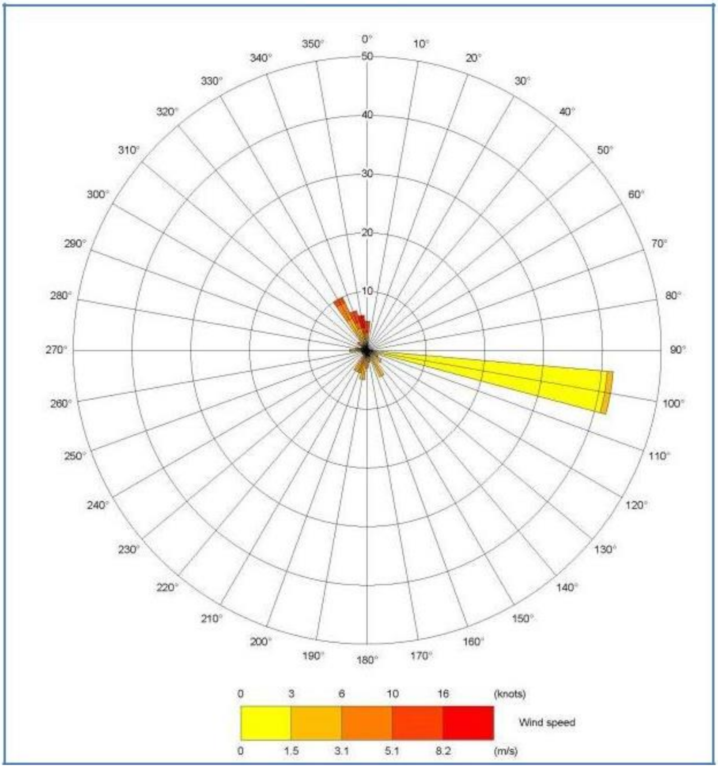

Figure 100: Ajab Shir wind rose (November 2014)

Figure 101: The distribution of particles in Qobadlu coast (November 2014)

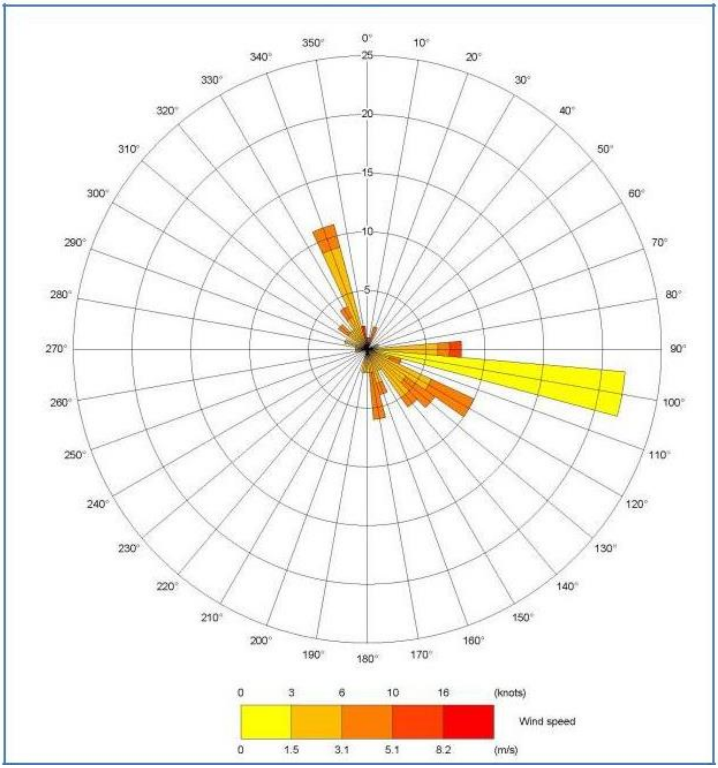

Figure 102: Ajab Shir wind rose (December 2014)

Figure 103: How particles are distributed in Qobadlu coast (December 2014)

As can be observed from the dispersion of particles in Qobadlu coast, it is clear that spreading of dispersed particles is during Summer and Autumn towards the lake. In other words, released particles resulted from the salt recovery process, scattered towards west and northwest.

It is also clear that, by moving away from the source of particles, spreading (even 100 to 200 m), the concentration of pollutant reduced and reaches less than

5 micro gr/cm^3. The maximum emission of dispersed particles towards land occurring in July, August, and minimum extension is in October, November. In other words, based on the result modelling, the extension of dispersed particles in October, December is more towards the lake.

2-9- Urmia Coast Modelling

The city of Urmia is located west of the Urmia Lake (Figure 104). Coordinates of a supposed salt recovery area and coordinates of studied are presented in Table 27 & Table 28 respectively.

Figure 104The studied area in the west of the Urmia lake (coast of Urmia city)

Table 27: Coordinates of the hypothetical range of salt extraction in the coast of Urmia city

Coordinates	Head number				Area (District)
	1	2	3	4	
X	525300	525345	525346	525301	38S
Y	4157640	4157646	4157632	4157627	

Table 28: Coordinates of the desired area in the modeling of Urmia city beach

Coordinates	min	max	Area (District)
X	523820	526819	38S
Y	4159128	4156136	

In continuation, the results of particles spreading modelling during Summer and Autumn 2014 and separately for each month, and related rose wind are presented (Figure 105 to Figure 118).

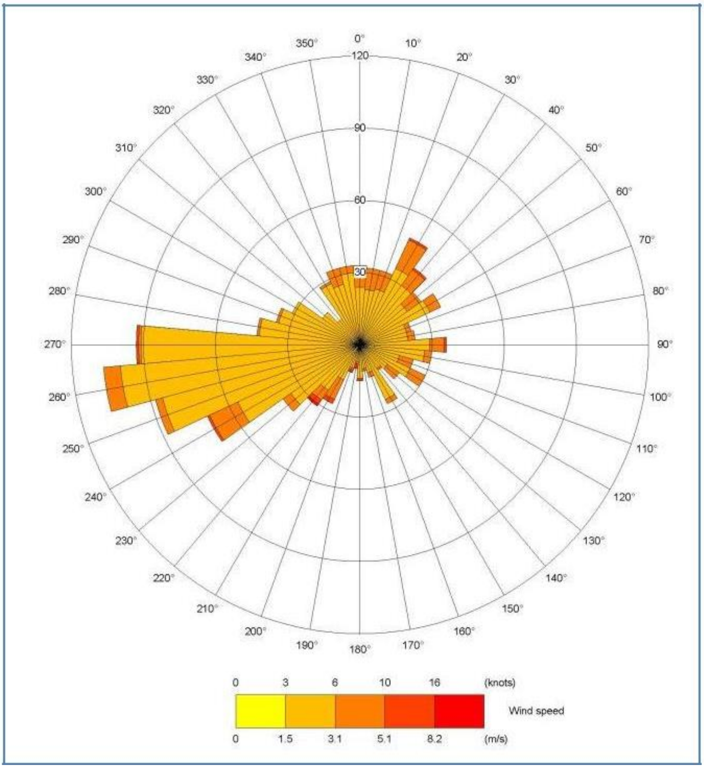

Figure 105: Urmia wind rose (summer and autumn 2014)

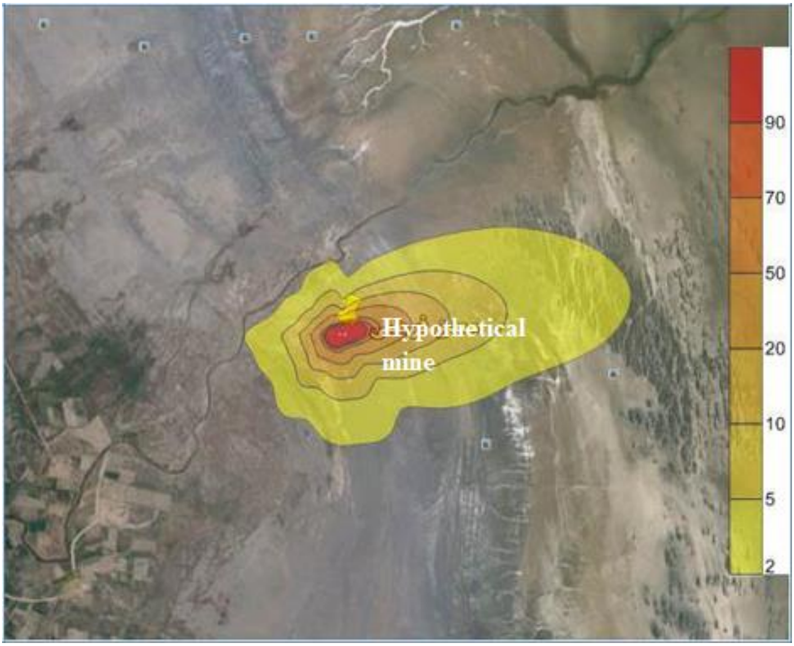

Figure 106: The distribution of particles on the coast of Urmia city (summer and autumn 2014)

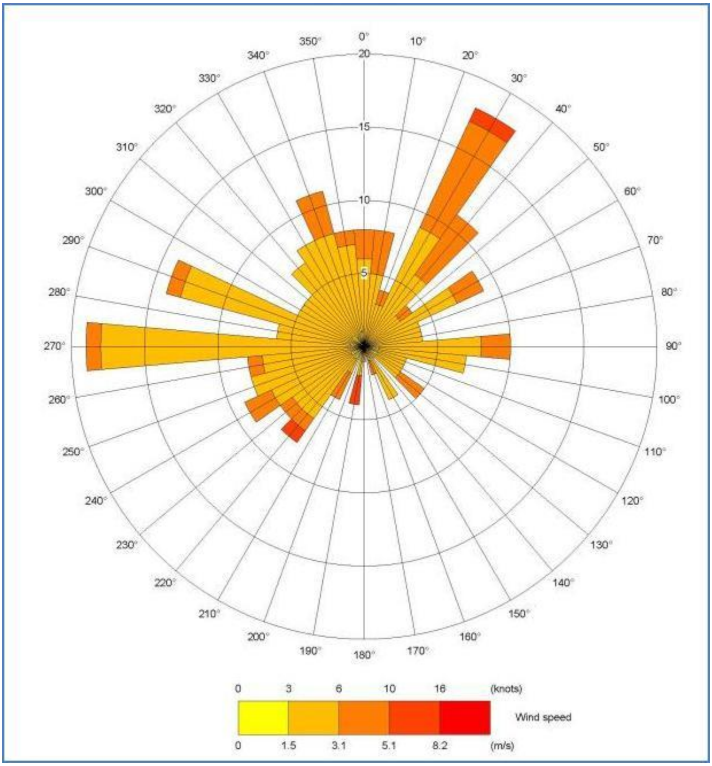

Figure 107: Urmia wind rose (July 2014)

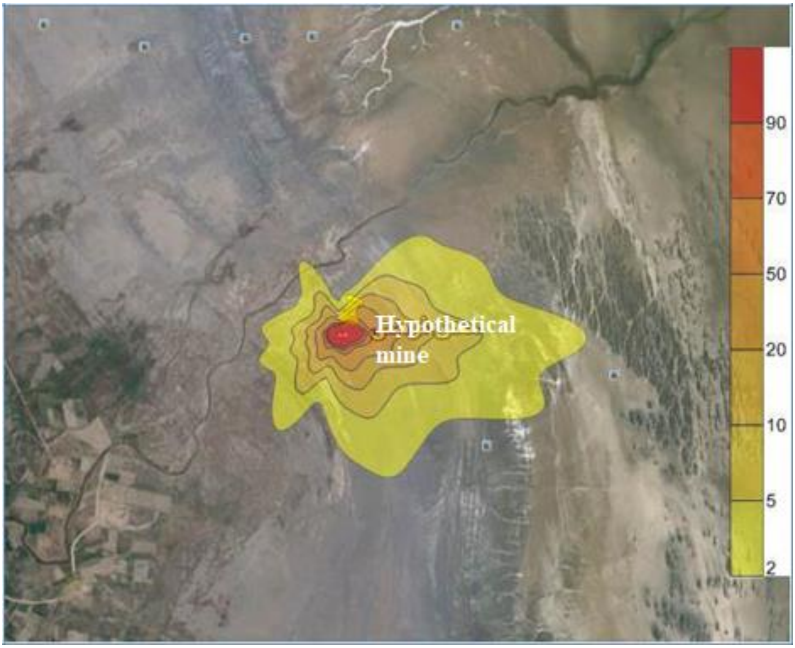

Figure 108: The distribution of particles on the coast of Urmia city (July 2014)

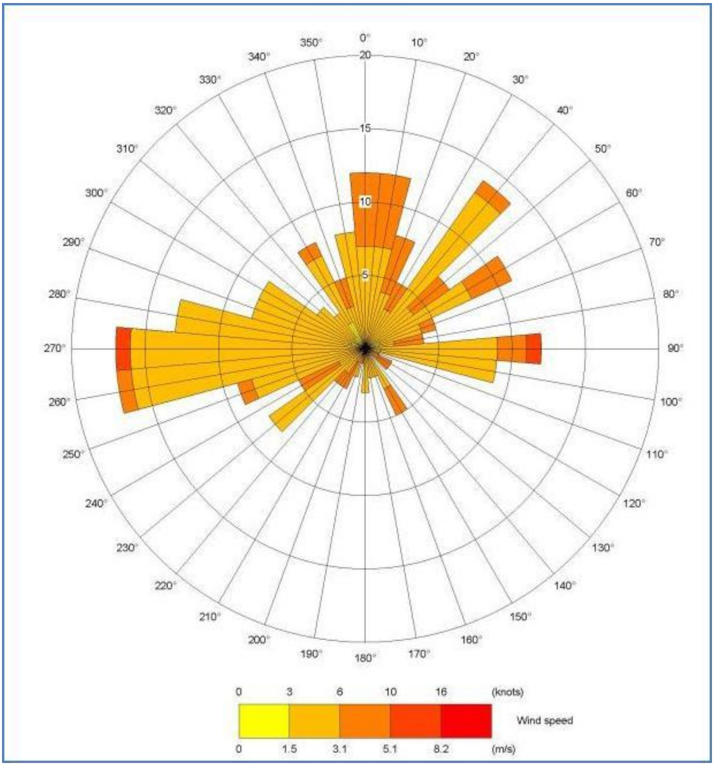

Figure 109: Urmia wind rose (August 2014)

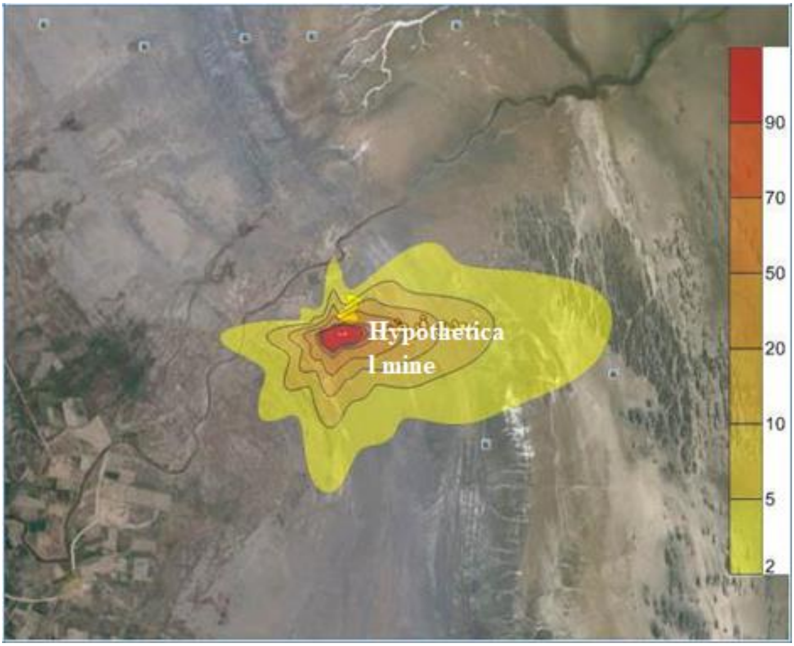

Figure 110: The distribution of particles on the coast of Urmia city (August 2014)

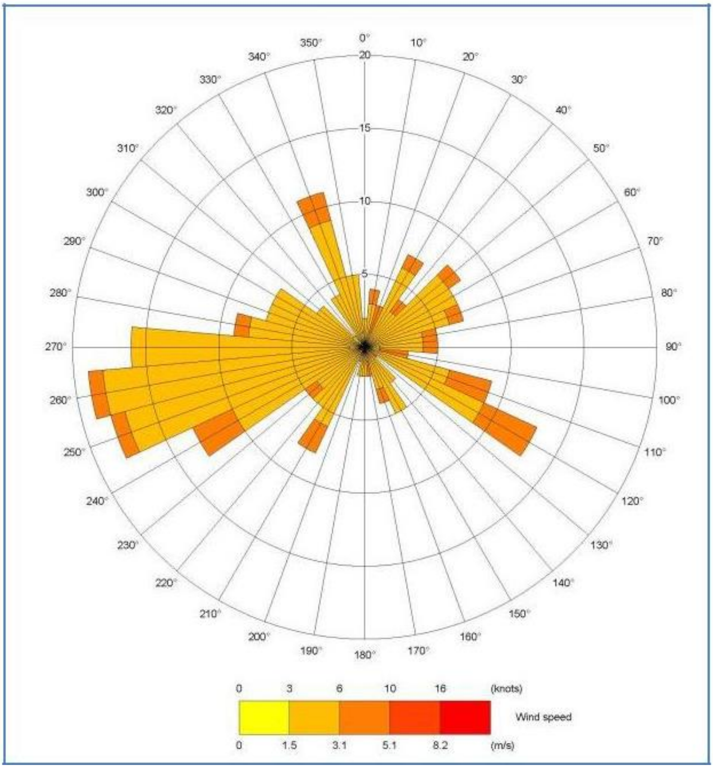

Figure 111: Urmia wind rose (September 2014)

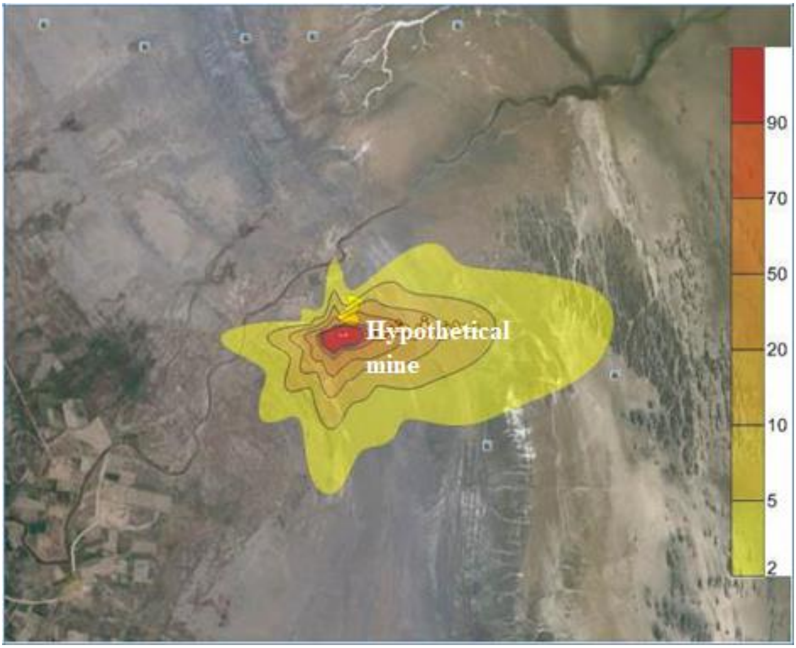

Figure 112: The distribution of particles on the coast of Urmia city (September 2014)

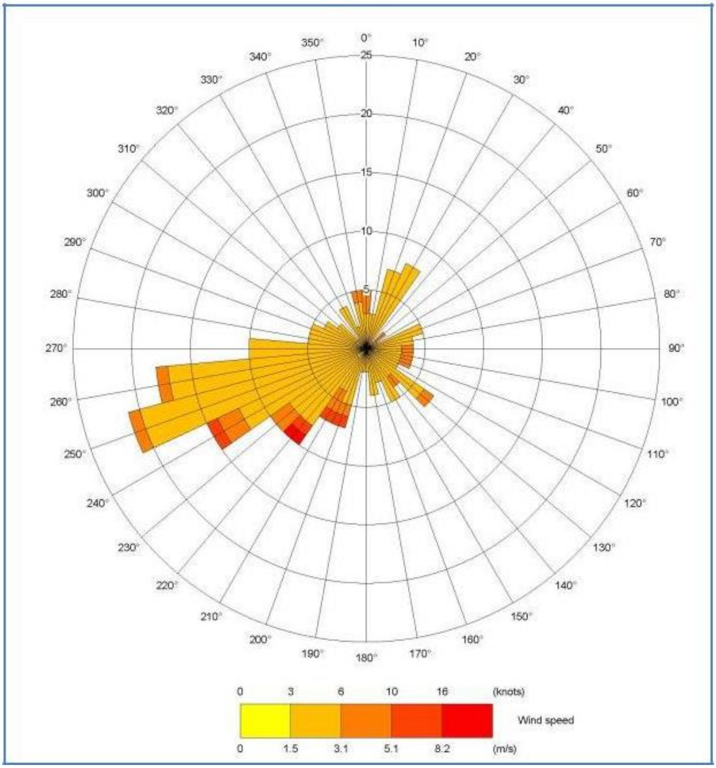

Figure 113: Urmia wind rose (October 2014)

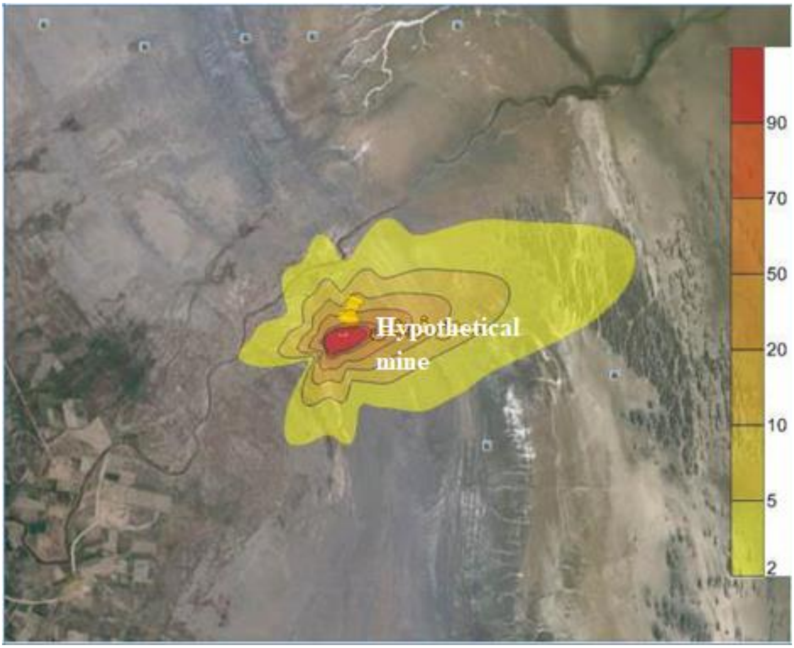

Figure 114: The distribution of particles on the coast of Urmia city (October 2014)

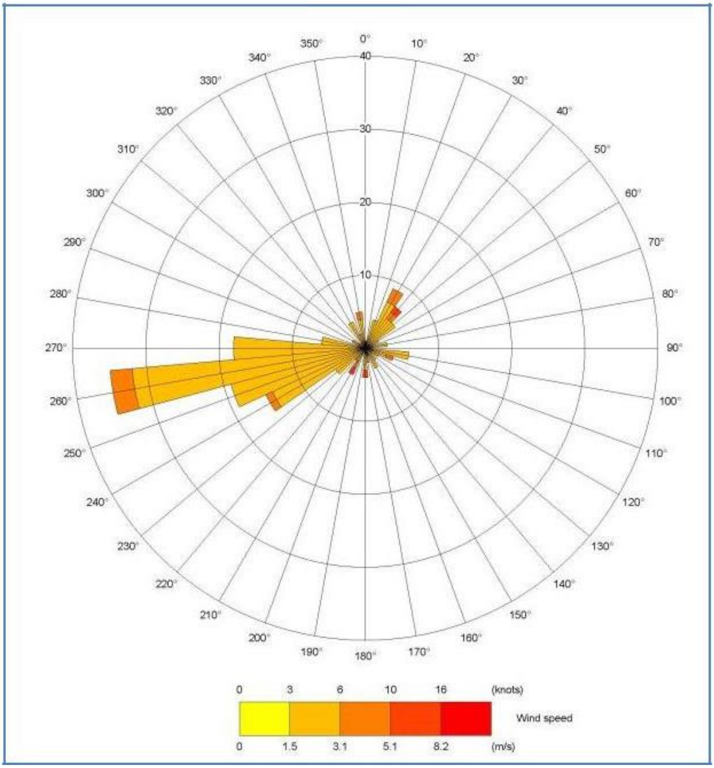

Figure 115: Urmia wind rose (November 2014)

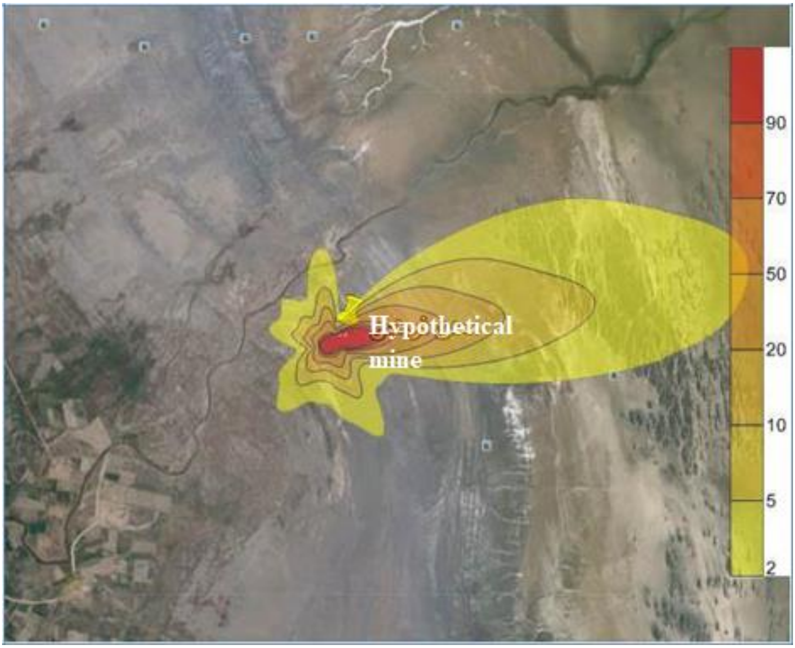

Figure 116: The distribution of particles on the coast of Urmia city (November 2014)

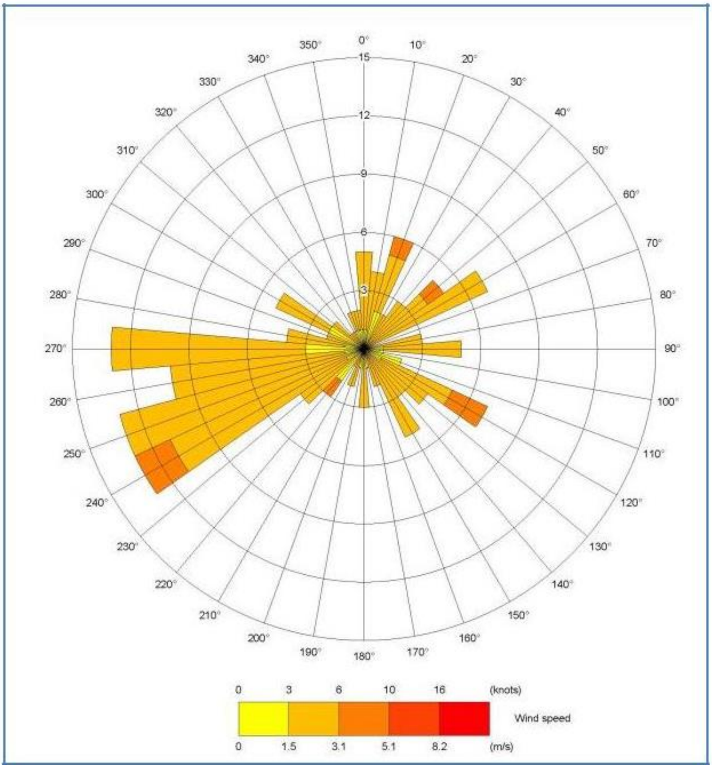

Figure 117: Urmia wind rose (December 2014)

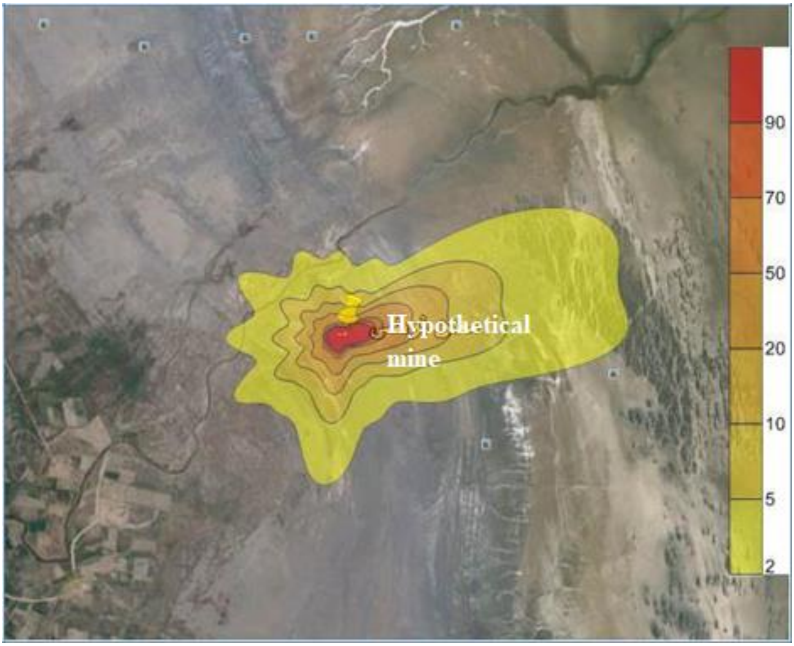

Figure 118: The distribution of particles on the coast of Urmia city (December 2014)

In this zone, extension of dispersed particles during the Summer and Autumn are eastward (i,e, towards the lake), and particles dispersion, towards land is very low, so that at a very short distance from salt mining zone in land side (about 100 to 150 m), the concentration of particles become very low.

The maximum extension of particles during August and September are westwards (inland), and minimum extension of particles occurring during October and November.

Based on the available wind roses, it can be seen that during Autumn, wind directions are almost uniform than in Summer, and prevailing wind is west to east.

2-10- Modelling of the NW side of the Lake (North of Qarabagh)

In order to study the particles spreading around the entire of lake resulting from salt mining, this area also, selected for investigation, by using the Salmas meteorological information (Figure 119).

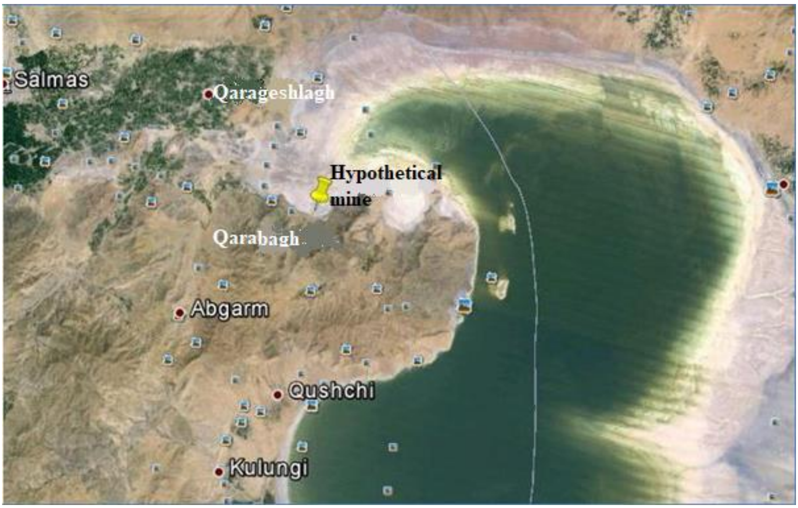

Figure 119: The studied area in the northwest of Lake Urmia (north of Qarabagh village)

Coordinate of a hypothetical salt recovery piles, and coordinates of studied area are given in Table 29 & Table 30 respectively.

Table 29: Coordinates of the hypothetical range of salt extraction on the north coast of Qarabagh village

Coordinates	Head number				Area (District)
	1	2	3	4	
X	505091	505098	505132	505125	38S
Y	4219833	4219843	4219815	4219806	

Table 30: Coordinates of the desired range in modeling the northwest coast of Lake Urmia (north of Qarabagh village)

Coordinates	min	max	Area (District)
X	503108	507108	38S
Y	4221826	4217826	

In continuation, the results of particles spreading modeling in NW coast of Urmia for Summer and Autumn and separately for each month and related wind rose are presented (Figure 120 toFigure 133).

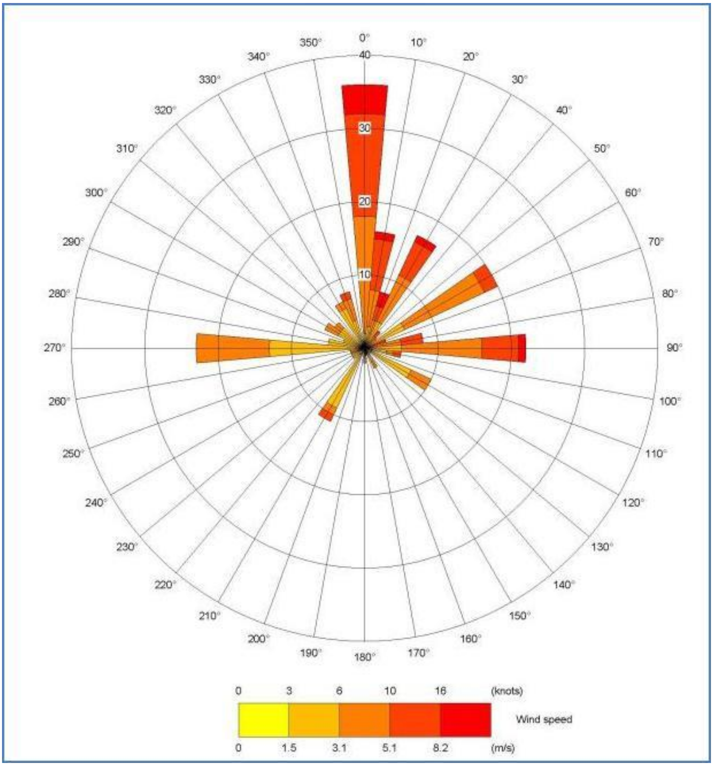

Figure 120: Salmas wind rose (summer and autumn 2014)

Figure 121: The distribution of particles in the north coast of Qarabagh village (summer and autumn 2014)

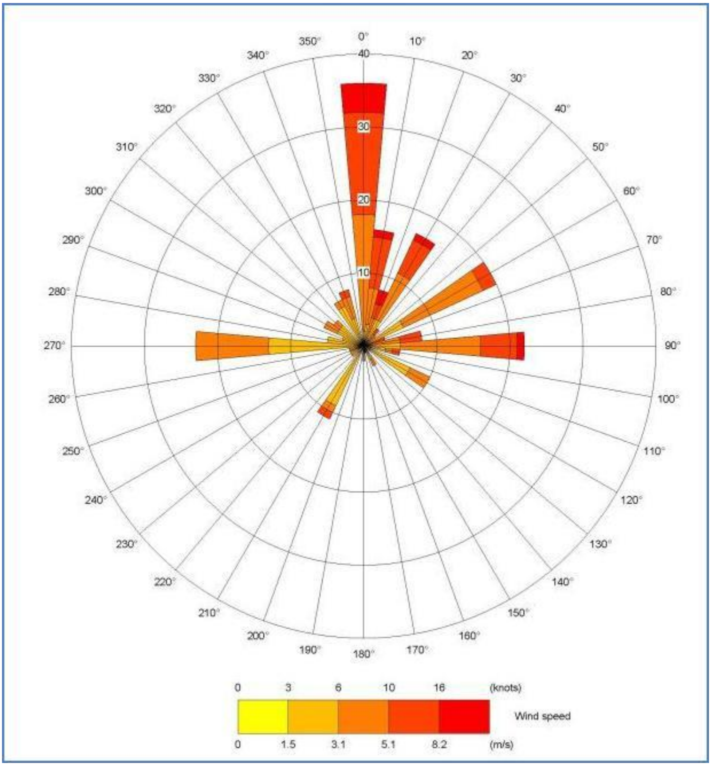

Figure 122: Salmas wind rose (July 2014)

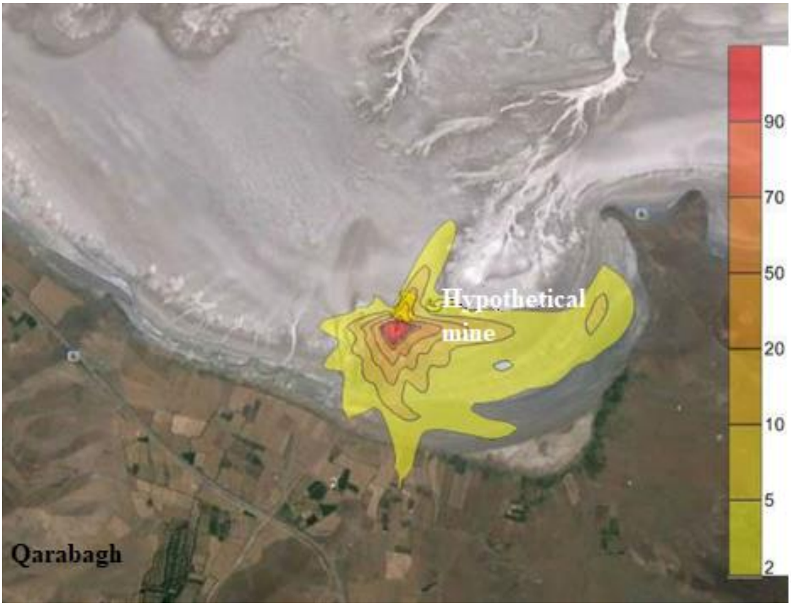

Figure 123: The distribution of particles on the north coast of Qarabagh village (July 2014)

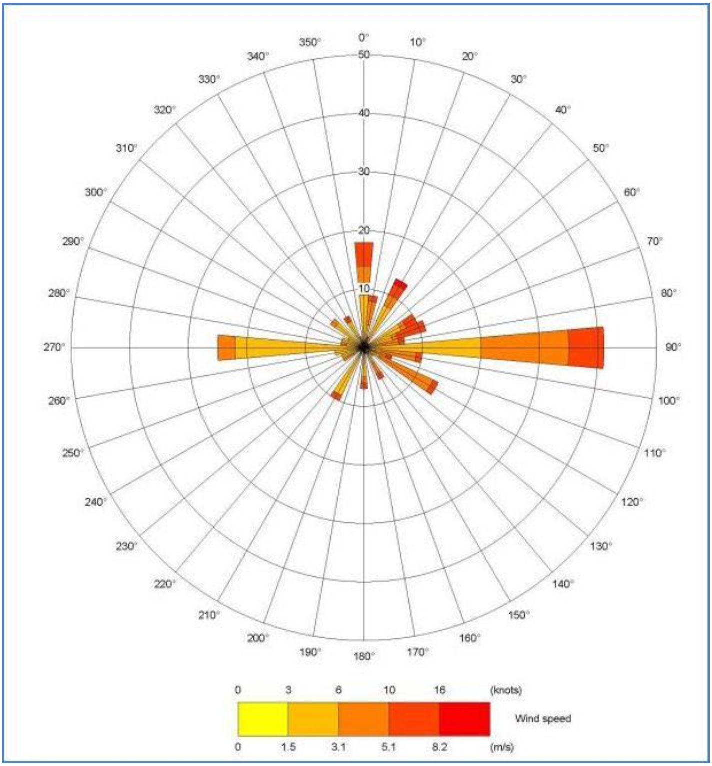

Figure 124: Salmas wind rose (August 2014)

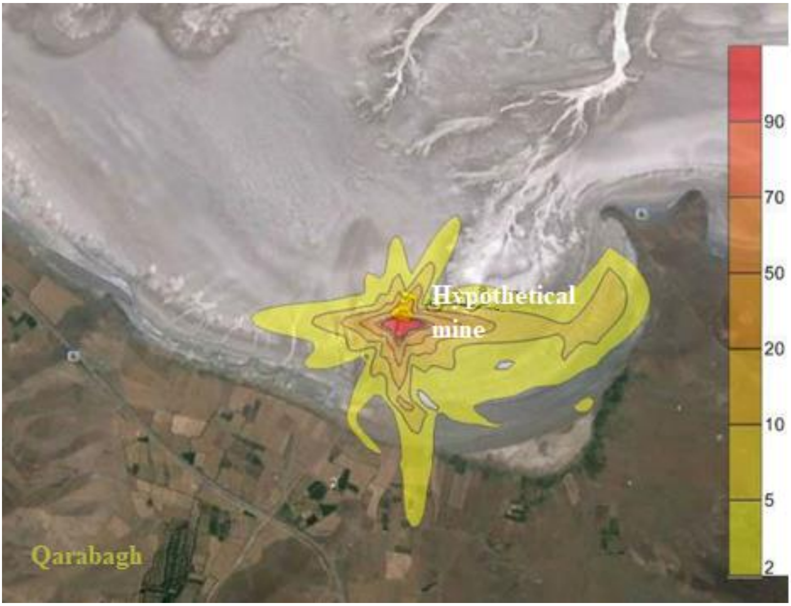

Figure 125: The distribution of particles on the north coast of Qarabagh village (August 2014)

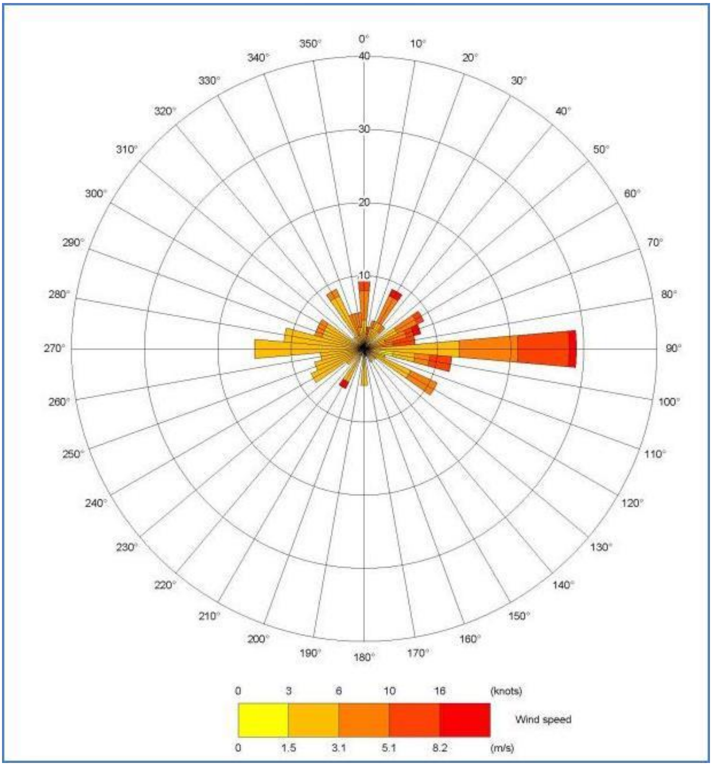

Figure 126: Salmas wind rose (September 2014)

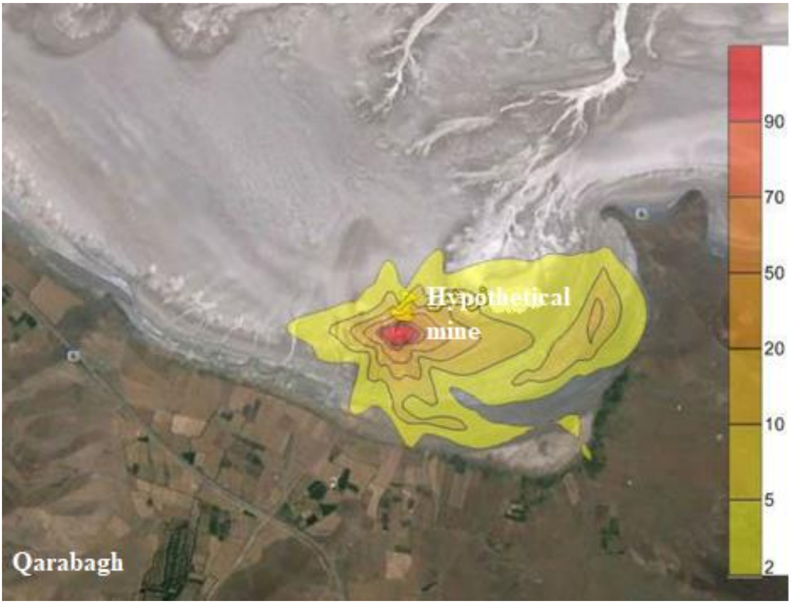

Figure 127: The distribution of particles on the north coast of Qarabagh village (September 2014)

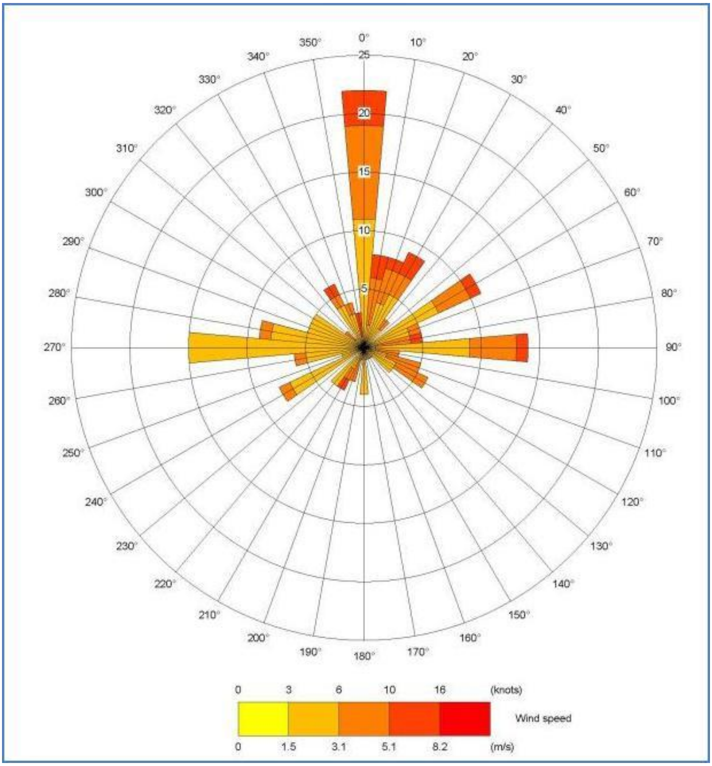

Figure 128: Salmas wind rose (October 2014)

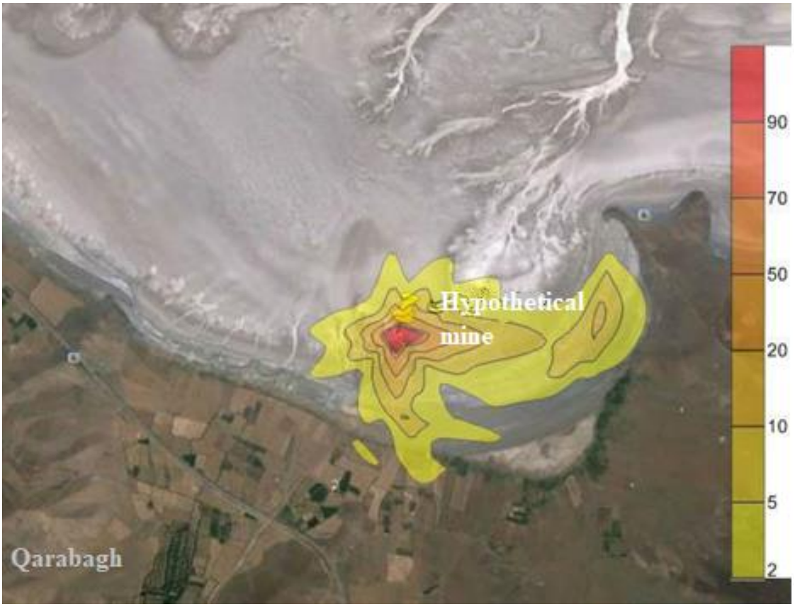

Figure 129: The distribution of particles on the north coast of Qarabagh village (September 2014)

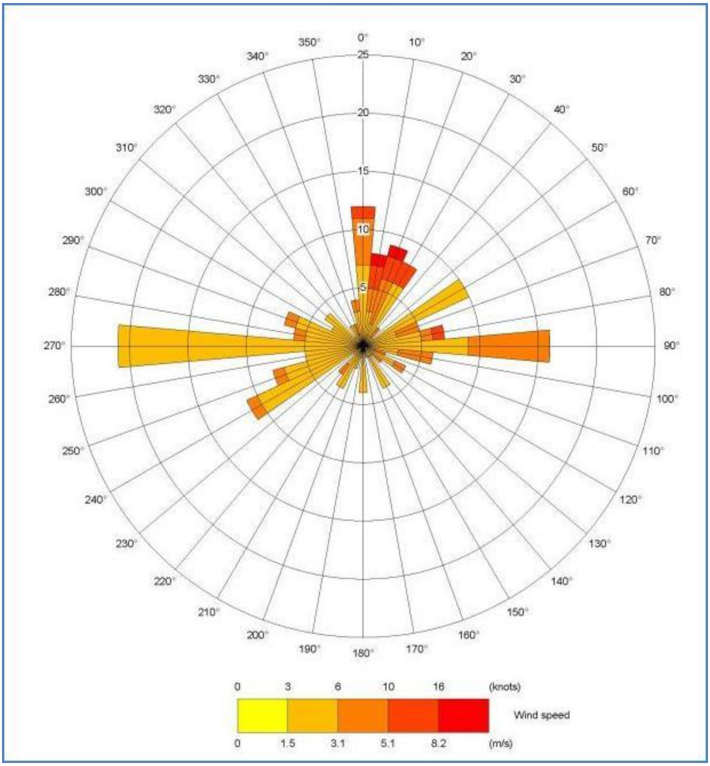

Figure 130: Salmas wind rose (November 2014)

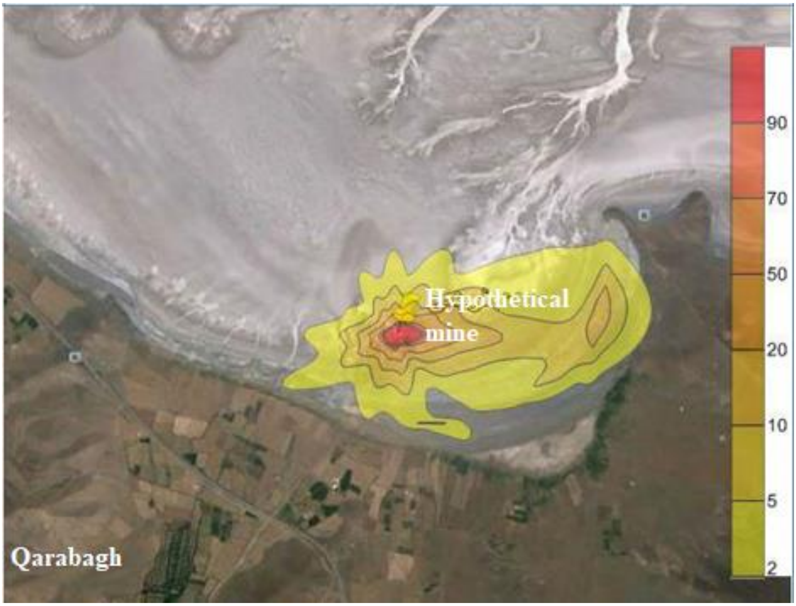

Figure 131: The distribution of particles in the north coast of Qarabagh village (November 2014)

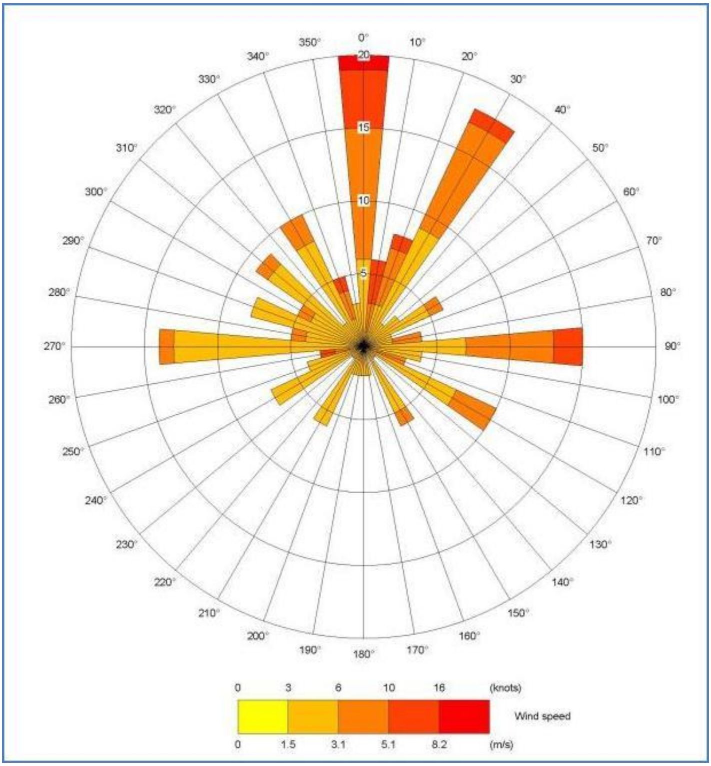

Figure 132: Salmas wind rose (December 2014)

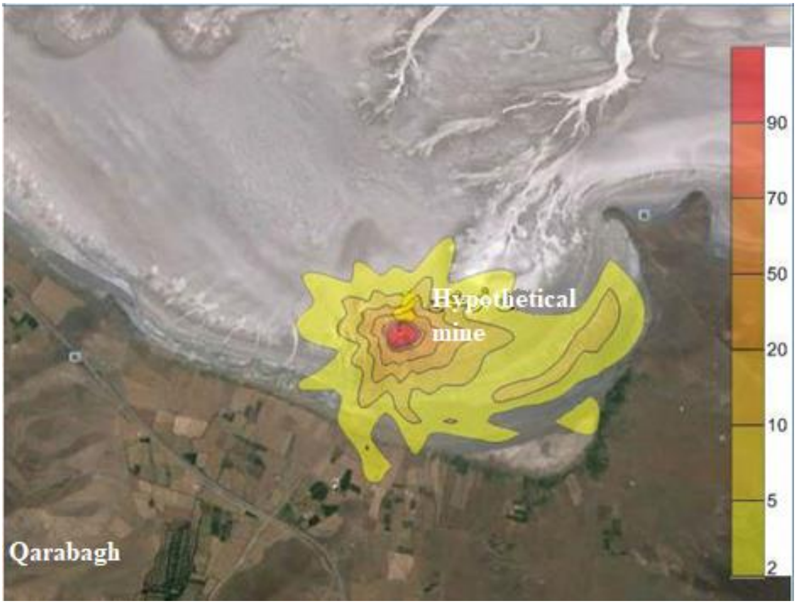

Figure 133: The distribution of particles on the north coast of Qarabagh village (December 2014)

On the basis of obtained diagrams, it can be observed that expansion of particles in the northern coast of Qarabagh (NW of Urmia Lake), is more eastward, then southward, which it means that particles expansion is towards the lake. In this area, most particles spreading are toward Qarabagh village during October and November.

Rose winds show that wind directions are mainly southward in Octeber and November, and most wind direction is eastward in November.

In Other words, during Autumn most wind direction is towards the lake.

Based on the obtained results of particles spreading modelling together with location of mine and prevailing wind direction, it is probable dusts of mining activities, reach to the urban areas. Hence, particles sensing is necessary.

2-11- Uncertainty and model sensitivity analysis

2-11-1- Sensitivity Analysis

Any kind of variation in import parameters, caused export variation and its results. Hence, several scenarios for sensitivity analysis and model uncertainty are as follows:

- Oscillation in pollutant resources amounting to ± 25%
- Oscillation in length of roughness amounting to ± 25%
- Oscillation in height of wind speed measuring amount to ± 25%

The amount of model sensitivity with above mentioned parameters presented in Table 31 and Figure 134.

Table 31: Sensitivity of the model to different parameters

Scenario	The amount of difference with the normal state (%)
Increase emissions by 25%	9.2 %
Reducing emissions by 25%	58.2 %
Increase the roughness length by 25%	12 %
Reduction of roughness length by 25%	19 %
Increasing the height of wind speed recording by 25%	55 %
Reducing the height of the wind speed record by 25%	42 %

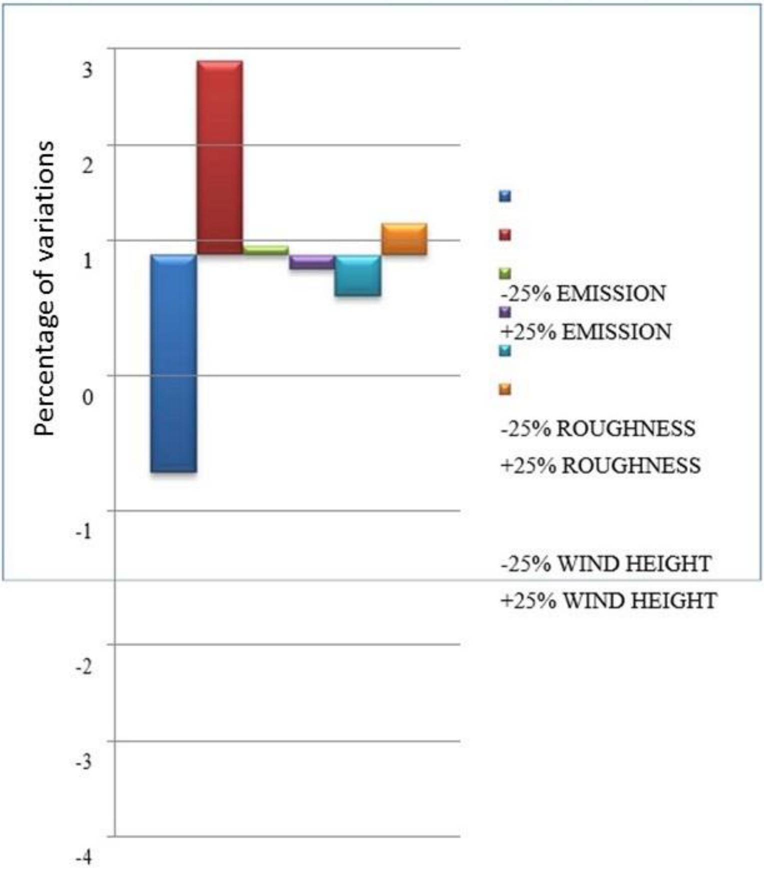

Figure 134: The results of data sensitivity analysis

It can be seen that the amount of model sensitivity to oscillation of pollutant resources, are more than the other investigated parameters, and is about ± 3%.

2-11-2- Model Uncertainty

Generally, the errors in modelling are as follows:

- The errors arising from physical theory of model while using special models (such as ADMS), the errors caused by physical theory of modifies is unavoidable, and might be reduced from one software to another software. For example, if all data for modelling are the same for both ADMS and AERMOD software's, inputs each of these software will provide a different solution for the concentration at a given point, due to the difference in the physical modelling theory used in the model.
- Errors in input data
  This sort of errors, arising from uncertainty in input model such as, Meteorological, Geographical and diffusion resources. Repeating measurements will reduce the errors.
- Errors from model simplifying
  A major error in any kind of modelling is simplifying the model. It is worth to mention that with calibration of model and changing parameters, errors will be reduced and a better result can be obtained. The model simplifying used in this study are resources modelling and gridding model.

Reference:

Aganbati, A., 2006., "Geology of Iran", Organization of Geology and Mineral Exploration of the country.

Arizona Department of environmental Quality, 2004, Revised PM10 State Implementation Plan for the Salt River Area.

Australian Government, NPi, 2012, National Pollutant Inventory Emission Estimation Technique Manual for Mining Version 3.1.

Darvishi Khatouni, J., 2011, "Limnology and paleolimnology report of Urmia Lake", Marine Geology Management, Iran Geology and Mineral Exploration Organization.

Darvishi Khatouni, J., Narimisa, S., Mohammadi, A., and Salehipour Milani. 2010, "Environmental contribution of Lake Urmia from river water and water supply needed to maintain the optimal water level, by examining the effects of development plans on Lake Urmia", the 14th conference of the Geological Society of Iran and the 28th meeting of Earth Sciences, Urmia University, Iran.

Department of Environmental Quality, State of Utah, 2015, Emission Factors for Paved and Unpaved Haul Roads.

EPA, Section 13.2.2, 2006, US Environmental Protection Agency, Emission Factor Documentation for the AP-42. Unpaved Roads.

EPA, Section 13.2.5, 2006, US Environmental Protection Agency, Emission Factor Documentation for the AP-42. Industrial Wind Erosion.

EPA, Section: 13.2.4, 2006, US Environmental Protection Agency, Emission Factor Documentation for the AP-42. Aggregate Handling and Storage Piles.

Esm Hosseini, M., Solatifar, S., 2009, "Compilation of the technical knowledge of extracting sodium sulfate from Urmia Lake water", Department of Chemistry, Faculty of Sciences, Urmia University, Journal of Science Thought, Applied Chemistry, Semnan University, 4th year.

Fariborzi-Iraqi, F. Salari, A., 2009, principles and criteria of the dimensions and weights of cargo transportation, published by Arg.

Greeley, R. and Iversen, J.D., 1987. Wind as a geological process: on Earth, Mars, Venus and Titan (No. 4). CUP Archive.

http://www.gostareshonline.com/culture-arts/1363419-%DB%8C%DA%A9-%DA%AF%D8%B2%D8%A7%D8%B1%D8%B4-

%D8%A8%D8%A7%D9%86%D9%85%DA%A9.html

http://www.gsi.ir/Branches/Lang_fa/Page_05-01-04/Start_0/GroupId_05-01/TypeId_0/ReportsId_1579/PageLimit_25/Action_MoreInfo/WebsiteId_8/%D9%86%D9%85%D8%A7%D9%8A%D8%B4.%D8%A7%D8%B7%D9%84%D8%A7%D8%B9%D8%A7%D8%AA.%D8%B4

http://www.ngdir.ir/minemineral/PMineMineralChapterDetail.asp?PID=3902]

Kelts, K. & Shahrabi, M., 1986, “Holocene sedimentology of hypersaline Lake urmia, Nortwestern Iran”, Palaeogeography, Palaeoclimatology, Journal, Vol. 54: 105-130.

Najafi, G., Najafi, P., 2013, "Necessity and ways to revive Lake Urmia". Scientific monthly of agriculture and rural environment.

Ravi, S., Zobeck, T.M., Over, T.M., Okin, G.S. and D'ODORICO, P.A.O.L.O., 2006. On the effect of moisture bonding forces in air-dry soils on threshold friction velocity of wind erosion. Sedimentology, 53(3), pp.597-609.

Sajjadi, A., Hashemian, J., 2001, "Extraction of mineral salts from Lake Urmia", Proceedings of the first conference of Lake Urmia.

Shah Hosseini, M. Amini, A., Shahrabi, M., 2003., "Sedimentological study and formation environment of young biogenic carbonate deposits around Lake Urmia and investigation of their relationship with the lake", 7th Conference of Geological Society of Iran.

Wilcox D. C., Turbulence Modeling for CFD (Third Edition)-2006.

Yaping Shag, 2000, A simple expression for wind erosion threshold friction velocity, Journal of Geophysical Research, Vol. 105, No. D17, Pages 22,437-22,443.